NORTH ATLANTIC MARINE TEPHROCHRONOLGY: A TOOL FOR RECONSTRUCTING EVENTS AND PROCESSES DURING THE PENULTIMATE GLACIAL-INTERGLACIAL CYCLE

Marion Kuhs

A Thesis Submitted for the Degree of MPhil
at the
University of St Andrews

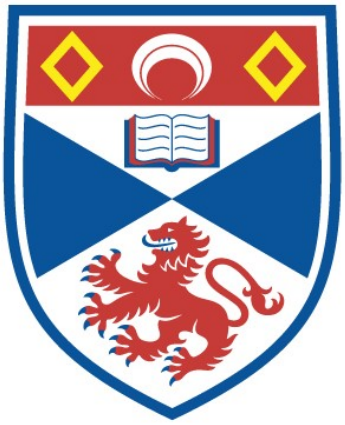

2016

North Atlantic marine tephrochronology: A tool for reconstructing events and processes during the penultimate glacial-interglacial cycle

Marion Kuhs

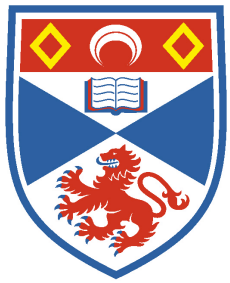

University of
St Andrews

This thesis is submitted in partial fulfilment for the degree of MPhil
at the
University of St Andrews

30th of September 2015

Declarations

1. Candidate's declarations:

I, *Marion Kuhs*, hereby certify that this thesis, which is approximately 31,000 words in length, has been written by me, and that it is the record of work carried out by me, or principally by myself in collaboration with others as acknowledged, and that it has not been submitted in any previous application for a higher degree.

I was admitted as a research student in September, 2010 and as a candidate for the degree of MPhil in November, 2014; the higher study for which this is a record was carried out in the University of St Andrews between 2010 and 2015.

Date: 30/09/2015

2. Supervisor's declaration:

I hereby certify that the candidate has fulfilled the conditions of the Resolution and Regulations appropriate for the degree of MPhil in the University of St Andrews and that the candidate is qualified to submit this thesis in application for that degree.

Date: …30/09/2015… signature of supervisor ……

3. Permission for publication: (*to be signed by both candidate and supervisor*)

In submitting this thesis to the University of St Andrews I understand that I am giving permission for it to be made available for use in accordance with the regulations of the University Library for the time being in force, subject to any copyright vested in the work not being affected thereby. I also understand that the title and the abstract will be published, and that a copy of the work may be made and supplied to any bona fide library or research worker, that my thesis will be electronically accessible for personal or research use unless exempt by award of an embargo as requested below, and that the library has the right to migrate my thesis into new electronic forms as required to ensure continued access to the thesis. I have obtained any third-party copyright permissions that may be required in order to allow such access and migration, or have requested the appropriate embargo below.

The following is an agreed request by candidate and supervisor regarding the publication of this thesis:

PRINTED COPY

Embargo on all of print copy for a period of 1 year on the following ground:

- Publication would preclude future publication

Supporting statement for printed embargo request:
Chapter 4, which also contains unpublished data from co-author Dr Mark Chapman (University of East Anglia), is planned to be published. Proposed journal for publication is Quaternary Science Reviews.

ELECTRONIC COPY

a) Embargo on all of electronic copy for a period of 1 year on the following ground:
    - Publication would preclude future publication

Supporting statement for electronic embargo request:
Chapter 4, which also contains unpublished data from co-author Dr Mark Chapman (University of East Anglia), is planned to be published. Proposed journal for publication is Quaternary Science Reviews.

Date: 30/09/2015……
Signature of supervisor ……

Abstract

The focus of this thesis is the analyses of tephra deposits found in the penultimate glacial–interglacial interval of the marine sediments from Integrated Ocean Drilling Project (IODP) Site U1304, southern Gardar Drift, North Atlantic. The location and the high-resolution of U1304 are ideal to investigate changes in deep-ocean ventilation, sea-surface circulation pattern well as ice-sheet dynamics. Especially, the climate conditions during the Last Interglacial (LIG) with warmer annual temperature and higher global sea-level are of particular interest because this period is often seen as an analogue to predicted future climate scenarios.

By means of geochemical and shard size analyses the transport mechanism of the tephra deposits were determined. The tephra deposits found during the penultimate glacial (Marine Isotope Stage 6 (MIS 6)) were transported by iceberg–rafting. Comparison of individual shard geochemistry with the geochemistry of Holocene volcanic systems from Iceland showed that the shards originated from different volcanic systems on Iceland. Combining source evidence with Icelandic Ice Sheet (IIS) flow models for the Last Glacial Maximum (LGM) suggests that the IIS had marine calving margins to both the north and south of Iceland during the late MIS 6 and that icebergs could have been transported to the U1304 core site by following surface ocean circulation patterns similar to those that prevailed during the LGM.

In contrast, one of the analysed tephra horizons deposited during MIS 5e at the U1304 core site can be correlated with the known 5e-Eem/RHY-I isochron in the tephrostratigraphical framework of the North Atlantic. The 5e-Eem/RHY-I tephra is also found in the nearby marine sediment core MD99-2253. In both cores, U1304 and MD99-2253, the 5e-Eem/RHY-I tephra occurs just above the onset of fully-interglacial deep-ocean ventilation, indicated by an abrupt shift in foraminiferal benthic $\delta^{13}C$. Aligning both cores on a common timescale with the 5e-Eem/RHY-I age of 121.99 ± 1 ka as an additional tie-point, suggests that the onset to full-interglacial conditions occurred synchronously at both core sites. This finding provides the opportunity to

develop a new event-based stratigraphy, reliably sub-dividing MIS 5e into an early and later phase.

Table of Contents

List of Figures

Chapter 1 Introduction

Chapter 2 Material and Methods

Chapter 3 Ice-Rafted Tephra in the Glacial North Atlantic

Chapter 4 The Stratigraphic Sub-Division of MIS 5e in the North Atlantic

List of Tables

Chapter 1 Introduction

Chapter 3 Ice-Rafted Tephra in the Glacial North Atlantic

Chapter 4 The Stratigraphic Sub-Division of MIS 5e in the North Atlantic

Chapter 6 Appendix A

List of Abbreviations

AABW	Antarctic Bottom Water
AMOC	Atlantic Meridional Overturning Circulation
AVS	Askja Volcano Systems
BIS	British Ice Sheet
CV	Critical Value
D/O	Dansgaard-Oeschger
dc	Detrital Carbonates
EGC	East Greenland Current
EIS	European Ice Sheets
EMPA	Electron Microprobe Analyses
EVZ	Eastern Volcanic Zone
FEEA	Facility for Earth & Environmental Analysis
FIS	Fennoscandian Ice Sheet
GIS	Greenland Ice Sheet
GNAIW	North Atlantic Intermediate Waters
GRIP	Greenland Ice Core Project
GVS	Grímsvötn Volcano Systems
HE	Heinrich Event
hsg	Haematite-Stained Grains
IIS	Icelandic Ice Sheet
IODP	Integrated Ocean Drilling Program
IRD	Ice-Rafted Debris
ISO	Iceland-Scotland Overflows
KVS	Krafla Volcano Systems
LC	Labrador Current
LGM	Last Glacial Maximum
LIG	Last Interglacial

LIS	Laurentide Ice Sheet
LSW	Labrador Sea Water
MIS	Marine Isotope Stage
NAC	North Atlantic Current
NADW	North Atlantic Deep Water
NEEM	North Greenland Eemian Ice Drilling
NHIS	Northern Hemisphere Ice Sheet
Np (s)	*Neogloboquadrina pachyderma* (sinistral)
NSIW	Norwegian Sea Intermediate Water
pg	Pumice Grains
RVZ	Reykjanes Volcanic Zone
SC	Similarity Coefficient
SDF	Statistical Distance Function
SIC	South Iceland Current
SPG	Sub-Polar Gyre
$\overline{SS}$	Mean Sortable Silt
SST	Sea Surface Temperature
SSW	Southern Sourced Waters
STG	Sub-Tropical Gyre
TAU	Tephrochronology Analytical Unit
TIMS	Thermal Ionization Mass Spectrometry
VBVS	Veidivötn-Bárdarbunga Volcano Systems
VPDB	Vienna Pee Dee Belemnite
WDS	Wavelength Dispersive Spectrometer
WVZ	Western Volcanic Zone

Collaboration Statement

Foraminiferal benthic and planktonic carbon and oxygen stable isotope data as well as bulk sediment weight percentage data of U1304 that have been used throughout this thesis, have been contributed by Prof David A. Hodell. Moreover, he supplied the residue of U1304 for the interval 15.47 to 24.52 mcd, which allowed me carry out IRD, tephra and fauna analyses over this interval.

Dr Mark Chapman provided so far unpublished proxy data from MD99-2253 used in Chapter 4.

Chapter 3 is based on and Chapter 2 contains parts of the following publication: Kuhs, M. et al., 2014. Iceberg-rafted tephra as a potential tool for the reconstruction of ice-sheet processes and ocean surface circulation in the glacial North Atlantic. *Geological Society, London, Special Publications*, 398(1), pp.141–155.

Chapter 4 is planned to be published under the title: 'The stratigraphic sub-division of MIS 5e in the North Atlantic', by Marion Kuhs, William E.N. Austin, Mark R. Chapman, David A. Hodell. Proposed journal for publication will be Quaternary Science Reviews.

Acknowledgements

First of all I have to thank Professor William Austin for taking me on as his student and always providing me with interesting ideas and new directions how to extend my research projects. I am very grateful to Bill for giving me opportunities like taking part in the research cruise to Svalbard and the Arctic Ocean.

A big thank you goes to Dr Katherine Roucoux who became my second supervisor in the final stage of my studies and who has provided extremely useful feedback on my research.

I thank Fiona Hibbert for introducing me into the research environment in St Andrews and always giving me good advice regarding academic and other relevant matters.

Peter Abbott has always been available for my many questions regarding tephra analyses. Thanks for your patience.

I am grateful to Dr Mark R. Chapman and Professor David A. Hodell for sharing data and samples for my project. Without these data, the thesis in its current form would not have been possible.

Furthermore, I would like to thank, Dr Chris Hayward, Mike Hall, Donald Herd, Andrews Mackie for their help and advice regarding the geochemical analyses of tephra (i.e. preparations of the samples and running the WDS electron microprobe).

This study could not have been completed without the financial support received from the Natural Environment Research Council (NERC through) the NERC studentship (NE/G007373) and would like to acknowledge the support of the Integrated Ocean Drilling Project.

None of this would have been possible without the love and patience of my family, especially Stefan and Nora. Thank you for all you support and encouragement.

CHAPTER 1 Introduction

1.1. Sub-Orbital Climate Fluctuations in the Northern Hemisphere

Geological records show that the Earth has experienced numerous glacial-interglacial cycles. During the most recent glacial periods of the late Quaternary, the Earth was covered with large ice-sheets which reached into the mid-latitudes, whereas these ice-sheets were restricted to the polar regions during interglacial periods. These glacial-interglacial cycles have been recorded in various marine and terrestrial palaeoclimate records, for example in the benthic foraminiferal $\delta^{18}O$ records of marine sediment cores (Pisias et al. 1984; Martinson et al. 1987; Lisiecki & Raymo 2005) and $\delta^{18}O$, δD and/or dust concentration of the high-latitude ice cores (Petit et al. 1999; Augustin et al. 2004; NGRIP Members 2004; Jouzel et al. 2007; Svensson et al. 2011). Furthermore, climate records from the North Atlantic region also show that climate fluctuations on a sub-orbital timescale occurred during past glacial and interglacial periods. Dansgaard-Oeschger (D/O) cycles are examples of millennial-scale fluctuations, which are characterized by rapid (typically a few decades) warming of 10 ± 5°C (Severinghaus & Brook 1999; NGRIP Members 2004). In contrast to the abrupt warming from cold stadials into warm interstadials, D/O cycles are generally characterised by gradual cooling (typically a few hundreds to thousands of years) (Dansgaard et al. 1982; Dansgaard et al. 1993; Dokken et al. 2013). Within the last glacial cycle, packages of D/O cycles forming a gradual cooling trend followed by a marked rapid warming are referred to as Bond Cycles. The last and coldest event within a Bond Cycle, often occurring immediately before the rapid warming is called a Heinrich Event (HE). These HEs represent major episodes of iceberg-rafting from the North Hemisphere Ice Sheets (NHIS) and yielded distinctive sediment layers (Heinrich Layers; HL) containing glacially transported debris from the adjacent continents. One of the characteristic lithologies of such major ice-rafting events within the North Atlantic's HLs are detrital carbonates. Geochemical analysis has shown that these detrital carbonates originated from bedrock sources to the north and east of the Hudson Bay (Andrews & Tedesco 1992; Bond et al. 1992; Gwiazda et al. 1996; Hodell & Curtis 2008; Hodell et al. 2008).

Even though the Laurentide Ice Sheet (LIS) is seen as the major source of ice-rafted debris (IRD) during a HE, there is evidence that the European Ice sheets (EIS) also contributed (Revel et al. 1996; Grousset et al. 2000). For example, preceding the peak of detrital carbonates, high concentration of basaltic glass and haematite-stained grains were observed during major IRD events (Bond 1997). The source of basaltic glass is thought to be Iceland (Bond 1997) and haematite-stained grains are thought to derive from Red Bed source areas enclosing the North Atlantic (Habicht 1979; Bond & Lotti 1995; Bond 1997; Peck et al. 2007). The time interval between HEs ranged from about 5 ka up to 15 ka (Bond et al. 1993). Bond & Lotti (1995) also identified IRD-events with a short periodicity of ~ 1.5 ka. These events coincide with a surface cooling of the North Atlantic, corresponding with the southwards migration of the North Atlantic polar front. This hydrographic response and/or driver allowed icebergs to travel further south in the North Atlantic before they melted and released IRD to the ocean floor.

Sediment records of last glacial age suggest that IRD from the Fennoscandian Ice Sheet (FIS) were transported by the Norwegian Sea Current northwards, before the current turned southwards, entering the North Atlantic by passing first eastern and then southern Iceland as it travelled west (Ruddiman 1977). This South Iceland Current (SIC) (Robinson et al. 1995) then travelled west before it turned south again and joined the counterclockwise surface circulation of the sub-polar gyre (SPG) (Figure 1.1). The East Greenland Current (EGC) transported icebergs from the Greenland Ice Sheet (GIS) and Icelandic Ice Sheet (IIS) to the south, entering the North Atlantic over the Denmark Strait where they became entrained in the SPG. The southward extent of the gyre itself depends on the actual prevailing climate state. During times when sub-polar water extended as far south as Spain (McIntyre & Ruddiman 1972) the cyclonic gyre was able to transport IRD-loaded icebergs much further south than today. During glacial periods, the highest deposition rate of IRD was between 46°N and 50°N, forming the so-called IRD belt (Ruddiman 1977). Despite the fact that icebergs have been sighted as far south as 28°N in recent times, this does not mean that they still carry significant amounts of IRD (Andrews 2000). IRD are largely carried within 1-3 m of the bottom of an iceberg

and under prevailing climate conditions the majority of IRD are already released before the icebergs pass 60°N (Andrews 2000).

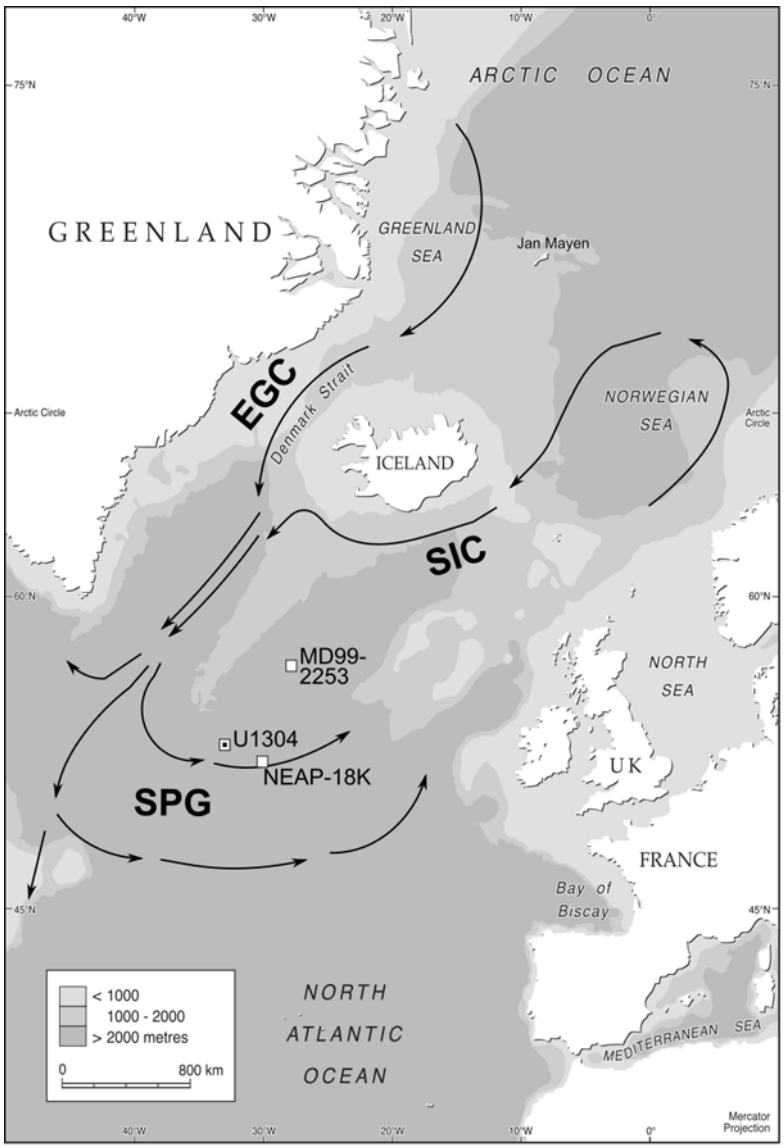

Figure 1.1: Location of IODP Site U1304 sediment core from the Gardar Drift, North Atlantic and locations of additional key cores used in this study. NEAP-18K see Hall et al. (1998); MD99-2253 see Chapman (2012) and Farmer (2012). Glacial surface ocean circulation after Ruddiman & Glover (1972), Ruddiman (1977) and Robinson et al. (1995). EGC: East Greenland Current, SIC: South Iceland Current, SPG: Sub-Polar Gyre.

1.1.1.

1.1.2. Climate Drivers

In general, trajectories of icebergs are determined by surface water circulation. Today, the majority of icebergs in the North Atlantic calve from outlet glaciers of the GIS and are carried by the Labrador Current (LC) and the EGC to the south as far as 28°N/48°W (Andrews 2000). Reconstructions (McIntyre & Ruddiman 1972; Ruddiman 1977; Bond & Lotti 1995; Robinson et al. 1995) and models (Watkins et al. 2007) of past surface circulation patterns show that they were similar to today's patterns. A dominant feature in the Northern Hemisphere is the counterclockwise surface circulation around a low pressure centre at high-latitudes. In the North Atlantic the SPG appears to have been a persistent feature of glacial and interglacial times (McIntyre & Ruddiman 1972; Ruddiman 1977; Robinson et al. 1995). However, during interglacials the gyre tends to be more weakly developed and has a smaller spatial extent (Ruddiman & Glover 1972).

A reduction of the Atlantic meridional overturning circulation (AMOC) is implicated in D/O cycle behaviour and is probably caused by a reduction of water density, driven by salinity and/or temperature changes, which lead to a reduction in deep water formation. In the Nordic Seas, an increased freshwater input caused by enhanced river run-off (e.g. Clark et al. 2001) or meltwater discharge from ice-sheets (e.g. van Kreveld et al. 2000) had the potential to weaken North Atlantic Deep Water (NADW) formation. As a result of the AMOC slow-down, the North Atlantic's supply of deep Southern Ocean-sourced water penetrated further north and reached shallower depths; in turn the northward surface transport of heat is reduced. The latter allowed the southwards expansion of the North Atlantic polar front and the transport, as well as the melting, of icebergs towards lower latitudes. Over time the reduced export of NADW caused a warming in the Southern Ocean, where meltwater input from destabilised ice-sheets subsequently reduced the formation of Antarctic Bottom Water (AABW) (Maslin et al. 2001). Together with the build-up of heat in the sub-tropical North Atlantic (Carlson et al. 2008) and the eventual mixing of high salinity surface waters in the North Atlantic, the strengthening of the AMOC and the resumption of the NADW formation is thought to

have occurred (Schmidt et al. 2004). As a consequence, the North Atlantic's polar front retreats to the north, which restricts iceberg transport and melting to higher latitudes. Due to this northward shift of the North Atlantic polar front, the renewed heat transport supplies moisture to the north which, in turn, allows renewed ice-sheet growth. On the other hand, this renewed warming can also act to destabilise ice-sheets, leading to an increased meltwater input and consequently to the next stadial phase. This millennial-scale behaviour in the North Atlantic's D/O cycle has been explained and termed the ocean "salt oscillator" (Broecker et al. 1990; Schmidt & Hertzberg 2011). The AMOC plays an important role in the heat exchange between the two hemispheres which leads to the so-called 'bi-polar see-saw' pattern, i.e. while the northern hemisphere rapidly warms, the southern hemisphere gradually cools (Broecker 1998; Blunier & Brook 2001; Severinghaus 2009).

During the Last Interglacial (LIG), it has been suggested that the intensity of the SPG played an important role in the observed surface cooling events. Southward movement of Artic water reduced the SPG and strengthened the sub-tropical gyres (STG), which allowed the North Atlantic Current (NAC) to bring warmer and saltier water into the Nordic Sea. Again, this northward transport of heat and moisture supported ice-sheet growth and deep water formation (Mokeddem et al. 2014).

1.1.3. Climate Proxies

Pioneering work in the early 1970s used microfossil and IRD distribution patterns in marine sediments of the North Atlantic to show changes of surface water masses (McIntyre & Ruddiman 1972; CLIMAP Project Members 1976; Bond & Lotti 1995). This concept of using faunal/IRD abundance variation as a proxy for changes in water temperature/salinity, and hence changes in water mass properties, is still commonly used today. The relative abundance of *Neogloboquadrina pachyderma* (sinistral) (*N. pachyderma* (s)), a planktonic foraminifera which prefers to live in cold polar waters can be used as an indicator for changes of the North Atlantic polar front position (Ruddiman & Mcintyre 1981). Furthermore, foraminiferal planktonic $\delta^{18}O$ has been

used to establish surface water conditions such as temperature and salinity changes. To unravel the contribution of temperature in planktonic $\delta^{18}O$ changes, foraminiferal Mg/Ca analyses have been performed in parallel, because the Mg/Ca ratios in foraminifera shells increase exponentially with increasing temperature (Lea et al. 1999; Barker et al. 2005). Palaeoclimate proxies are often subtle and difficult to interpret because they tend to be influenced by more than one parameter (see above $\delta^{18}O$) and much care has to be taken for their interpretation. Thus, generally more than just a single proxy (i.e. multiproxy approach) has to be considered in the reconstruction of past climate conditions. The development of new as well as the improvement of well-established proxies is a continuing field of research in paleoclimatology. Further proxies for sea surface temperature (SST) reconstruction are for example alkenone index U^{k}_{37} (Pelejero & Grimalt 1997), Tex_{86} and complex microfossil assemblages transfer functions. The methods are time consuming and more expensive than *N. pachyderma* (s) relative abundance counts, which in the sub-polar North Atlantic have been shown to provide a robust indicator of abrupt climate transition in the surface ocean (e.g. Austin & Hibbert, 2012).

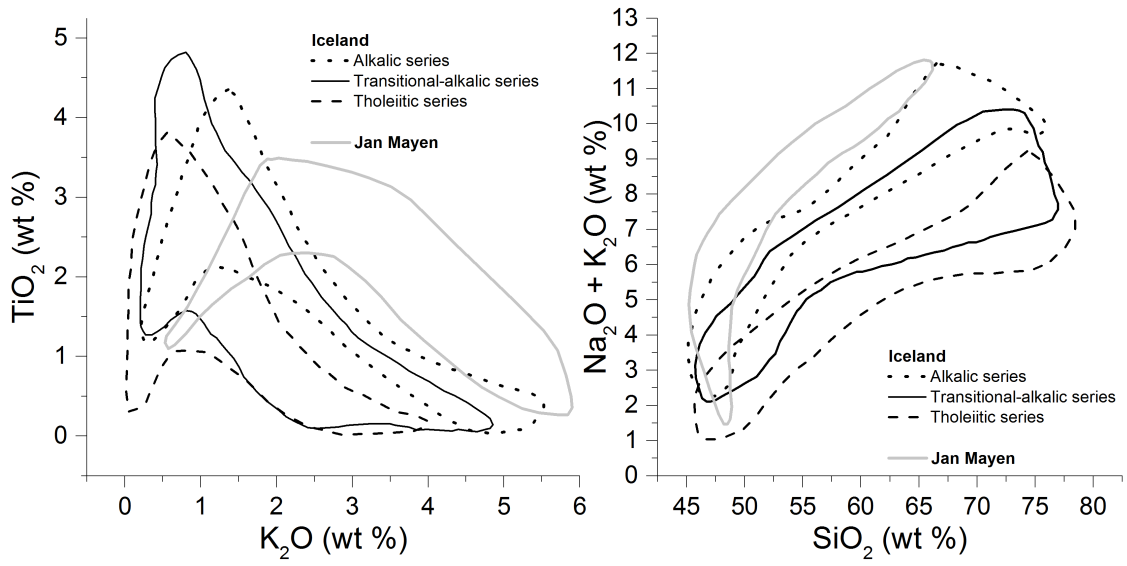

Figure 1.2: Left: TiO_2 versus K_2O and **Right:** Total alkali-silica plots with Jan Mayen rock suite (Imsland 1984; Maaløe et al. 1986) and Icelandic rock suites: Alkalic, Transitional-alkalic and Tholeiitic series (Jakobsson et al. 2008).

Sand-size debris (≥ 150 μm), delivered by glaciers to their calving margins and transported by icebergs to the open ocean not only give an insight into surface circulation patterns, but also hold the potential through detailed provenance studies to shed light on ice-sheet dynamics. By means of visual inspection, the IRD lithology can be identified, which can help to determine possible source regions for these grains. Detrital carbonates, for example, have characteristic sugary textures and are commonly associated with source rocks from Hudson and Baffin Bay (Andrews & Tedesco 1992; Bond et al. 1992). They have been interpreted as having been delivered by LIS-sourced icebergs and are widely held as the diagnostic lithology for a HE (Andrews & Tedesco 1992). Due to the common geological history of the North Atlantic's continental margins, certain lithologies can potentially originate from several areas neighbouring the North Atlantic. For example, haematite-stained quartz from Red Bed sources could be delivered from the LIS (Bond & Lotti 1995), GIS (van Kreveld et al. 2000), FIS (Habicht 1979) or British Ice Sheet (BIS) (Peck et al. 2007). In addition, igneous debris such as pumice, obsidian and basalts have several potential source areas as, Icelandic volcanic province (Bond & Lotti 1995; Lacasse et al. 1996; Lackschewitz & Wallrabe-Adams 1997), British Tertiary Province (Knutz et al. 2001; Hibbert et al. 2010) and offshore sources such as Rockall Bank (Scourse et al. 2009). Even though Jan Mayen could also be the source origin for volcanic glass in the North Atlantic, in general these tephra are associated with Icelandic eruptions (Bond & Lotti 1995; Lacasse et al. 1996; Hafliðason et al. 2000; Brendryen et al. 2010). IRD provenance studies based solely on the visual inspection of the IRD components need to be interpreted with care, as one and the same lithology could have been derived from different source areas around the North Atlantic. Additional analyses, such as isotope or geochemical analyses could help to narrow down these source region options. Dolomitic limestone from northeastern Canada has a distinctive lead isotope (Gwiazda et al. 1996) and $\delta^{18}O$ signature (Hodell & Curtis 2008). By means of isotope analyses, detrital carbonates associated with HEs can be tied to these regions around the Baffin and Hudson Bay. Hodell & Curtis (2008) and Hodell et al. (2008) also showed that the 'Laurentide carbonate' signature, as well as its distinctive Ca/Sr ratio, is carried in the fine fraction of the bulk sediments. This is

of particular interest because while the coarse material from a specific source region might be missing, the source-signature can still be present in the fine fraction of the sedimentation records in distal areas and can still be identified by the analyses of bulk sediments rather than the discrete components of the IRD. Furthermore, geochemical analyses of tephra can help to identify whether they are derived from Jan Mayen or Iceland because of the distinct potassium rich nature of the Jan Mayen volcanic source. These two potential tephra sources in the North Atlantic can usually be separated with the help of $Na_2O + K_2O$ vs. SiO_2 and Ti_2O vs. K_2O plots (Figure 1.2). While the visual inspection and identification of IRD might have its pitfalls, it remains a relatively quick and low-cost method which can provide a first evaluation of past conditions. Other methods, e.g. $^{40}Ar/^{39}Ar$ dating of Hornblende (Hemming et al. 1998) are often limited by the quantity and/or quality of the material required for such analyses.

1.2. Last Interglacial North Atlantic Climate

The Last Interglacial is often generalised as the 'Eemian', a term first introduced by the Dutch biologist and naturalist Pieter Harting (Harting 1874). While working on sediments near Amersfoort he discovered sequences of clay and sands containing a rich variety of Lusitanian and Mediterranean molluscs which he could not correlate to any of the known stratigraphic units of that time (Bosch 2000). Therefore, he named this unit Eemian after the nearby river Eem (Bosch et al. 2000; Kukla et al. 2002). In the following years the Eemian stratigraphical unit was found in various places in Northern Europe (Bosch et al. 2000). Jessen & Milthers (1928) used an extensive pollen investigation to introduce the first biostratigraphy for the Eemian in Denmark and northwest Germany (Bosch et al. 2000), which was later adapted by Zagwijn (1961) to develop a pollen stratigraphy for the Netherlands (Cleveringa et al. 2000; Kukla et al. 2002). However, the record from this stratotype location at Amersfoort is interrupted by erosion and periods of non-deposition, which became especially apparent when the stratotype record was compared with the records from a new location at Amsterdam Terminal (Cleveringa et al. 2000). This location contains detailed faunal and flora

records and has been proposed as the parastratotype for the Northern and Central Netherlands (Cleveringa et al. 2000; Gans et al. 2000; Van Leeuwen et al. 2000).

The terrestrial Last Interglacial at these localities can be defined by a vegetation sequence of temperate forests sandwiched between open vegetation of the penultimate/last glacial. The durations of the terrestrial Last Interglacial varies between 11,000-13,000 years (Müller 1974; Turner 2002) in northwest Europe to about 15,000-16,500 in southwest Europe (Sánchez Goñi et al. 1999; Shackleton et al. 2003; Tzedakis 2003). These regional differences in the duration of the LIG were probably caused by the time needed for plant species to migrate across Europe from the south to the north, highlighting that the upper or lower (or both) LIG boundaries could not have been synchronous.

The most commonly used stratigraphy for marine records is the Marine Isotope Stratigraphy and initially it was thought that the whole of MIS 5 represented the LIG. However, Shackleton (1969) suggested a different interpretation of MIS 5, proposing that only the earliest part (MIS 5e) expressed the LIG of northern Europe. Based on the astronomical tuned marine timescale, the MIS 5e sub-stage lasted from 128 ka to 116 ka (Imbrie et al. 1984), which fits very well with the duration of the Eemian calculated by Müller (1974). The 11,000 years duration was based on varve counts from a record in Bispingen, Germany (Müller 1974). In the following decades various investigations were made to attempt to resolve the question about the duration as well as the synchronicity of ocean-terrestrial LIG sequences. Indirect ocean-land correlations suggest a duration for the LIG between 15,000-23,000 years (Sánchez Goñi et al. 2000 and therein). Turon's (1984) investigation of direct ocean-land correlation, based on a very low resolution marine pollen record, suggested that MIS 5e and the Eemian were synchronous. The marine sediment core MD95-2042 from the Iberian margin has probably allowed the best insight into ocean-land correlation until now. Extensive work has been carried out on this high resolution sedimentary core by Sánchez Goñi et al. (2000) and Shackleton et al. (2003) and they were able to show that the Eemian and

MIS 5e were not synchronous. The Eemian actually started 2,000 years later than the foraminiferal benthic $\delta^{18}O$ plateau and 6,000 years later than the MIS 6/5e boundary, i.e. after all the major NHIS that grew during MIS 6 had already melted (Shackleton et al. 2003). Furthermore, they discovered that the LIG conditions on land persisted into MIS 5d (Shackleton et al. 2003). The simultaneous rise of steppic vegetation and decline of Eurosiberian trees combined with the disappearance of the Mediterranean vegetation occurred shortly after a transition to positive benthic $\delta^{18}O$ (Sánchez Goñi et al. 2000; Shackleton et al. 2003). This finding actually suggests that the end of the Eemian occurred after the high latitude ice-sheets had already grown (Sánchez Goñi et al. 2000; Shackleton et al. 2003). The data from MD95-2042 allowed the identification of four different climate phases during the Eemian; a: Mediterranean, b: temperate oceanic, c: cold oceanic, d: temperate oceanic (Sánchez Goñi et al. 1999; Sánchez Goñi et al. 2000). Interestingly in the MD95-2042 record, the Eemian thermal optimum occurred in the early stage, whereas records from northern Europe show the thermal optimum in the so-called middle Eemian (Sánchez Goñi et al. 2000). This apparent 'lag' of the thermal optimum in northern Europe compared with southern Europe might be related to palaeoceanographic observations made in the adjacent North Atlantic Ocean. Over recent years more evidence has emerged that the Nordic Seas remained colder for much longer than the sub-polar North Atlantic (Bauch & Kandiano 2007; Van Nieuwenhove et al. 2011). The delayed optimal interglacial conditions in the Nordic Seas were probably a result of a prolonged deglaciation at the start of MIS 5 causing a reduced AMOC. The warming of the Nordic Seas probably occurred after the AMOC strengthened and allowed enhanced northward heat transportation in the surface and near-surface ocean (Van Nieuwenhove et al. 2011; Bauch et al. 2012).

Millennial-scale climate fluctuations, similar to D/O events observed during the last glacial, were also observed in various marine sediment cores during the MIS 5e (Fronval et al. 1998; Oppo et al. 2006; Müller & Kukla 2004; Mokeddem et al. 2014). The most complete series of the MIS 5e cooling events were found in the in Iceland and Norwegians Seas (Fronval et al. 1998) and the North Atlantic (Oppo et al. 2006; Bauch

et al. 2012; Mokeddem et al. 2014), but single events could also be identified elsewhere. During these surface cooling events (C28–C26), IRD signals were present but were not as strong as during their glacial counterparts and were primarily identified by planktonic $\delta^{18}O$ and foraminiferal abundances changes (Fronval et al. 1998; Oppo et al. 2006; Mokeddem et al. 2014). The majority of these surface cooling events were also related to the reduction of deep-ocean ventilation, indicating a weakened AMOC (Müller & Kukla 2004; Oppo et al. 2006).

1.3. Chronology

In palaeoclimatology the development of reliable age-models for past climate records is absolutely fundamental. Without a sound chronology it is not possible to raise conclusions of the duration and/or the frequency of certain climate fluctuations. Besides absolute ages, as derived from radiocarbon dating, tuning (e.g. orbital-tuning) is a common method to obtain age control. However, one drawback of this technique is the assumption of synchronicity of climate events over a wide areas which can potentially lead to circuit reasoning (Blaauw 2012). Therefore, tephra isochrones, i.e. volcanic glass derived from a single volcanic eruption and simultaneously deposited over a wide area and/or in different realms, became the focus of palaeoclimatologists over the last decades. Even though these tephra deposits do not necessarily provided an absolute age, they can be used to test the synchronicity of certain climate events as well as the accuracy of assigned age-models.

The quality of an age-model depends on various factors, including the availability of dating material, resolution of the records and uncertainties of the dating methods applied. These uncertainties are of particular importance for age-models based on benthic foraminiferal $\delta^{18}O$ stacks, such as LRO4 (Lisiecki & Raymo 2005). This age-model uses benthic $\delta^{18}O$ records as a proxy for global ice-volume, which allows marine records to be aligned to a common global timescale. There are several issues with this method, such as asynchronous changes of $\delta^{18}O$ across the ocean basins and local hydrological effects, which undermine the reliability of the benthic $\delta^{18}O$ stratigraphy on

sub-orbital timescales and particularly through glacial terminations; these can potentially lead to timescale uncertainties of several thousands of years (Lisiecki & Raymo 2005; Skinner & Shackleton 2005; Skinner & Shackleton 2006).

Another common method to create an age-model for marine records in the North Atlantic region is tuning of the surface proxies to the $\delta^{18}O$ records of Greenland ice cores. This approach assumes that the SST in the North Atlantic (recorded in the surface proxies) and the air temperatures (recorded in the $\delta^{18}O$) over the GIS changed synchronously (Bond et al. 1993; Shackleton et al. 2000). Annual layering in these ice cores provides the potential to date the records quite precisely. However, only one of the three available GIS timescales is solely based on annual layer counts: the GICC05 age-model. This model has defined age error estimates, in contrast to the ss09 timescale, but only continues back to 60 ka (Andersen et al. 2006; Rasmussen et al. 2006; Svensson et al. 2006; Vinther et al. 2006). The ss09 timescale is a combination of annual layer counts and modelling which covers the last 123 ka (Johnsen et al. 2001; NGRIP Members 2004). Due to the increased interest in the LIG, the NEEM ice core was subsequently drilled and the first chronology was published by Rasmussen et al. (2013). This GICC05modelext-NEEM-1, covering the last 122 ka b2k, is based on the alignment of the GICC05 counted model as well as its extension (GICC05modelext). Until now, no annual layer counts are available for the NEEM ice core and the disturbed ice structure of the Eemian section poses a significant challenge to this goal (Rasmussen et al. 2013).

Tuning marine surface proxies (e.g. *N. pachyderma* (s)) to the Antarctic methane record is a potential method to obtain age-control prior to Termination II (Hibbert et al. 2010). This method assumes that changes in methane concentration were synchronous between both hemispheres and therefore creates a link between Antarctica and the synchronous changes of Greenland air temperature and North Atlantic surface temperatures. The observed offset between temperature changes over Antarctica and Greenland on a millennial scale (EPICA Community Members et al. 2006; Blunier et al. 2007) would

lead to synchronisation uncertainty of about 200-800 years (Blunier et al. 2007), which is much smaller than the potential errors related in the tuning to benthic $\delta^{18}O$ stacks. Certain events, present in these climate records, such as the glacial-interglacial transition (Termination) or rapid warming events during D/O cycles, are used to gain age control for palaeorecords. These event-ages from the chosen timescale (e.g. GICC05, SPEMAP or LR04) can then be transferred to the target record and age-depth control is usually gained by linear interpolation between two tie-points/events.

1.3.1. MIS 5e Chronology

As highlighted above, numerous glacial-interglacial cycles are often recorded in marine sediment cores from the deep sea. These fluctuations in global ice-volume are reflected in the benthic foraminiferal $\delta^{18}O$ ratios (Shackleton 1969; Pisias et al. 1984), which were used to build the marine isotope stratigraphy (Emiliani 1955; Emiliani 1966; Shackleton & Opdyke 1973). Whereas Emiliani 1955 used uranium-series dating of the sediment to create an absolute timescale for MIS 5, Broecker & van Donk (1970b) and Martinson et al. (1987) used radiometric dated marine coral terraces and astronomical tuning, respectively (Shackleton et al. 2002).

Nowadays, it is widely considered that Emiliani's dating method does not provide results of the necessary precision and accuracy (Shackleton et al. 2002). Even though Martinson's approach yielded lower average errors than Broecker & van Donk (1970b), ±5,000 years compared to ±6,000 years at that time, improvements in thermal ionization mass spectrometry (TIMS) could reduce errors of the U-Series dating of coral reef carbonates from raised marine terraces to 1,000 years (Kukla et al. 2002; Shackleton et al. 2002). However, Thompson & Goldstein (2006) showed that orbitally tuned foraminiferal $\delta^{18}O$ stacks from the SPECMAP age-model of Martinson et al. (1987) are in good agreement[1] with their own independent U/Th ages, except for the last glacial maximum and MIS 7/6 transition. Another age model, LR04, is based on orbitally tuned

[1] average difference is 1.3 ka (Thompson & Goldstein 2006)

benthic $\delta^{18}O$ stacks which is tied to additional ages derived from ^{14}C dates obtained from the component $\delta^{18}O$ benthic records, GRIP-ice core ages and U/Th ages for Termination II for the first 130 000 years (Lisiecki & Raymo 2005).

For MIS 5e, Shackleton et al. (2002; 2003) developed a stratigraphy based on foraminiferal benthic $\delta^{18}O$ from marine sediment core MD95-2042, Iberian Margin. On this timescale, MIS 5e started at 132 ka and ended at 115 ka (Shackleton et al. 2002). They defined a benthic $\delta^{18}O$ plateau, beyond which benthic $\delta^{18}O$ values become more positive (Shackleton et al. 2003) and defined the start and end of this plateau from 128 ± 1 ka to 116.1 ± 0.9 ka, respectively (Stirling et al. 1998; Shackleton et al. 2003). These ages are derived from U/Th dated corals from Western Australia to define the MIS 5e plateau, assuming the synchronicity of the sea-level highstand between both hemispheres and its direct imprint upon the benthic $\delta^{18}O$ record.

1.3.2. Tephrochronology

In contrast to the chronology described above and dating tools such as ^{14}C-dating, tephrochronology does not necessarily provide absolute ages, but instead offers the potential to test correlations between records from different environments and in particular the synchronicity of climate changes over a wide area, such as the North Atlantic (Turney et al. 2004; Davies et al. 2004; Abbott et al. 2011). Thus, tephrochronology is a very important tool in palaeoclimatology, especially when dealing with long records, because the range and uncertainty of many dating methods is increasingly limited back in time e.g. the limit for radiocarbon dating is about 50,000 BP (Reimer et al. 2009). Therefore, the geochronology constraints for marine sediment records covering the penultimate glacial–interglacial cycle are rather limited. Establishing a regional tephrochronology over different realms allows for both, the correlation of records across the North Atlantic region and for the testing of the synchronisation of climate events without absolute age-control.

Iceland is one of the world's most active volcanic regions and produced the majority of tephra layers composing the tephrostratigraphical framework for the North Atlantic area (Hafliðason et al. 2000). One of the most widely distributed ash layers is the Vedde Ash which is thought to originate from the Katla volcano system in South Iceland. The Vedde Ash is found in terrestrial records all over Europe (Turney et al. 1997; Sandgren et al. 1999; Wastegård et al. 2000; Schoning et al. 2001; Davies et al. 2005; Blockley et al. 2007), is also present in Greenland ice cores (Grönvold et al. 1995; Mortensen et al. 2005) and marine sediment cores (Ruddiman & Glover 1972; Mangerud et al. 1984; Kvamme et al. 1989; Austin et al. 1995; Peters et al. 2010). Tephra layers with a potential as isochronous markers and tephra used in IRD provenance studies can be distinguished by certain characteristics which are inherent to their transport mechanisms to the marine environment.

The main transport mechanism of tephra, and the only way to deposit Icelandic tephra over a wide geographical region, is by wind and atmospheric deposition. During an eruption the volcanic material is ejected into the atmosphere and transported by the prevailing wind. Due to gravity effects the larger particles fall out earlier and only very fine material will tend to be transported to distant regions, resulting in the often observed decrease in shard size with distance from the source volcano (Sparks et al. 1981). These so-called primary air-fall tephra layers are considered to be instantaneously deposited (Turney et al. 2006; Brendryen et al. 2010). Therefore, when the same tephra layer is found in different realms, such as ice cores and ocean sediments, these isochrons offer the potential to test the synchronicity of rapid and abrupt climate transitions, such as D/O warming events. In the marine environment, tephra can be deposited by secondary transport mechanisms, such as sea-ice-rafting and iceberg-rafting. These two transport mechanisms have a major role in the North Atlantic during glacial periods, when extensive sea-ice coverage was present and ice-sheet calving margins characterised the region. When tephra falls out of the air column on to sea-ice instead of land, the tephra will be transported by sea-ice-rafting until the sea-ice melts and it then becomes a secondary deposit on the sea-floor. The time delay between

the eruption and the final deposition is thought to be months or years (Brendryen et al. 2010).

	Primary air-fallen tephra deposit	Sea-ice-rafted tephra deposit	Iceberg-rafted tephra deposit
Geochemical population of the tephra deposit	Homogeneous (single geochemical population)	Homogeneous (single geochemical population)	Heterogeneous (multiple geochemical populations)
Covariant with IRD concentration	No	No	Yes
Shard size distribution[1]	Well-sorted	Well-sorted	Poorly-sorted
Time from eruption until deposit	Instantaneously	Instantaneously	100's of years
Potential use as	Isochron in Tephrochronology	Isochron in Tephrochronology	Ice-rafted-debris provenance indicator

Table 1.1: Characteristics of the three different types of tephra deposits based on Lackschewitz & Wallrabe-Adams (1997), Austin et al. (2004) and Brendryen et al. (2010).

Sea-ice-rafted tephra and primary air-fall tephra have in theory, many characteristics in common. Shards transported by these processes should have a very similar geochemical composition, reflecting a single or several eruptions close in time from a single volcanic system (Brendryen et al. 2010). The second attribute is a well-sorted shard size distribution which is caused by the gravity related processes described by Sparks et al. (1981). Even though the deposition of sea-ice-rafted tephra is not an instantaneous process, they can still be very useful marine marker horizons. In contrast, iceberg-rafted tephra deposits are characterised by a mixed geochemical population and their abundance co-vary with the abundance of IRD (Lackschewitz & Wallrabe-Adams 1997; Austin et al. 2004; Brendryen et al. 2010) and have a poorly-sorted shard size distribution (Lackschewitz & Wallrabe-Adams 1997; Austin et al. 2004). Iceberg-rafting can, of course, potentially lead to a lag of hundreds of years between the actual eruption event and deposition on the sea-floor and caution must always be applied in the use of such markers as truly isochronous (Brendryen et al. 2010).

[1] The degree of sorting can potentially be influenced by secondary depositional processes such as bottom currents.

1.4. Aims and Objectives

The focus of the presented thesis is the application of tephra related analyses in palaeoceanography as a tool for reconstruction of the climate during the penultimate glacial-interglacial cycle. Tephra have become an established regional indicator of IRD provenances in the North Atlantic and are widely used as isochronous markers. Their use as a tracer of potential IRD source regions provides an insight into the dynamics of the corresponding ice-sheet and/or hydrographic processes controlling the IRD delivery. Therefore, iceberg-rafted tephra deposited during the MIS 6 could help to estimate the expansion of the IIS, i.e. if the IIS had active marine-terminating calving margins and to evaluate potential surface ocean circulation pattern during the penultimate glacial. The application of tephra as a chronological tool offers the opportunity to test assigned age-models and to identify potential lags or leads of certain climate (proxy) events. During the MIS 5e several sediment cores recorded a delayed onset of 'fully'-interglacial deep-ocean ventilation. The identification of the widespread tephra isochron 5e-Eem/RHY-I in further high-resolution marine sediment cores from the North Atlantic could not only test the synchronicity of 'fully'-interglacial deep-ocean circulation, but also the validation of assigned age-models of these marine records. In turn these findings might help to improve the chronostratigraphy of the MIS 5e in the North Atlantic. In order to address these main objectives tephra deposited from the penultimate glacial-interglacial section of the marine sediment core U1304 was identified and on the basis of detailed geochemical and shard size analyses of tephra amongst other aspects, the following key research questions have been addressed in this thesis:

Q1: How extensive was the IIS during MIS 6, and did the IIS have active marine-terminating calving margins during that period?

Q2: What were the characteristics of the North Atlantic's surface ocean circulation pattern during MIS 6 and how did it compare to the pattern for the Last Glacial described in the literature?

Q3: Can the widespread tephra isochron 5e-Eem/RHY-I be reliably identified in the MIS 5e section of marine sediment core U1304? If so, can it be used to improve the chronostratigraphy of MIS 5e in the North Atlantic?

Q4: Did the delayed onset of 'fully'-interglacial deep-ocean ventilation in MIS 5e observed in North Atlantic sediment records occur as a synchronous event?

1.5. Thesis Structure

Chapter 1 gives a general introduction to the background and context of the topics relevant to this thesis. The materials and methods used for analyses presented in this thesis are described in detail in Chapter 2. In Chapter 3, the work related to answering the key research questions Q1 and Q2 are discussed; while Chapter 4 addresses the research questions Q3 and Q4. A summary and outlook are given in Chapter 5. All the necessary supplementary data are provided in the appendices.

CHAPTER 2 Material and Methods

2.1. Regional Setting

The 244 m long U1304 record was collected during Expedition 303 of the IODP in 2004 and was recovered from a water depth of 3082 m on the eastern flank of the Reykjanes Ridge on the southern Gardar Drift (Lat 53°03'N, Long 33°32' W), within the sub-polar North Atlantic (Figure 2.1) (Expedition 303 Scientists 2006b; Hodell et al. 2009). The U1304 Site was chosen with the aim to recover a high resolution record which not only captured changes in the North Atlantic Deep Water (NADW) and sea surface temperature (SST) but also changes in the input of ice-rafted debris (IRD) into the Central North Atlantic (Expedition 303 Scientists 2006b).

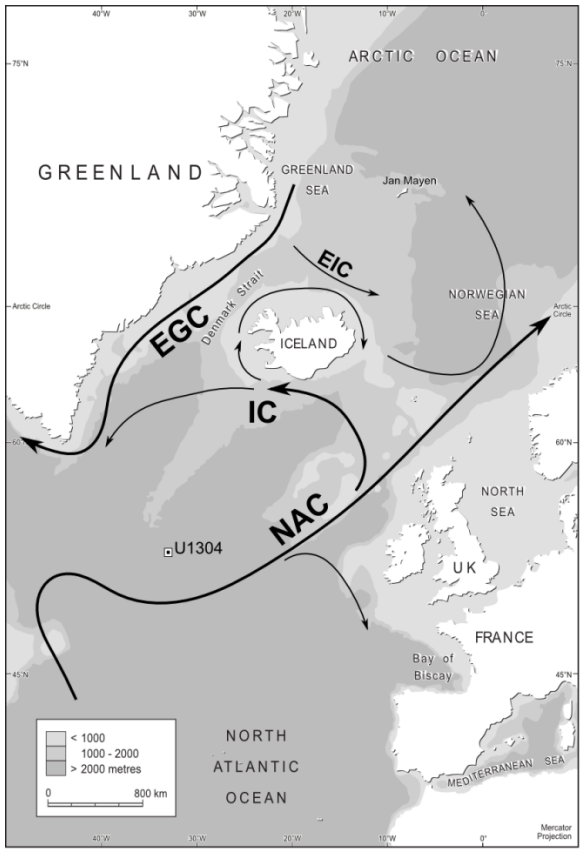

Figure 2.1: Location of IODP Site U1304 sediment core from the Gardar Drift, North Atlantic. Modern surface ocean circulation after Fratantoni (2001) and Ran et al. (2011). EGC: East Greenland Current, EIC: East Iceland Current, IC: Irminger Current, NAC: North Atlantic Current.

Today, the North Atlantic Current (NAC) passes over the core site and transports warm surface water north-eastwards to the Nordic Sea (Figure 2.1). Iceland-Scotland Overflows (ISO) mix with overlying Labrador Sea Water (LSW) travelling south-westwards and represent the dominant water body at this site today (Bianchi & McCave 2000; Hodell et al. 2009). During glacial periods, Southern Sourced Waters (SSW) dominated depths below 2000 meters and Glacial North Atlantic Intermediate Waters (GNAIW) dominated the upper water column (Hodell 2009).

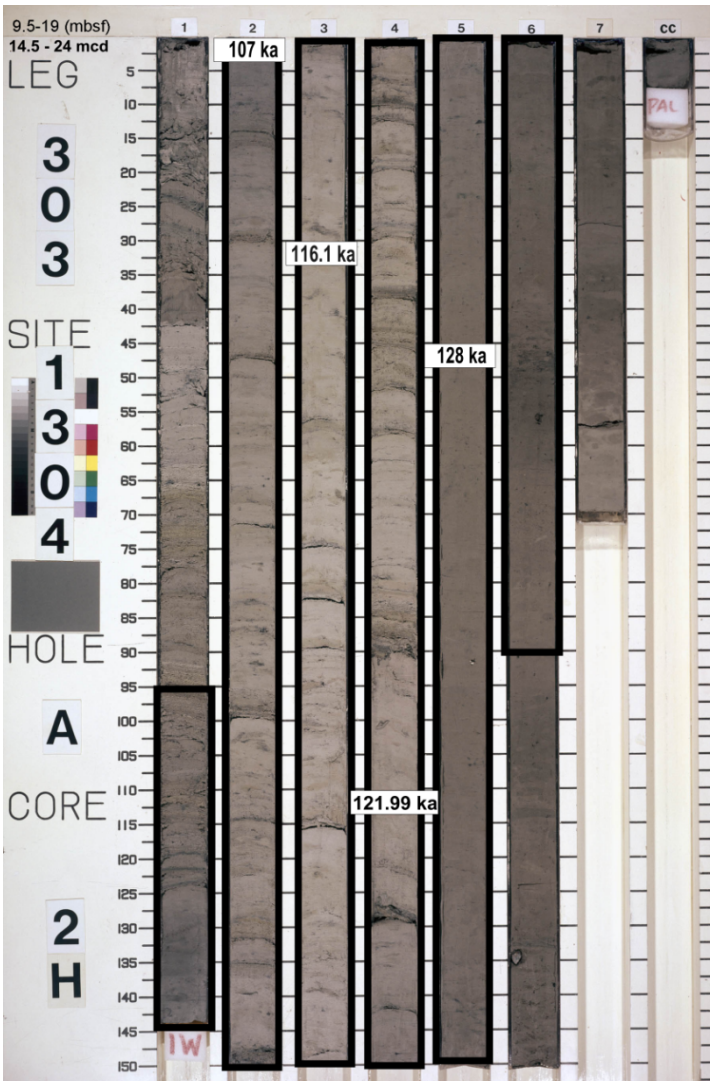

Figure 2.2: Core photograph of 1304-A-2H (Expedition 303 Scientists 2006b). Positioning of stratigarphical tie-points used in this study are marked: MIS 5e benthic $\delta^{18}O$ plateau (128 – 116ka), C24 (107 ka) and the 5e-Eem/EHY-I (121.99ka). The interval studied is marked by the rectangle.

The sediments core U1304 comprise interbedded diatom and nannofossil oozes (Expedition 303 Scientists 2006b; Mazaud et al. 2009). Deposits from the MIS 6 interval are dominated by nannofossil oozes with grey clay and moderate to high bioturbation (Expedition 303 Scientists 2006b) (Figure 2.2 & 2.3). Termination II (22.5 meter composite depth (mcd)) is marked by a peak in IRD concentration and around zero weight % $CaCO_3$ (Figure 2.4). During MIS 5e and MIS 5d laminated diatom oozes and mats become common, inhibiting bioturbation, yielding an undisturbed, high resolution record (sedimentation rate 40 cm/ka) for the MIS 5e (Hodell et al. 2009).

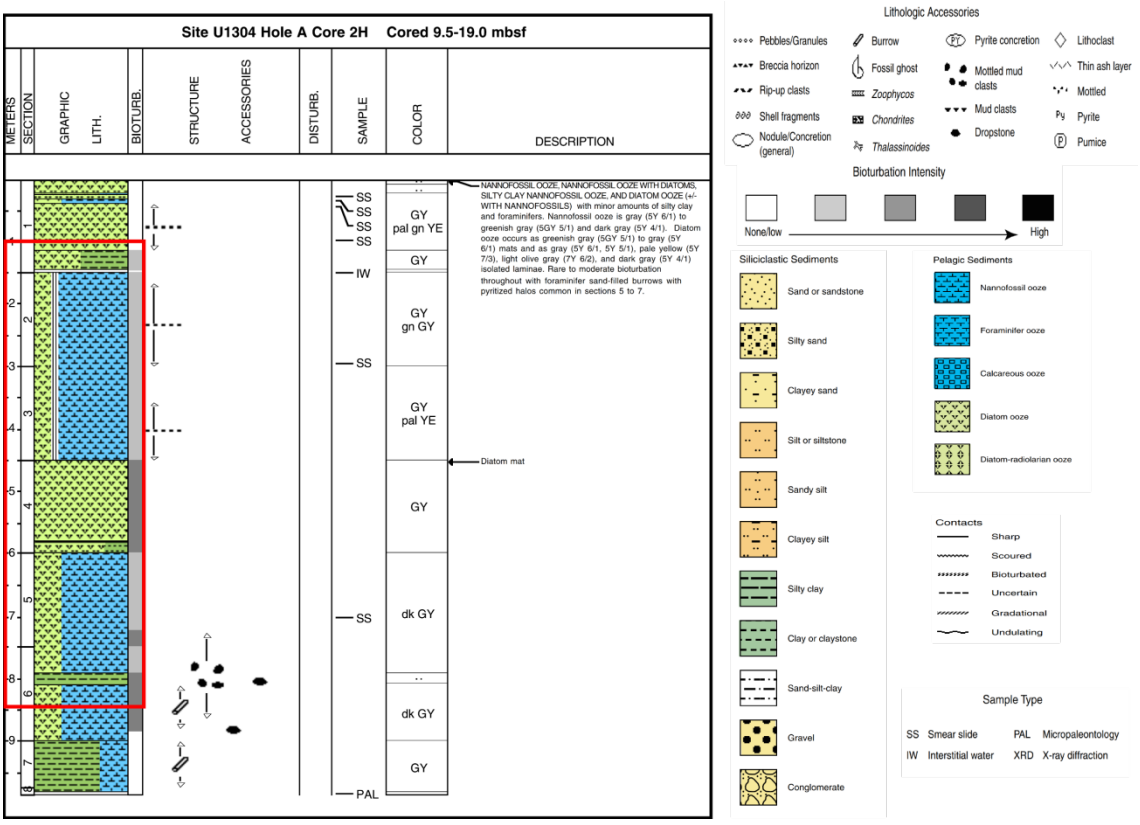

Figure 2.3: Visual description of the core 1304-A-2H (Expedition 303 Scientists 2006b). Interval studied is indicated by the red rectangle.

The age-model for the interval 15.47 mcd to 24.52 mcd of the marine core U1304 was created by Hodell et al. (2009) and is based on tuning to MD09-2042 benthic $\delta^{18}O$

records, itself anchored to the radiometric timescale for the last interglacial period created by Shackleton et al. (2003) (Figure 2.4). Hodell et al. (2009) determined the MIS 5e plateau (Figure 2.4), a period of low and relative constant benthic foraminiferal $\delta^{18}O$ values, between 22.6 mcd and 17.7 mcd, which corresponds to an interval from 128 ka to 116 ka, respectively (Shackleton et al. 2003) (Figure 2.4). A further tie-point was used at 16.07 mcd, where a peak in planktonic $\delta^{18}O$ values in MIS 5d represents the C 24 (Figure 2.4) (McManus et al. 1994). McManus et al. (1994) and Rousseau et al. (2006) used the Greenland ice core tuning of surface proxies (planktonic $\delta^{18}O$, *Neogloboquadrina pachyderma* sinistral (*Np* (s)) and IRD percentage to determine the age of this event to be 107 ka. For the purpose of this study these published alignments have been used to constrain the timing of records produced.

More information about the site location, detailed description of the stratigraphy and isotope data is published by Expedition 303 Scientists (2006a), Hodell et al. (2009) and Mazaud et al. (2009).

Professor D.A. Hodell (University of Cambridge) kindly provided the sample residues, which were used in this study. These same samples were previously used for the study at this site (see Hodell et al. 2009). These residues had been prepared from sub-samples of the core taken at 5 cm intervals with a sample depth of 2 cm between 24.52 - 15.47 mcd. After processing (i.e. freeze drying, weighing and sieving), stable isotope analyses as well as faunal counts were carried out, which are presented in detail by Hodell et al. (2009). Only methods which were used in this study are described in detail hereafter.

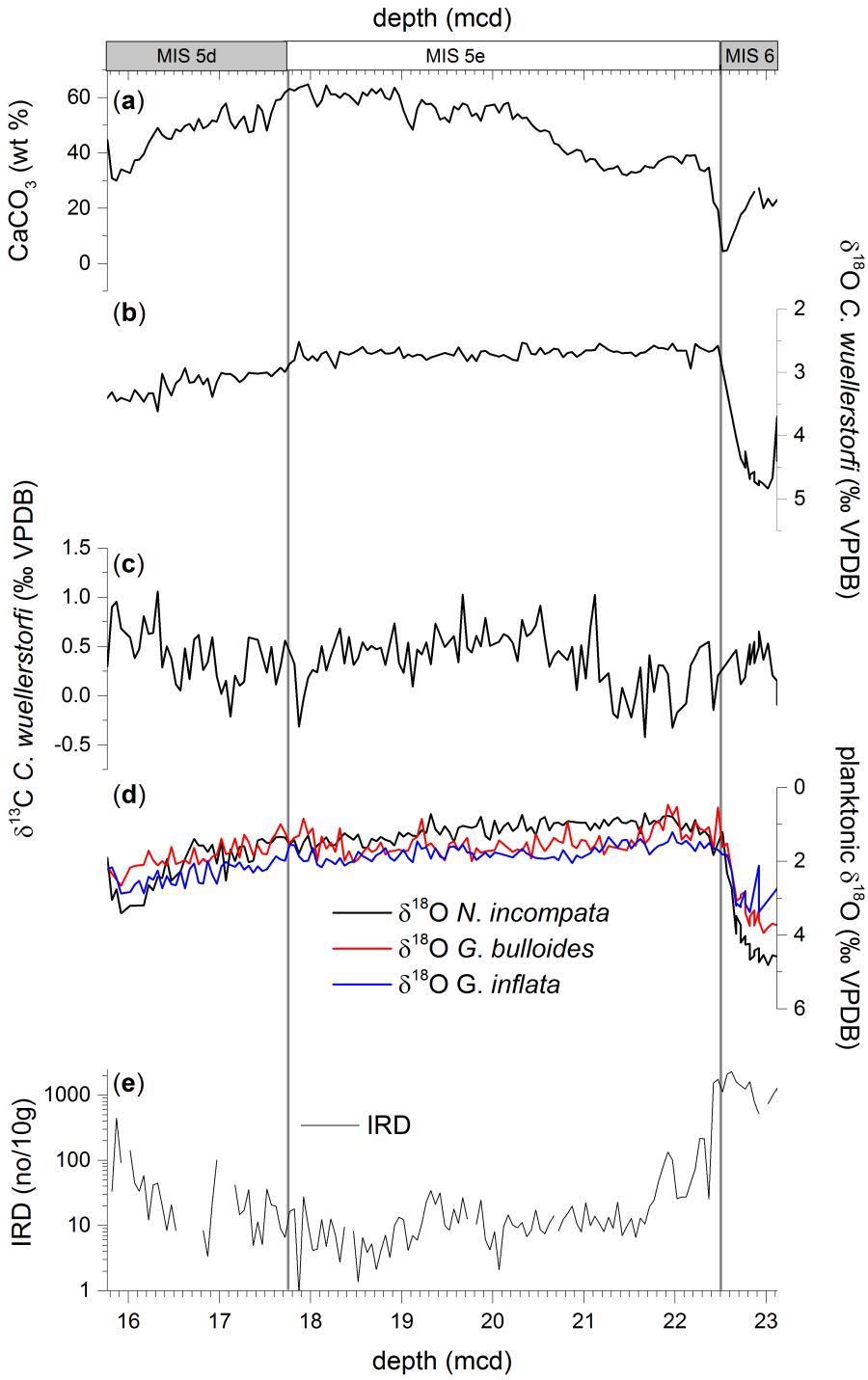

Figure 2.4: Stratigraphical framework for IODP Site U1304 based on Hodell et al. (2009). (**a**) $CaCO_3$wt%, (**b**) benthic $\delta^{18}O$ *C. wuellerstorfi*, (**c**): benthic $\delta^{13}C$ *C. wuellerstorfi*, (**d**) planktonic $\delta^{18}O$, *N. incompata* (black), *G. bulloides* (red), *G. inflata* (blue), (**e**) IRD concentration (log-scale).

2.2. Quantitative Analyses

An initial quantitative analysis (>150 µm sieved fraction) of tephra shards, lithic grains, *N. pachyderma* (s) and the sum of all other planktonic foraminifera species was performed. With the aid of a microsplitter, the samples were halved n times until the residue evenly covered a 42-cell gridded picking tray. Under a stereomicroscope the four components were counted for a representative fraction of the sample, i.e. until ≥ 300 planktonic foraminifera specimens (i.e. combined values of *N. pachyderma* (s) and others foraminifera species) were observed. The results were expressed as *N. pachyderma* (s) percentages, grain and shard numbers per g dry sediment. All these measurements were recorded against meter composite depth (mcd).

$$\text{Total number grains in the split} = \frac{\text{total number grains counted}}{\text{numbers of square counted}} \text{ x } 42 \qquad (1)$$

where *42* is the number of cells in the picking tray.

$$\text{Total number of grains within sample} = \text{total number grains in split} \times n \qquad (2)$$

where n is the number of splits.

$$\text{Concentration (grains/g)} = \frac{\text{total number of grains in sample}}{\text{dry weight of sediments processed}} \qquad (3)$$

$$Np\text{ (s) \%} = \frac{\text{total number of } Np \text{ (s) in sample}}{\text{total number of planktonic species counted in sample}} \times 100 \qquad (4)$$

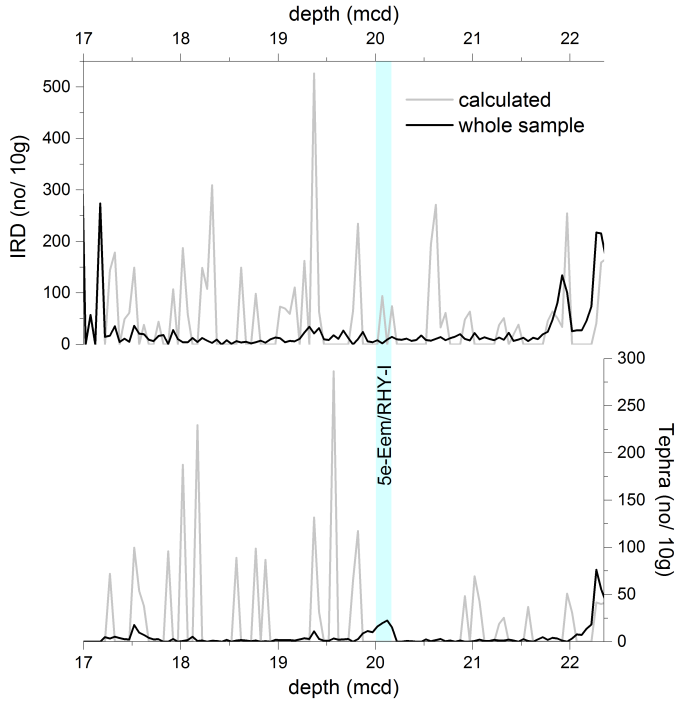

Figure 2.5: IRD grains and Tephra shards (no/10g) versus depth. Comparing IRD (upper panel) and tephra (lower panel) concentrations based on two different counting methods. **Calculated**: Only a fraction of each sample was counted (until reaching ≥ 300 planktonic foraminifera specimens). **Whole sample**: *all* IRD grains and tephra shards found in each sample were counted. This method was only used in the interval 17.22 – 22.32 mcd. Position of 5e-Eem/RHY-I isochron is highlighted in light blue.

While dealing with high volume samples (glacial), the method for determination of the grain/shard concentration described above yields good estimates. However, this method leads to less representative results when the samples are smaller (e.g. interglacial periods when IRD concentrations were very low and lithic grains occur only sporadically). It is likely that the heterogeneous mixing of samples' different components during the process of splitting will result in difference in the calculated concentration based on lithic/ tephra counts and the analysis of the whole sample, i.e. counting *all* IRD and tephra shards found in the entire sample (Figure 2.5). Therefore, for the interval 17.22 – 22.32 mcd all lithic grains and tephra shards which could be found in the whole sample were counted (Figure 2.5 & 2.6). Based on these counts the concentration given in grains/shards per gram are calculated (Equation 3). Note that the

whole count method yields at about 20 mcd a clear peak in tephra concentration which is independent of the IRD concentration, this relation is of importance for interpreting tephra transport mechanism.

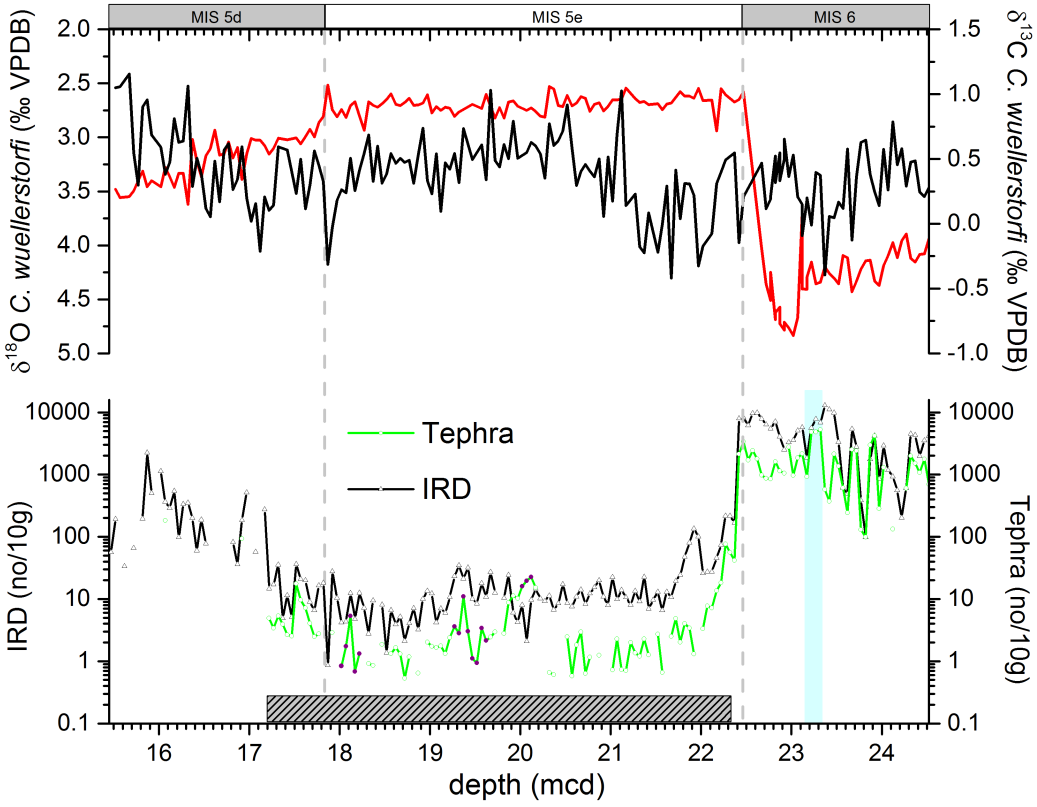

Figure 2.6: Overview of the U1304 core over the depth range analysed in this thesis. The light blue area (Chapter 3) and purple dots (Chapter 4) indicate depths for which detailed tephra analyses (geochemical and shard size) have been perfomed. The hatched box shows the depths interval for which the whole tephra and IRD count has been performed.

2.3. IRD Lithology, Tephra Composition and Morphology

Tephra shards were classified by colour into rhyolitic or basaltic shards, colourless or brown, respectively. Initially the lithic grains were grouped into five components: quartz, haematite-stained grains, detrital carbonate, basaltic and undifferentiated grains (labelled as nID). During the whole sample counting for the interval 17.22 – 22.32 mcd the additional classification of four lithological components was introduced: coarse crystalline grains, mica, pumice and hornblende.

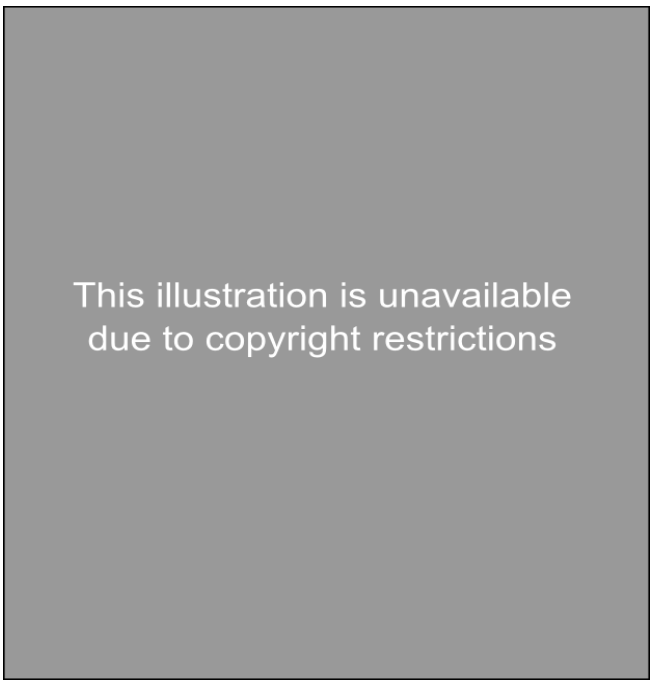

Figure 2.7: This illustration is unavailable due to copyright restrictions

During initial quantitative analyses a horizon (23.32 mcd- 23.17 mcd) of high tephra concentration was identified, which was chosen to be the focus of the detailed analyses for the MIS 6. The tephra shards from these four samples (23.32 mcd, 23.27 mcd, 23.22 mcd, 23.17 mcd) recovered from the penultimate glacial section of the U1304 (Chapter 3) were grouped on the basis of the close morphological analysis under the stereomicroscope. ---------- This material is unavailable due to copyright restrictions. ----------.

2.4. Tephra Geochemistry

The geochemical analyses of tephra horizons found in the record from IODP Site 1304 were undertaken at the Tephrochronology Analytical Unit (TAU) at the Grant Institute, University of Edinburgh and Facility for Earth & Environmental Analysis (FEEA) at the University of St Andrews. For these analyses the tephra shards (> 150 µm) were picked using a stereomicroscope, stuck on double-side tape and embedded in epoxy resin (Araldite® (AY103-1/HY991)) on 28 mm diameter moulds. This mounting method was used for the electron microprobe analyses (EMPA) conducted in June 2011 (EMPA 2) at FEEA and in May/June 2012 (EMPA 3 & 4) at TAU. For the sample preparations for the analyses at TAU in October 2010 (EMPA 1), the mounting procedure described by Steele & Engwell (2009) was followed, with the difference that aluminium silicate powder and Araldite® were used for frosting and gluing, respectively. After mounting the slides/discs were ground, polished and carbon-coated. These tephra preparations were carried out by M. Kuhs with assistance and help from Andrews Mackie (University of St Andrews), Donald Herd (University of St Andrews), Chris Hayward (TAU, University of Edinburgh) and Dr Peter Abbott (University of Swansea). The tephra shards found in the MIS 5e interval of the U1304 record have a high vesicular morphology with very thin walls, which requires a very precisely executed preparation. For this reason, the sample preparation of tephra shards for the electron microprobe analyses in March 2015 (EMPA 5) was undertaken by Mike Hall at TAU (University of Edinburgh).

At TAU the major and minor elements were determined by of a wavelength dispersive spectrometer (WDS) electron microprobe (Cameca SX100). An accelerating voltage of 15 kV, a beam diameter of 5 microns, an initial beam current of 2 nA (to reduce Na loss) and later a beam current of 80 nA were applied (Hayward 2012). At FEEA the WDS electron microprobe (JEOL JXA 800) was operated with the following settings: accelerating voltage of 15 kV, a beam current of 10 nA and a beam size of 5 microns. For the primary calibrations of both WDS electron microprobes a series of synthetic

oxides, pure metals and minerals was used (Table 6.1 in Appendix A). Lipari was used as secondary standard for rhyolitic glass during all EMPA. The secondary standards for basaltic glass were BHVO-2G (EMPA 1, 2, 5) and BCR-2G (3, 4, 5). The results are expressed as oxide weight percentages after normalisation to 100 % and are presented on an anhydrous basis. During EMPA 2 at FEEA up to five analyses per tephra shard were carried out. The mean of these different measurements, which was calculated after removing outliers and inclusions, was used for further analyses.

2.5. Shard Size Analyses

By means of a reticule on a stereomicroscope the maximum grain size of the tephra shards (> 150 µm fraction) was measured in order to gain an understanding of shard size distribution. However, it is important to highlight that shard size analyses can be influenced by the shape of the shard, i.e. elongated shards can pass through a 150 µm sieve, even though their maximum diameter is > 150 µm. The results are presented in frequency plots and the median ($Md_\varphi=\varphi_{50}$), mode, standard deviation (σ_φ) and skewness α_φ were calculated. In sedimentology it is common to quote the grain size in φ:

$$\varphi = -\log_2 r \tag{5}$$

where r is the grain size diameter in mm. For easier use of grain size equations and comparison with published data, the tephra shard sizes were transformed into φ; σ_φ and α_φ were derived by the following equations (Sparks et al. 1981):

$$\sigma_\varphi = {}^1\!/_2\,(\varphi_{84} - \varphi_{16}), \tag{6}$$

$$\alpha_\varphi = \frac{{}^1\!/_2\,(\varphi_{84} + \varphi_{16}) - Md_\varphi}{\sigma_\varphi} \tag{7}$$

However, the shard size analyses were only carried out on tephra shards found in sample depths where tephra shards were also geochemically analysed.

- Chapter 3 (Glacial): for each of the samples geochemically analysed (23.32 mcd, 23.27 mcd, 23.22 mcd and 23.17 mcd), the maximum dimension of at least 300 basaltic shards was randomly measured.
- Chapter 4 (Interglacial): every shard (rhyolitic as well as basaltic) found in the intervals, 20.17-19.92 mcd, 19.62-19.27 mcd, 18.22-18.02 mcd, was measured for sizes prior to the geochemical analyses. The total shard number found in the interglacial samples is quite low (varies between 2 to 23 shards per sample), therefore the calculated shard size distribution for this interval might not be significant.

2.6. Statistical Tests

In order to identify similarities between different geochemical populations, to test the accuracy (see Appendix A) of the two different WDS systems and to evaluate whether the two datasets from EMPA 1 and EMPA 2 could be merged, the following two statistical tests were used. The similarity coefficient (Borchardt et al. 1972) gives the similarity between two populations and is defined as:

$$d_{(1,2)} = \frac{\sum_{k-1}^{n} R_k}{n} \tag{8}$$

where $d_{(1,2)} = d_{(2,1)}$ is the similarity coefficient between two samples 1 and 2, n is the number of oxides, and R is X_{k1}/X_{k2} if $X_{k2} \geq X_{k1}$ or X_{k2}/X_{k1} if $X_{k1} > X_{k2}$. X_{k1} is the concentration of oxides k in sample 1 and X_{k2} is the concentration of the oxide k in sample 2. Only oxide weight contributions greater than 1% were include in these analyses. Calculated values closer to 1 indicate a higher similarity. (Begét et al. 1992) suggested the following categorisation: Samples with values between 1 and 0.95 are identical; values between 0.95 and 0.90 are not identical but are likely to have the same source; all values below 0.90 indicates that there is no significant relationship between the populations.

The statistical distance function D^2 highlights samples without similarities Perkins et al. (1995), Perkins et al. (1998) and Pearce et al. (2008).

$$D^2 = \sum_{k=1}^{n} (X_{k1} - X_{k2})^2 / (\sigma_{k1}^2 + \sigma_{k2}^2) \quad (9)$$

where n is the number of oxides, X_{k1} and X_{k1} is the average concentration and σ_{k1} and σ_{k2} are the standard deviations of the average of the k-th oxide in the samples 1 and 2. Calculated D^2 values were compared to critical values (Cv) of the 99 % confidence level. If the calculated values were greater than the critical value then the null hypothesis, that the samples are identical, can be rejected. However, smaller values can suggest that a correlation exists, but this is not necessarily the case (Pearce et al. 2008). Therefore, if several populations (POP A, POP B, ...) were tested and the result is as follows:

$$\text{Pop A} = \text{Pop B} \wedge \text{Pop C} = \text{Pop B} \wedge \text{Pop A} \neq \text{Pop C}$$

then, none of these populations were identified as being identical. Only oxides with an average weight percentage greater than 0.1 % were used.

2.7. Secondary Data

2.7.1. Stable Oxygen and Carbon Isotope Measurement of Foraminifera Tests

The use of stable isotopes in aquatic records is based on the concept that foraminiferal carbonate test records the isotopic signature of the surrounding water in which they live. However, the oxygen isotopic signal of foraminifera test is not only depending on the water's isotopic composition but also on the water temperature (Epstein et al. 1951; Epstein et al. 1953; Emiliani 1955) and any vital effects (e.g. Duplessy et al. 1970; Spero et al. 1997). The latter are often a combination of various processes, which can result in 'out- of equilibrium' test calcification. Studies on stable oxygen isotope are

very important tool for reconstructions ice volume changes, palaeotemperature and palaeosalinity, whereas carbon isotopes provide information on changes in productivity of the ancient oceans and the carbon cycle.

In this study the stable oxygen and carbon isotope measurements of three planktonic foraminifera (*Globigerina bulloides*, *Neogloboquadrina incompata* and *Globorotalia inflata*) and one epi-benthic foraminifera (*Cibicidoides wuellerstorfi*) which were published in Hodell et al. (2009) were used. The analyses were carried out by means of a Finnigan-MAT-252-isotope ratio mass spectrometer coupled with a Kiel III carbonate preparation device. The estimated analytical error is better than ± 0.1 ‰ with respect to both ratios and is reported on the Vienna Pee Dee Belemnite (VPDB) scale through NBS-19 standard.

CHAPTER 3 Ice-Rafted Tephra in the Glacial North Atlantic

The reconstruction of ice-sheet processes and ocean surface circulation during Marine Isotope Stage 6 in the North Atlantic.

3.1. Abstract

----------This material is unavailable due to copyright restrictions----------

---

3.2. Introduction

Figure 3.1: This illustration is unavailable due to copyright restrictions

3.2.1. Aims and Objectives

----------This material is unavailable due to copyright restrictions----------

3.3. Material and Methods

----------This material is unavailable due to copyright restrictions----------

---

----------This material is unavailable due to copyright restrictions----------

Figure 3.2: This illustration is unavailable due to copyright restrictions

3.4. Results and Discussion

3.4.1. Geochemical Analyses

----------This material is unavailable due to copyright restrictions----------

Figure 3.3: This illustration is unavailable due to copyright restrictions

Figure 3.4: This illustration is unavailable due to copyright restrictions

3.4.2. Tephra Populations

----------This material is unavailable due to copyright restrictions----------

---

----------This material is unavailable due to copyright restrictions----------

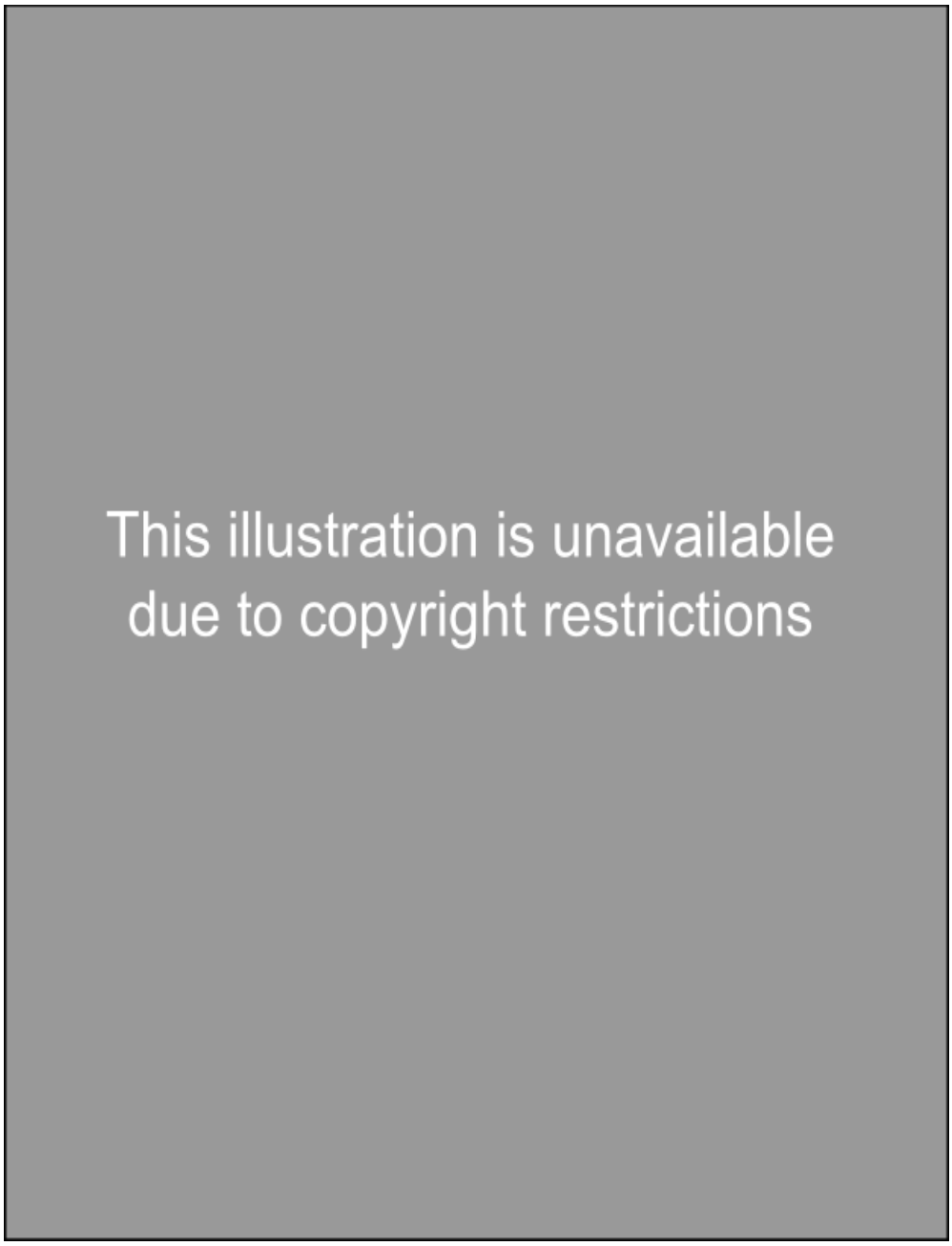

Figure 3.5: This illustration is unavailable due to copyright restrictions

---

---This material is unavailable due to copyright restrictions----------

Figure 3.6: This illustration is unavailable due to copyright restrictions

---

----------This material is unavailable due to copyright restrictions----------

3.4.3. Shard Size Distribution

Figure 3.7: This illustration is unavailable due to copyright restrictions

---

Table 3.1: This table is unavailable due to copyright restrictions

---

----------This material is unavailable due to copyright restrictions----------

3.4.4. Transport Mechanism

----------This material is unavailable due to copyright restrictions----------

Figure 3.8: This illustration is unavailable due to copyright restrictions.

----------This material is unavailable due to copyright restrictions----------

---

----------This material is unavailable due to copyright restrictions----------

Figure 3.9: This illustration is unavailable due to copyright restrictions

---

----------This material is unavailable due to copyright restrictions----------

3.5. Conclusion

----------This material is unavailable due to copyright restrictions----------

---

CHAPTER 4 The Stratigraphic Sub-Division of MIS 5e in the North Atlantic

The 5e-Eem/RHY-I isochron: A marker to improve the stratigraphic sub-division of MIS 5e in the North Atlantic

4.1. Abstract

Climate models developed over the past decades suggest that climate conditions in our future might be similar to the Marine Isotope Stage 5e (MIS 5e) climate. During the MIS 5e annual mean temperature is thought to have been ~1.5°C warmer (Turney & Jones 2010) and global sea-level about six meters higher (Kopp et al. 2009) than currently observed. The identification of synchronous deposited tephra horizon (tephra isochrons) in the North Atlantic region is of high importance because the correlation between different palaeorecords can help us to improve our understanding about the rapidity and variability of a much warmer climate. The widespread 5e-Eem/RHY-I tephra isochron was identified in the MIS 5e interval of the marine sediment core U1304, southern Gadar Drift, North Atlantic. In U1304 the 5e-Eem/RHY-I isochron is found shortly after the delayed onset of fully- interglacial deep-ocean ventilation, which is a basin-wide observed phenomenon in the North Atlantic. The unique position of 5e-Eem/RHY-I does not only provide the opportunity to develop a new event-stratigraphy in the North Atlantic region, but also offers an important link between the North Atlantic and Nordic Sea, which can potentially provide insights into MIS 5e climate fluctuations.

4.2. Introduction

The Last Interglacial (LIG), which is better known in the marine oxygen isotope stratigraphy as MIS 5e, was a period when annual mean temperature is thought to have been ~ 1.5°C warmer (Turney & Jones 2010) and global sea level about six meters higher (Kopp et al. 2009) than the present day. For a long time it was assumed that the

MIS 5e climate was quite stable, until sub-orbital climate fluctuations were first discovered during the last interglacial interval of the Greenland ice cores[1] high-latitude marine sediment cores and subsequently in the mid-latitude records of the North Atlantic. More recently, Galaasen et al. (2014) showed that deep-ocean circulation changes even occurred on a centennial-scale within MIS 5e. Furthermore, it became increasingly evident that the climatic optimum was rather short-lived (~ 10 ka) (Shackleton 1969) and the onset of full-interglacial conditions probably did not occur before the middle of the MIS 5e interval (Sánchez Goñi et al. 1999; Shackleton et al. 2003). With the prospect of an increase of mean annual temperature and higher global sea-levels, MIS 5e has been seen as a potential analogue for certain future climate scenarios and has been the focus of attention across the climatological scientific community. In short to understand the non-anthropological-influenced MIS 5e climate fluctuations might help to evaluate the future dimension of the possible climate fluctuations ahead. If used critically, knowledge of climatic mechanisms in operation during the MIS 5e may help us to understand climatic functioning in an anthropogenically warmed world.

One of the largest challenges in palaeoceanography is to create robust and precise age-models for past climate records, especially when dealing with records continuing beyond the effective radiocarbon dating limit of around 50,000 years, which makes radiocarbon consequently unsuitable for LIG. Age models beyond this dating limit often use astronomical tuning (Martinson et al. 1987; Lisiecki & Raymo 2005), radiometric dating (Stirling et al. 1998; Shackleton et al. 2003), ice layer counting and ice flow modelling (NGRIP Members 2004; Andersen et al. 2006; Parrenin et al. 2007) to obtain their age-control. These ages are assigned to distinctive events, for example, to the rapid warming of D/O cycles as seen in the $\delta^{18}O$ record of the Greenland ice cores. These ice core ages can then be transferred to marine records with the help of wiggle matching

[1] The initially observed rapid climate changes observed in the Greenland Ice Core Project (GRIP) core (GRIP Members 1993) were later identified as an artefact caused by post-deposition processes (Chappellaz et al. 1997; Landais et al. 2004).

between Greenland ice cores $\delta^{18}O$ and marine surface proxies (e.g. Austin & Hibbert 2012). Age estimates at any given depth between two assigned ages/events are often derived by linear interpolation. The fundamental assumption of this (correlation) method is that the events used as tie- (or control) points occurred synchronously in different regions/settings. However, it is known that benthic $\delta^{18}O$ changes can be asynchronous across different ocean basins (Skinner & Shackleton 2005; Lisiecki & Raymo 2009) and are also influenced by other effects, such as the hydrological effect (Skinner & Shackleton 2006), which potentially leads to errors of several thousand years in the global benthic stacks. Thus, over the recent decades the focus of attention in palaeoceanography became the identification of isochronous tephra horizons (Lowe 2011; Davies et al. 2012) which is a method that has the potential to solve many of the problems associated with the assumption of synchrony between palaeoclimate records. Tephra, i.e. volcanic glass which was erupted by a volcano and transported by wind, falls out of the air-column and becomes deposited on sea-ice or the ocean floor. Tephra transported in this way is thought to be deposited instantaneously (Brendryen et al. 2010) across vast areas (e.g. Vedde Ash). This is in contrast to tephra transported by icebergs which may take hundreds of years before it is deposited in the ocean (Brendryen et al. 2010). Although tephra isochrones do not provide absolute ages, their relative ages are very useful to check whether climatic events happened synchronously or not, and test existing age-models (Austin & Hibbert 2012). Hibbert et al. (2010) used the NGRIP $\delta^{18}O$ records (ss09sea timescale) as their tuning target for the surface proxies (*N. pachyderma* (s) % and ITRAX XRF calcium profile) to develop their MD04-2822 age-model from 0ka to 124ka. The presence of North Atlantic Ash Zones (NAAZ) I and II in the Greenland ice core as well as MD04-2822 confirmed their event stratigraphy and tuning (Hibbert et al. 2010).

4.2.1. Aims and Objectives

In this chapter, tephra shards (and ice-rafted debris (IRD)) from the marine sediment core from the Integrated Ocean Drilling Program (IODP) Site U1304 (from here onwards only referred to as: core U1304) are examined. By means of geochemical and

shard size analyses of the tephra shards we identify a known tephra isochron: 5e-Eem/RHY-I. To provide a provisional age estimate for 5e-Eem/RHY-I, the Shackleton MIS 5e age-model (Shackleton et al. 2003; Shackleton et al. 2002) was assigned to U1304 as well as to MD99-2253 (56°21'78N, 27°48.95W, 500 km to the NE of U1304), and additional data was used to estimate sedimentation rate at the core Site U1304 (Figure 4.1). Using the 5e-Eem/RHY-I age of 121.99 ± 1 ka as an additional tie-point shows that the onset of fully- interglacial benthic $\delta^{13}C$ occurred in both cores simultaneously, sub-dividing the MIS 5e in an early and late phase. Based on this new event-stratigraphy we propose sub-division of MIS 5e in: early MIS 5e and late MIS 5e.

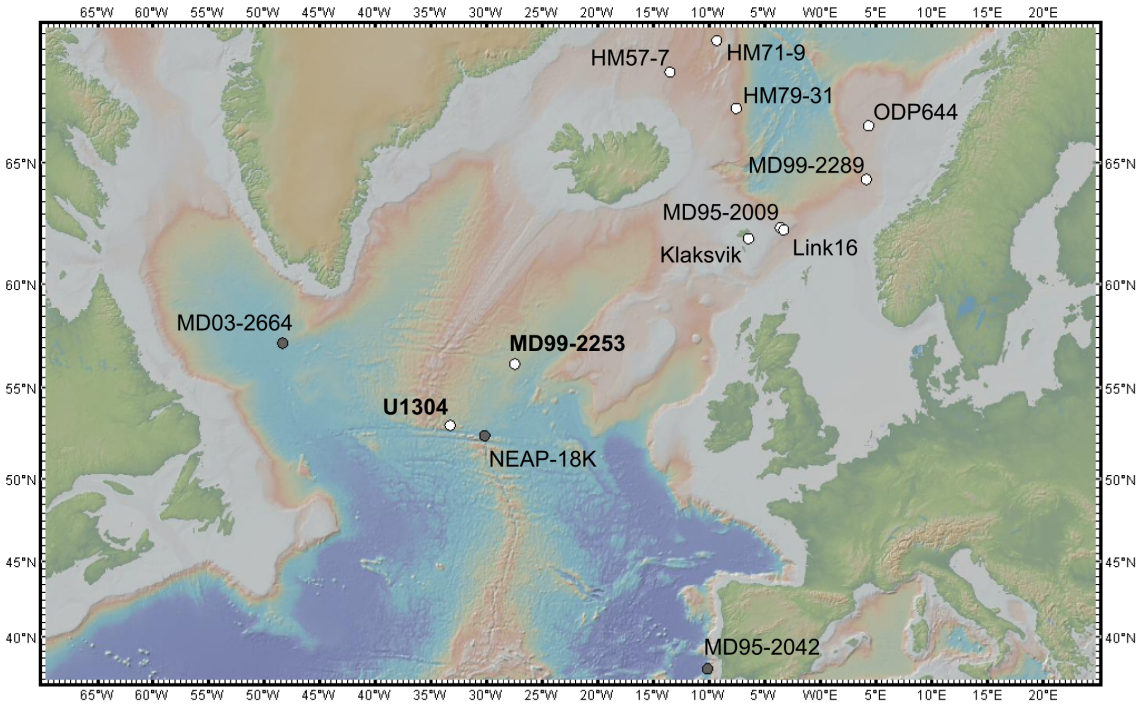

Figure 4.1: Locations of key cores used in this study, U1304 and MD99-2253, and additional cores mentioned in the discussion: **White circle***:* 5e-Eem/RHY-I isochron bearing cores (please refer for reference to Table 4.2). **Bold font**: key cores U1304 see Hodell et al. (2009) and MD99-2253 see Chapman (2012). **Grey circles**: further cores mentioned in the discussion MD03-2664 see Galaasen et al. (2014), NEAP-18K see Hall et al. (1998) and MD95-2042 see Sánchez Goñi et al. (2000) and Shackleton et al. (2003). Map was created with GeoMapApp (Ryan et al. 2009) (http://www.geomapapp.org).

4.3. Material and Methods

Please refer to Chapter 2 (Material and Methods) where all relevant material and methods are discussed.

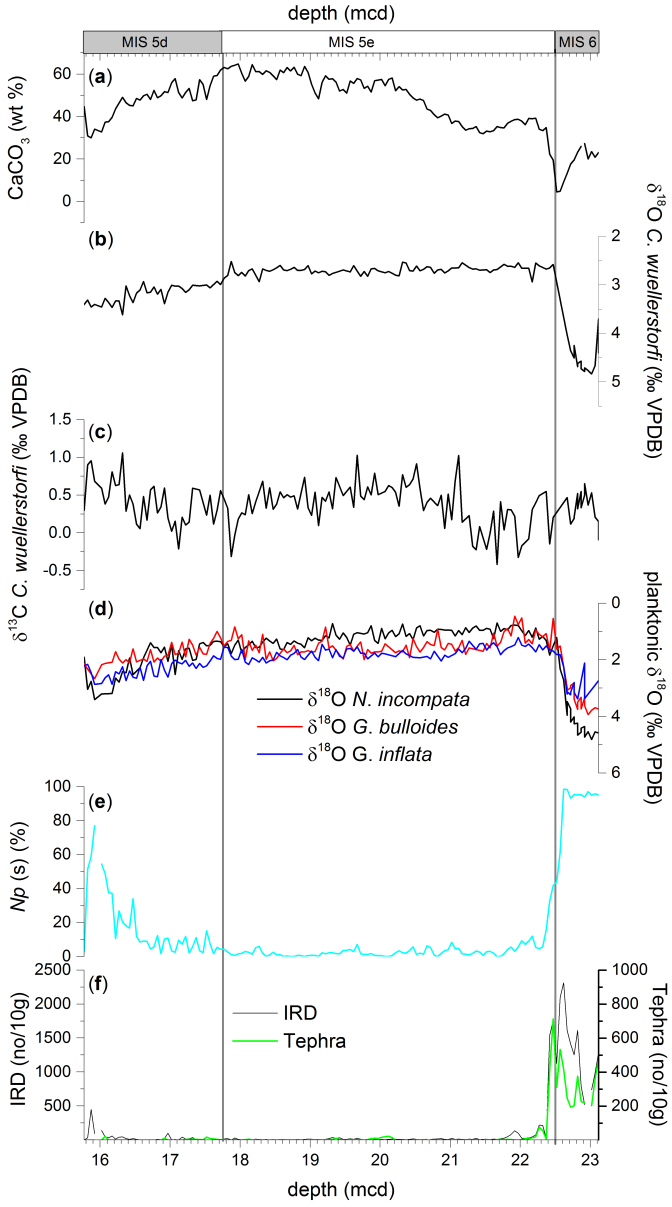

Figure 4.2: Stratigraphical framework for IODP Site U1304 based on Hodell et al. (2009). (**a**) bulk sediment $CaCO_3$wt%; (**b**) benthic $\delta^{18}O$, *C. wuellerstorfi*; (**c**) benthic $\delta^{13}C$, C. *wuellerstorfi*; (**d**) planktonic $\delta^{18}O$; *N. incompata* (black), *G. bulloides* (red), *G. inflata* (blue); (**e**) percentage abundance of *N. pachyderma* (s) (*Np* (s)) (light blue) (Kuhs et al. 2014); (**f**) Ice-rafted debris (IRD; black) and tephra (green) concentration (*this study*).

4.4. Results

The following results sections are organised according to primary and secondary data sources for reasons of transparency.

4.4.1. Secondary Data Sources[1]

4.4.1.1. Bulk sediment CaCO3wt%

Bulk sediment $CaCO_3$wt% in the core ranges from 4.5wt% to 65wt%. At the MIS 6/5 transition at around 22.5 mcd, $CaCO_3$wt% increases from ~4.5 to ~40 (Figure 4.2a). After a short interval of reduced values of 30wt%, $CaCO_3$wt% reaches two 'high-percentage' plateaus, followed by a steep decrease at 17.52 mcd. The first plateau extends from 20.17 mcd to 19.17 mcd and the second from 18.92 mcd to 17.72 mcd, with average $CaCO_3$wt% of 55.8 and 61.4, respectively (Figure 4.3a).

4.4.2. Stable Isotope Stratigraphy

4.4.2.1. Benthic foraminiferal $\delta^{18}O$

As described by Hodell et al. 2009, the transition from MIS 6/5 at around 22.7 mcd is marked by a steep decrease of benthic $\delta^{18}O$ when it changes from heavier glacial values (>4‰) to lighter interglacial values (<3‰). The benthic MIS 5e $\delta^{18}O$ plateau from 22.6 mcd to 17.7mcd was defined by Hodell et al. (2009) with average values of 2.69 ± 0.08‰. Within the plateau, at 22.17 mcd and 18.27 mcd, two $\delta^{18}O$ maxima occur as well as one minimum located at 17.87 mcd (Figure 4.3b). With average benthic $\delta^{18}O$ of 2.66 ± 0.07‰ the first half of this plateau (up to 20.32 mcd) is isotopically slightly lighter compared to the second part with average benthic $\delta^{18}O$ 2.73 ± 0.08‰. At 17.87 mcd benthic $\delta^{18}O$ increases gradually and reaches benthic $\delta^{18}O$ values about 3.5‰ during MIS 5d (Figure 4.2b & 4.3b).

[1] Professor David Hodell, University of Cambridge and Hodell et al. (2009)

4.4.2.2. Benthic foraminiferal $\delta^{13}C$

During the early part of MIS 5e benthic $\delta^{13}C$ shows some fluctuations, but in general it is isotopically light, similar to the glacial benthic $\delta^{13}C$ values. Only 1.5 meters (21.37 mcd), above the MIS 6/5 transition in the benthic $\delta^{18}O$ record, does the benthic $\delta^{13}C$ start to become isotopically heavier and, after a period of shifting values (21.02 mcd to 20.62 mcd), benthic $\delta^{13}C$ reaches a plateau (20.52-19.37 mcd) with an average value of 0.59 ± 0.18‰ (Figure 4.2c & 4.3c). Before reaching a second plateau (18.92-18.12 mcd) with an average benthic $\delta^{13}C$ of 0.48 ± 0.12‰, benthic $\delta^{13}C$ has an excursion to more negative values (19.12 mcd). At 17.87 mcd a benthic $\delta^{13}C$ minimum of -0.31 ‰ occurred, after which benthic $\delta^{13}C$ returns to heavier values of 0.41 ± 0.19‰[1] and continues at these values across the MIS 5e/5d transition (Figure 4.3c).

4.4.2.3. Planktonic foraminiferal $\delta^{18}O$

The planktonic $\delta^{18}O$ record exhibits similar trends to benthic $\delta^{18}O$, but with a greater degree of isotopic variability. A steep decrease of planktonic $\delta^{18}O$ is followed by more or less distinctive, species dependent, plateaus (Hodell et al. 2009) and a gradual increase to heavier values into MIS 5d (Figure 4.2d & 4.3d). During the MIS 5e interval *N. incompata* has lighter $\delta^{18}O$ compared to *G. bulloides*, with notable exceptions at the beginning of MIS 5e (22.47 mcd and ~22 mcd), at the end of the benthic $\delta^{18}O$ plateau (19.22 mcd) and towards the end of MIS 5e (from 18.32 mcd up-core) (Figure 4.3 d). *G. bulloides* has the most variable $\delta^{18}O$ record. After the very short-lived plateau, *G. bulloides* $\delta^{18}O$ increases and remains fairly stable (with values >1‰) until 18.62 mcd. During this interval two minima (20.82 mcd and 19.22 mcd) are recorded. Towards the end of MIS 5e *G. bulloides* $\delta^{18}O$ decreases in two steps to lighter values, interrupted by a rebound at 18.07 mcd and after the MIS 5e/ 5d transition *G. bulloides* $\delta^{18}O$ values becomes gradually heavier again (Figure 4.2d & 4.3d). During the MIS 5e *G. inflata* $\delta^{18}O$ is with some exceptions (e.g. 21.32 mcd -21.62 mcd, 18.57 mcd) heavier than *G.*

[1] These benthic $\delta^{13}C$ values are similar to the benthic $\delta^{13}C$ values of the second benthic $\delta^{13}C$ plateau (Figure 4.3c).

bulloides $\delta^{18}O$, but consistently isotopically heavier than *N. incompata* $\delta^{18}O$. The offset between *G. inflata* $\delta^{18}O$ and *N. incompata* $\delta^{18}O$ is greatest in the interval between 21.62 mcd and 19.57 mcd. During MIS 6, 22.7 mcd down-core, the relationship between *N. incompata* $\delta^{18}O$ *and G. inflata* $\delta^{18}O$ reverses and *N. incompata* $\delta^{18}O$ is heavier. The same can be observed during MIS 5d at around 16 mcd, which Hodell et al. 2009 defined as C24 (see Figure 4.2 d).

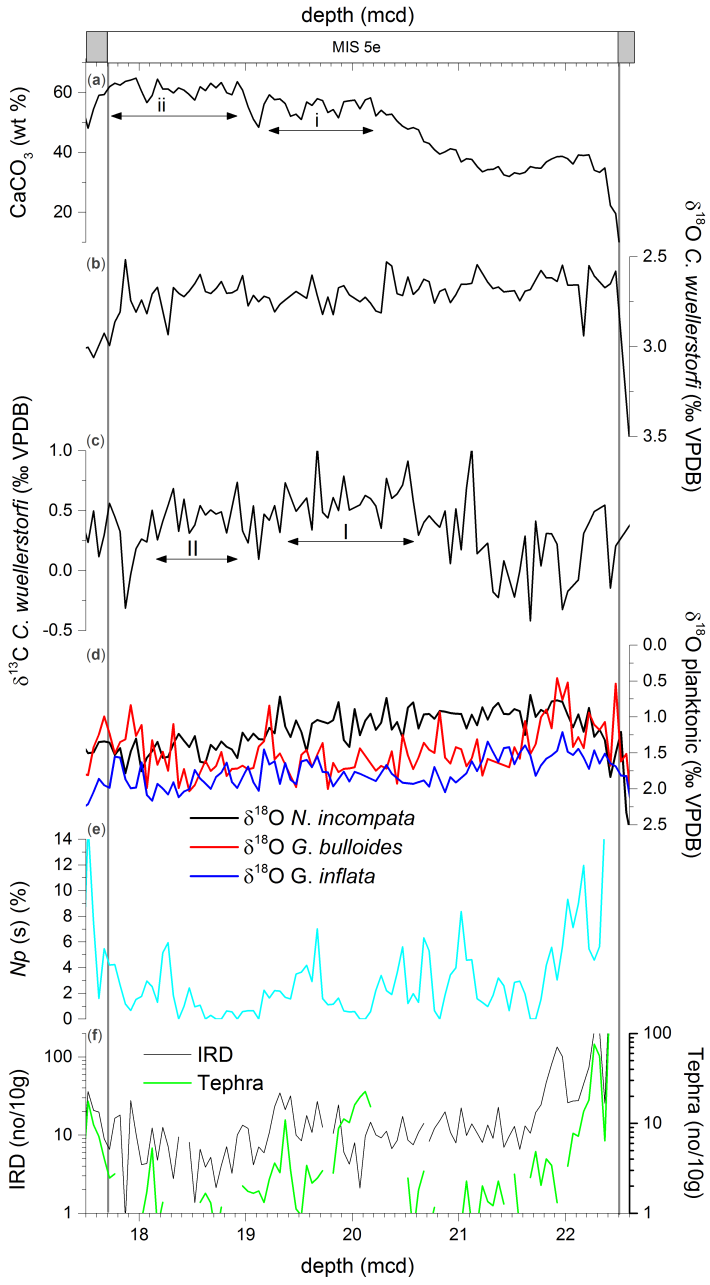

Figure 4.3: Stratigraphical overview of the benthic MIS 5e plateau for IODP Site U1304 based on Hodell et al. (2009)**.** (**a**) bulk sediment $CaCO_3$wt%; (**b**) benthic $\delta^{18}O$, *C. wuellerstorfi*; (**c**) benthic $\delta^{13}C$, *C. wuellerstorfi*; (**d**) planktonic $\delta^{18}O$; *N. incompata* (black), *G. bulloides* (red), *G. inflata* (blue); (**e**) percentage abundance of *N. pachyderma* (s) (*Np* (s)) (light blue); (Kuhs et al. 2014)*;* **(f)** Ice-rafted debris (IRD; black) and tephra (green) concentration (*this study*).(**i**),(**ii**) 1st and 2nd bulk sediment $CaCO_3$wt% plateau as described in Section 4.4.1.1.; (**I**) (**II**), 1st and 2nd *C. wuellerstorfi* $\delta^{13}C$ plateau as described in Section 4.4.2.2

4.4.3. Primary Data

4.4.3.1. N. pachyderma (s) percentage

At the end of MIS 6 *N. pachyderma* (s) % is very high with values around 95 %, and over the transition into MIS 5e it decreases sharply. During much of the MIS 5e *N. pachyderma* (s) % stays relatively low, with some intervals over the background level of 3-4 %, but it never exceeds 12 % (Figure 4.2e & 4.3e). At the start of MIS 5d *N. pachyderma* (s) % is nearly constant over the background level and varies between 10 % and 15 %, before it increases up to 78 % at 16 mcd, in phase with the planktonic $\delta^{18}O$ maximum and a major cooling interval (Figure 4.2.e).

4.4.3.2. IRD concentrations

During most of MIS 5e, IRD concentrations are very low; only at the beginning of this sub-stage do IRD concentrations exceed >100 IRD/10 g (Figure 4.2f & 4.3f; please note log scale). After 21.92 mcd the IRD concentrations decrease and reach a low concentration plateau (21.77-20.12 mcd) with average values of 12 IRD/10 g. The end of this plateau is marked by an IRD minimum at 20.07 mcd (2 IRD/10 g), which is followed by stepwise increases in IRD concentrations and an IRD peak at 19.32 mcd (35 IRD/10 g). Up-core, IRD concentrations decrease again, before they start to rise towards the end of MIS 5e. This last increase during MIS 5e is interrupted by a distinctive minimum at 17.87 mcd.

4.4.3.3. IRD composition

The most commonly found IRD lithologies within the MIS 5e interval are quartz and mica. Their combined average is 82 ± 13 % and only at 19.92 mcd do they contribute less than 50 %. Lithological indicators of provenance which occur in sufficient numbers are: haematite-stained grains (hsg), detrital carbonate (dc) and pumice grains (pg). Haematite-stained grains occur throughout the whole MIS 5e interval and were usually observed with percentages higher than, or similar to, those of detrital carbonate and pumice. At times when hsg % exceed their background level of ~10 % (Bond 1997) it is the dominant provenance indicator lithology. This occurs three times during the studied

interval: (i) MIS 6/5e transition – 21.57 mcd; (ii) 20.12-19.57 mcd and (iii) 18.72 mcd-end MIS 5e. Between 21.37-20.47 mcd dc % rises above hsg % and detrital carbonates become the most prominent lithological types as pumice grains are not present. However, at the end of this interval pumice grains (pg) start to appear again and persist until 20.12 mcd. There are two further intervals (19.62 mcd - 19.1 mcd and 17.82 mcd - 17.37 mcd) and one peak 18.6 mcd with pumice grain appearances. During the first interval (19.62 mcd-19.17 mcd) dc % also increases and peaks together with pg % at 19.62 mcd. Furthermore, as one might expect from their probably common source, pg % has a good correlation with the occurrence of tephra concentration (Figure 4.4).

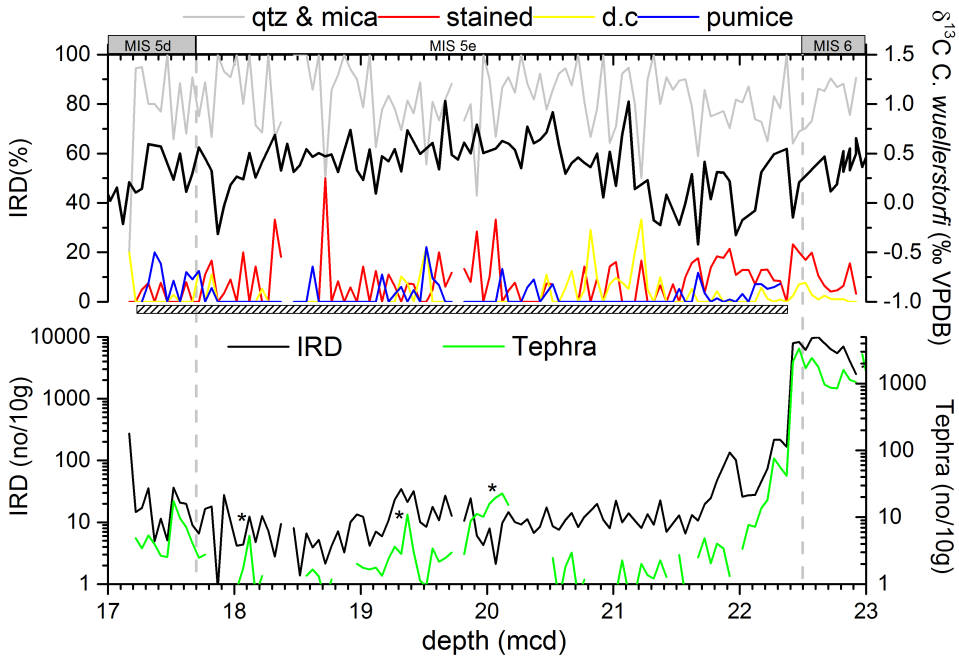

Figure 4.4: **IRD percentage, lithology and concentration for the IODP Site U1304. Upper panel:** quartz & mica % (grey), stained debris % (red), detrital carbonates (d.c) % (yellow), pumice % (blue), *C. wuellerstorfi* $\delta^{13}C$ (black). **Lower panel**: IRD (black) and tephra (green) concentration. **Grey hatched area**: all IRD and tephra which could be found in a single sample were counted and classified. For the samples above and below that interval only a fraction (until ≥ 300 planktonic foraminifera were counted) of the samples were counted and the (no/g) were calculated. * Tephra peaks analysed in the chapter.

4.4.3.4. Tephra concentration

When tephra shards are present their concentration generally correlates positively with IRD concentration (Figure 4.4). Several peaks of higher tephra concentration are present in the MIS 5e interval: 20.12 mcd with a minor peak at 19.92 mcd, 19.37 mcd and 18.12 mcd (Figure 4.4). In general, tephra concentration is several times lower than IRD concentration and only at the 20.12 mcd peak in tephra are the IRD concentrations in an opposing trend.

4.4.3.5. Tephra composition

The high concentration of tephra at around 20.12 mcd combined with a low IRD concentration gives the opportunity to identify this interval as a potential tephra isochron, i.e. the result of air-fall or sea-ice-rafting rather than iceberg-rafting. In addition, intervals around tephra the peaks at 19.37 mcd and 18.12 mcd, which are correlated with high IRD concentrations were geochemically analysed in order to investigate potential transport mechanisms and their potential volcanic source. The results of the geochemical analyses of tephra shards across these intervals are presented below.

. *Tephra in the 19.92 mcd - 20.17 mcd interval*

All colourless shards, with one exception at 19.92 mcd, analysed in this interval are of rhyolitic composition (Figure 4.5a) and can be associated with the tholeiitic rock suite of Iceland as illustrated in Figure 4.5a. Plotting the geochemical data on various oxide/oxide bi-plots show the homogenous composition of the shards found in this interval with FeO values around 3 wt%, and K_2O and Al_2O_3 varies between 1.79-2.0 wt% and 10.9-11.64 wt%, respectively (Figure 4.5). Geochemical data comparison of this U1304 MIS 5e horizon with other MIS 5e rhyolitic horizons derived from marine cores in the North Atlantic allows the correlation of the 19.92 mcd - 20.17 mcd tephra with the isochronous 5e-Eem/RHY-I horizon (Figure 4.5). This horizon is widespread and was first recognised in the Nordic Sea (Fronval & Jansen 1997; Wastegård & Rasmussen 2001; Brendryen et al. 2010; Abbott et al. 2014) and in lake sediments from

the Faroe Islands (Wastegård et al. 2005), but has recently been found in the marine record MD99-2253, from the North Atlantic (Davies et al. 2014). One colourless shard found in the sample at 19.92 mcd was identified to be of basaltic composition and is also geochemically characteristic of the tholeiitic series of Iceland (Figure 4.6).

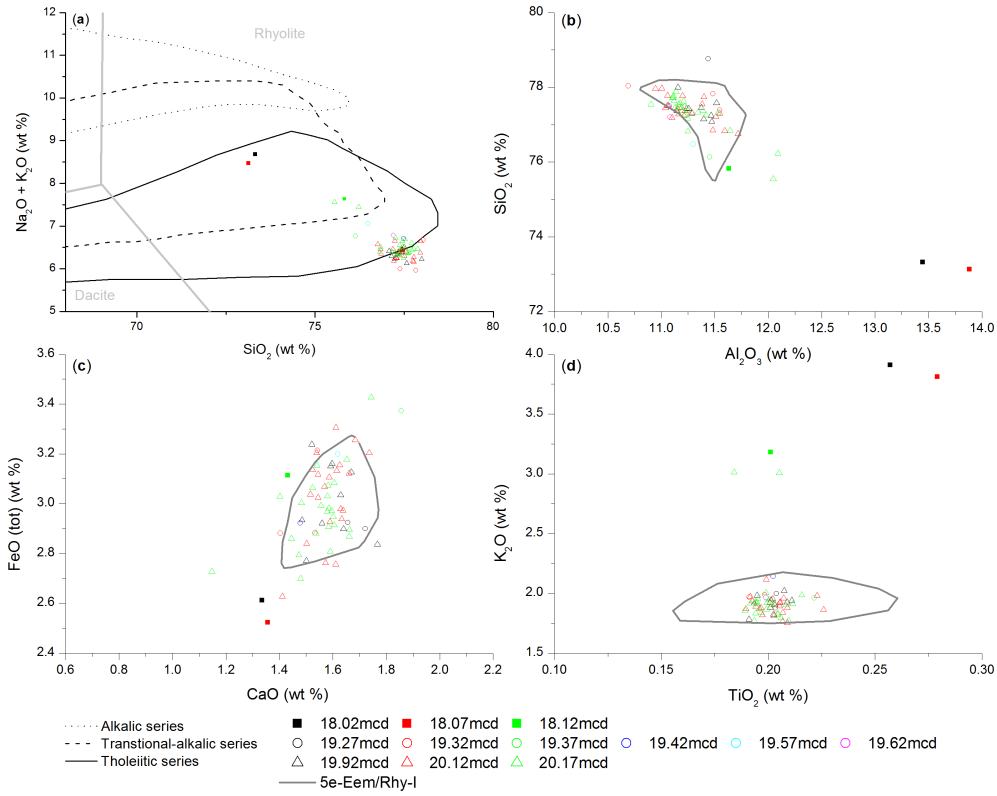

Figure 4.5: (**a**) Total alkali-silica plot shows the classification of shards into three different Icelandic rock suites: tholeiitic, transitional-alkalic and alkalic-series (Jakobsson et al. 2008). (**b**) SiO_2 versus Al_2O_3 v (**c**) FeO versus CaO (**d**) K_2O versus TiO_2 variation diagrams comparing rhyolitic shards from U1304 found in three intervals (18.02 mcd - 18.22 mcd, 19.27 mcd - 19.62 mcd, 19.92 mcd – 20.17 mcd) with published data of the 5e-Eem/RHY-I / 5e-Midt/RHY-I (Wastegård & Rasmussen 2001; Brendryen et al. 2010; Abbott et al. 2014; Davies et al. 2014). Chemical classification after Bas & Maitre (1986).

. *Tephra in the 19.27 mcd - 19.62mcd interval*

The rhyolitic tephra shards found in this interval have similar, though more variable, geochemistry to the shards analysed from 19.92 mcd - 20.17mcd. Based on the visual examination of various binary plots and statistical tests they also can be associated with

the 5e-Eem/RHY-I horizon (see Appendix C Table 8.1 & 8.2). In contrast to the previous interval, the basaltic shard concentration is higher in this interval and co-varies with the IRD concentration (Figure 4.4). The basaltic shards are geochemically heterogonous. Three shards can be affiliated with the Grímsvötn volcano system (GVS) and a further two shards have a similar geochemistry to the Krafla volcano system (KVS) (Figure 4.6). For the remaining shards no clear association with any of the compared volcanic system could be found, but the possibility that some of these have been derived from a volcanic system in the Western Volcanic Zone (WVZ) of Iceland cannot be discounted (Figure 4.6).

. *Tephra in the 18.02 mcd - 18.22 mcd interval*

The geochemistry of rhyolitic shards found in this interval varies from the geochemistry of the rhyolitic shards found in 19.92 mcd - 20.17 mcd and can be grouped into the transitional rock suite of Iceland (Figure 4.5a). They have higher K_2O% as well as lower CaO wt% and SiO_2 wt% than the 19.92 mcd -20.17 mcd tephra (Figure 4.5). Further differences are that 18.02 mcd - 18.07 mcd shards have higher TiO_2 wt% and Al_2O_3 wt% as well as lower FeO wt%. The 18.12 mcd shards have higher FeO wt% and similar Al_2O_3 and TiO_2 wt% (Figure 4) compared to the shards from the interval 19.92 mcd – 20.17 mcd. As well as the rhyolitic shards found in this interval, the basaltic shards also reveal that they are part of heterogeneous geochemical populations. In contrast to the rhyolitic shards, only two shards could be clearly identified as members of the transitional rock suit, whereas the remaining five basaltic shards are most likely to be representative of the tholeiitic rock suite, derived from the WVZ, Eastern Volcanic Zone (EVZ) and Reykjanes Volcanic Zone (RVZ) of Iceland (Figure 4.6).

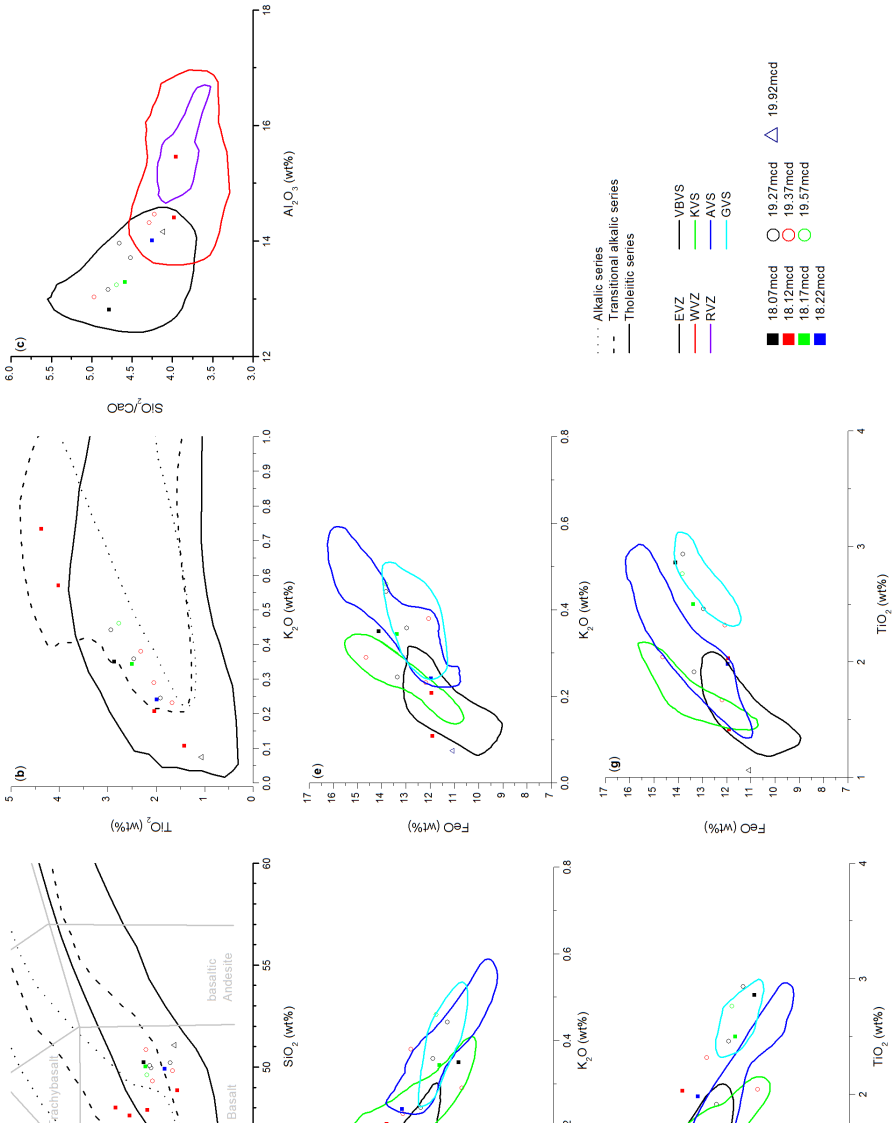

Figure 4.6: (**a**) Total alkali-silica plot (**b**) TiO_2 vs. K_2O oxide plot shows the classification of shards into three different Icelandic rock suites: tholeiitic, transitional-alkalic and alkalic-series (Jakobsson et al. 2008). Compositional envelopes from Jagan (2010) (**c**) and Oladottir et al. (2011) (**d-g**). (**c**) SiO_2/CaO vs Al_2O_3 plot allows differentiation between tephra derived from the Western volcanic zone (WVZ; *red*), Reykjanes volcanic zone (RVZ; *green*) or Askja (AVS), Krafla (KVS), Veidivötn-Baradagunga (VBVS) and Grímsvötn volcano system (GVS) summarised as Eastern volcanic zone (EVZ; *black*). (**d**) MgO vs. K_2O (**e**) FeO vs. K_2O; (**f**) MgO vs.TiO_2;(**g**) FeO vs. TiO_2 separate shards with a geochemical signature similar to VBVS (*black*), GVS (*light blue*) and KVS (*light green*) AVS (*dark blue*). Chemical classification after (Bas & Maitre 1986).

4.4.3.6. Tephra size distribution

Shard size measurements were grouped into intervals around the tephra concentration peaks. Size frequency plots for shards of each geochemical group are plotted for the sample depth: 20.17 mcd; 20.12 mcd; 19.92 mcd and samples intervals: 19.27-19.62 mcd and 18.02-18.22 mcd in Figure 4.7. In Table 4.1 maximum (Max) and minimum (Min) shards size; mean; median, $Md_{\varphi;}$ mode; standard deviation, σ_{φ} (sorting) and skewness α_{φ} for each group can be found.

The maximum and minimum shard size for the interval 19.92-20.17 mcd is 672 µm and 168 µm, respectively. The shard size distribution is relatively large with a median between 308 µm and 364 µm and very well to well-sorted (Table 4.1). In the two intervals, 19.27-19.62 mcd and 18.02-18.22 mcd, shard size analyses were carried out for basaltic and rhyolitic grains independently, as well for both combined. In the interval 19.27-19.62 mcd basaltic median value is larger than the rhyolitic median, they are 335 µm to 282 µm, respectively (Table 4.1). Whereas the basaltic shards are only moderately well sorted, the rhyolitic shards and the overall combined shard size distribution is well-sorted with shard size ranges from 565 µm to 106 µm (Table 4.1/Figure 4.7). For the interval 18.02-18.22 mcd the basaltic, rhyolitic as well as the overall combined shard size distribution (Table 4.1/Figure 4.7). With a median of 252 µm, this interval has the smallest average shard size.

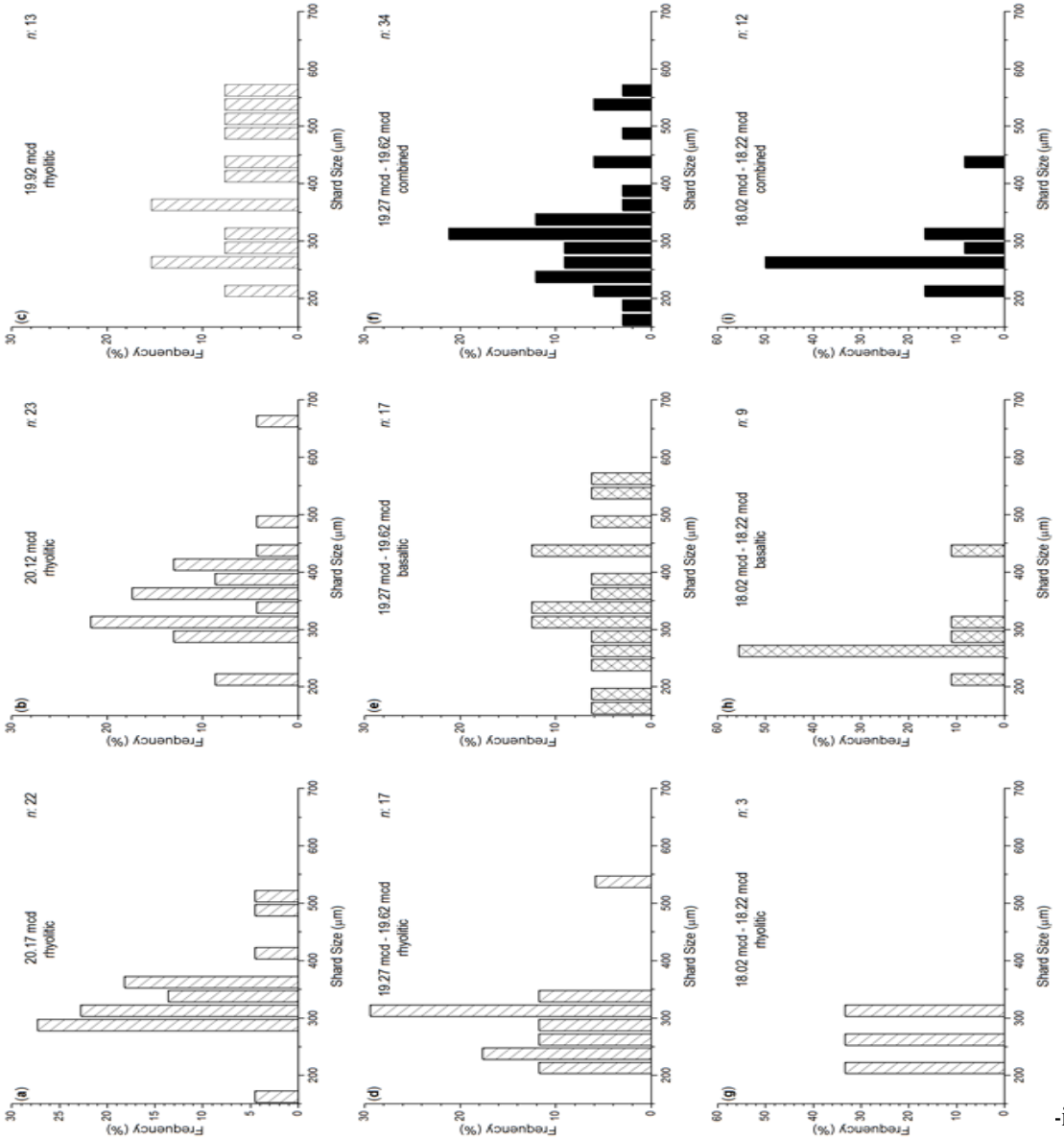

-**i**). (**a**) 20.17 mcd; (**b**) 20.12 mcd; (**c**) 19.92 mcd and samples intervals 19.27-19.62 mcd: (**d**) rhyolitic, (**e**) basaltic, (**f**) combined; 18.02-18.22 mcd: (**g**) rhyolitic (**h**) basaltic (**i**) combined. Filling of the bars corresponds to the tephra shards' geochemistry: Hatched bars: rhyolitic; cross-hatched: basaltic; black bars: rhyolitic and basaltic shards combined. *n*: number of measured tephra sizes. Note: samples only contain material >150µm

Min [ϕ/µm]		Mean [ϕ/µm]		median Md_φ [ϕ/µm]		Mode [ϕ/µm]		St. Dev. σ_φ [ϕ/µm]		Skewness α_φ [ϕ]
2.57	168.0	1.63	329.6	1.70	308.0	1.84	280.0	0.19	42.0	-0.27
2.16	224.0	1.52	359.1	1.46	364.0	1.70	308.0	0.29	70.0	0.29
2.16	224.0	1.45	383.4	1.46	364.0	1.46	364.0	0.50	127.1	0.05
3.24	105.9	1.74	316.1	1.70	308.9	1.65	317.7	0.45	98.5	-0.04
3.24	105.9	1.62	353.9	1.58	335.3	1.18	441.3	0.57	136.6	0.00
2.24	211.8	1.81	292.8	1.82	282.4	1.65	317.7	0.25	48.0	0.19
2.16	224.0	1.77	275.3	1.84	252.0	-	252.0	0.27	31.4	-0.22
2.16	224.0	1.87	280.0	1.99	252.0	1.99	252.0	0.13	24.1	-1.00
2.16	224.0	1.95	261.3	1.70	252.0	-	-	0.16	28.6	-0.26

Table 4.1: Maximum (Max) and minimum (Min) shards size; mean; median, $Md_{\varphi;}$ mode; standard deviation, σ_φ (sorting) and skewness α_φ (in units of [ϕ/µm]) of samples depth 20.17 mcd, 20.12 mcd, 19.92 mcd as well as the sample intervals 19.27 mcd - 19.62 mcd and 18.02 mcd - 18.22 mcd. All shards found in in each sample were measured along their long axis.

4.5. Discussion

4.5.1. Tephra Transport Mechanism

The rhyolitic shards from the 19.92-20.17 mcd are part of a single homogenous geochemical population, which can be affiliated with the known 5e-Eem/RHY-I isochron (Figure 4.5). The shard size analyses revealed a well-sorted population with median shard size varying between 308 µm and 368 µm (Table 4.1). This relatively large median sizes indicate that these shards were either transported by iceberg- or sea-ice-rafting to the core Site U1304 (Sparks et al. 1981; Brendryen et al. 2010). Iceberg-rafted tephra is characterised by a heterogonous population, poorly-sorted shard size distribution and co-variance to changes in IRD concentration. However, the tephra shards found in the interval 19.92-20.17 mcd have a well-sorted shard-size distribution and changes in shard concentration are not correlated to changes in IRD concentration. Thus, these shards were most likely to be transported by sea-ice-rafting. Even though, there is a short delay in timing of the sea-ice-rafted tephra deposits compared to air-fall deposits, they can still be seen as an effectively instantaneously deposition (Lackschewitz & Wallrabe-Adams 1997; Austin et al. 2004; Brendryen et al. 2010). Tephra shards found in the 19.27-19.62 mcd interval form a geochemically heterogeneous population. Shards from the KVS, WVZ, GVS and 5e-Eem/RHY-I-affiliated were found. The heterogeneous population combined with the large median and co-variability with IRD concentrations point towards an iceberg-rafted deposition. The presence of 5e-Eem/RHY-I-like shards suggest also secondary transport processes, such as bioturbation or increased bottom current speed (Abbott et al. 2014). The influence of secondary transport processes is further supported by the well to moderate to well-sorted shard size distribution. The heterogonous populations, relative large median size and covariance of tephra and IRD concentrations, suggest that shards from the 18.02-18.22 mcd interval were probably also transported by iceberg-rafting to the core site.

4.5.2. Chronology

Tephrochronology is, at the moment, the only method to test the synchronicity of sub-millennial events observed in different records because tephra isochrons are thought, under certain conditions, to be instantly deposited and can therefore test the "accuracy" of the assigned age-model. The discovery of the widespread 5e-Eem/RHY-I isochron in the U1304 record allows us to correlate the U1304 proxy data to other proxy records in which the 5e-Eem/RHY-I tephra was also found. This will not only give the opportunity to estimate potential lags or leads of certain environmental changes (e.g. surface cooling, deep-water ventilation decrease) but also to evaluate 5e-Eem/RHY-I ages from the records being compared.

The 5e-Eem/RHY-I tephra is also recorded in the marine sedimentary record MD99-2253 (56°21'78N, 27°48.95W) (Davies et al. 2014) (Figure 4.1). The proximity to U1304 makes MD99-2253 an ideal correlation record to test the U1304 event-stratigraphy and to evaluate the U1304 age-model and vice versa. MD99-2253 is located only 500 km to the NE of U1304 and its recovery depth is 2840m (only 242m shallower that U1304) and therefore one might reasonably assume that the benthic $\delta^{18}O$ changes observed are synchronous in both records. In the 18.58-18.59 mcd interval of MD99-2253, homogenous rhyolitic tephra were found and these have been correlated to the isochron 5e-Eem/RHY-I (Davies et al. 2014). The small shard sizes (25-50µm) and independence from IRD concentration changes suggest that this cryptotephra (non-visible volcanic-tephra) is a primary air-fallen deposit (Davies et al. 2014).

Shackleton's LIG timescale (Shackleton et al. 2002; Shackleton et al. 2003) was assigned to the benthic $\delta^{18}O$ record of MD99-2253[1]. The start and end of the benthic MIS 5 $\delta^{18}O$ plateau in MD99-2253 were defined as 19.68 mcd to 17.10 mcd, respectively. On this timescale, MIS 5e started at 132 ka and ended at 115 ka (Shackleton et al. 2002); the MIS 5e benthic $\delta^{18}O$ plateau lasted from 128 ± 1 ka to

[1] Chapman, unpublished proxy data

116.1 ±0.9 ka (Stirling et al. 1998; Shackleton et al. 2003). The MIS 5e plateau itself is defined as an interval beyond which benthic $\delta^{18}O$ values become positive (Shackleton et al. 2003). Hodell et al. (2009) used the same approach to generate a timescale for U1304. This 'Shackleton- method' to create a LIG timescale is widely-accepted, even though one has to bear in mind that there are certain caveats associated with the use of this age-model. Shackleton et al. (2003) used ages derived from U/Th dated corals from Western Australia to date the MIS 5e plateau, assuming the synchronicity of the sea-level highstand and its association with benthic $\delta^{18}O$ between both hemispheres.

Assigning the age 128 ± 1 ka and 116 ± 0.9 ka to the start (19.68 mcd) and end (17.1 mcd) of the MIS 5e $\delta^{18}O$ plateau results, based on a linear age-model, in an age of 122.93 ka for the 5e-Eem/RHY-I in MD 99-2253, which is about 1000 years older than the 5e-Eem/RHY-I age derived in the U1304 record (121.99 ka). Hence, if we accept that 5e-Eem/RHY-I tephra found in both cores is isochronous, then one or both of these records would require a non-linear age-depth relationship over the entire MIS 5e to reconcile the linear age-depth age estimates obtained. Both MD99-2253 and U1304- 5e-Eem/RHY-I ages lie within the conservative error estimates (±1ka) derived from the tie-point uncertainties.

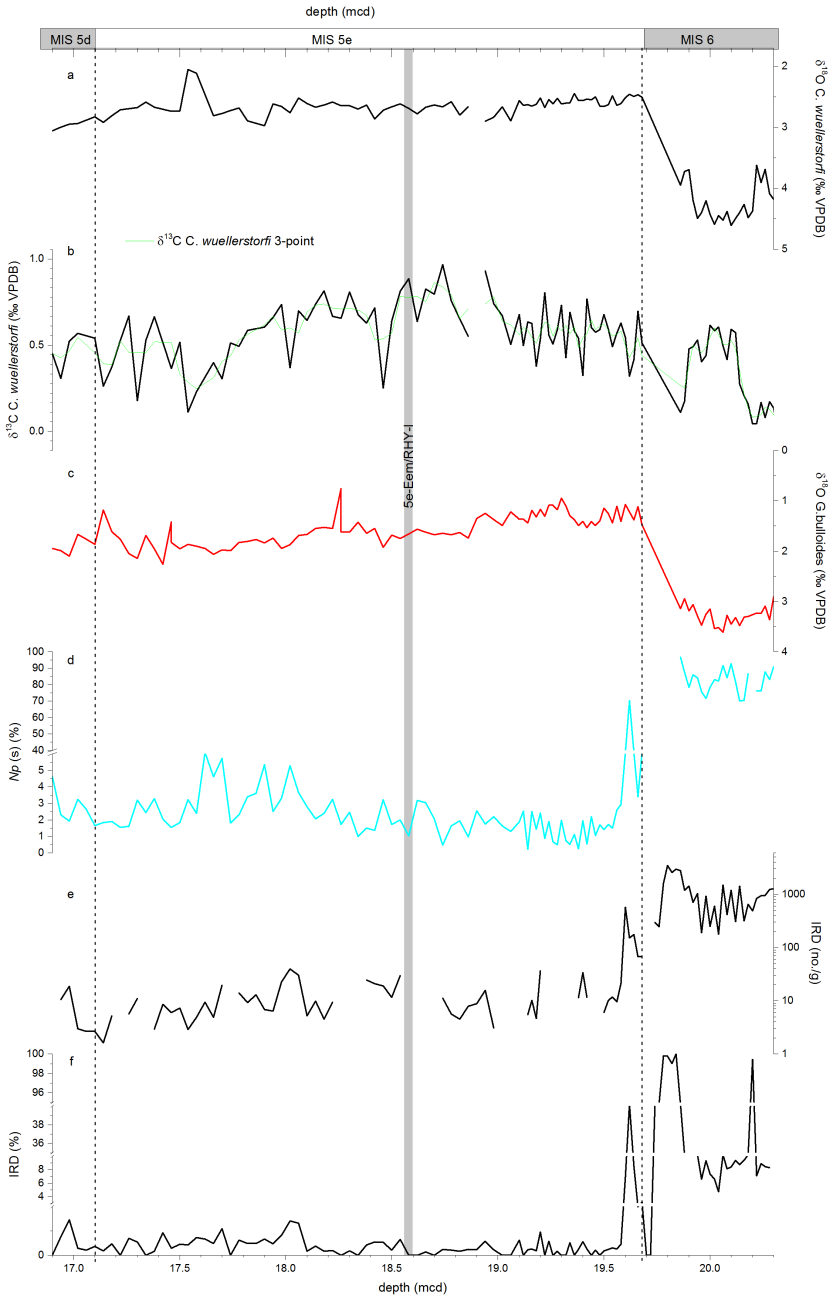

Figure 4.8: Stratigraphical framework for MD99-2233 (**a**) $\delta^{18}O$ *C. wuellerstorfi* (*black*); (**b**) $\delta^{13}C$ *C. wuellerstorfi (black)*, $\delta^{13}C$ *C. wuellerstorfi* 3-point running mean (*green*); (**c**) *G. bulloides* $\delta^{18}O$ (*red*); (**d**) percentage abundance of *N. pachyderma* (s) (*Np* (s)) (*light blue*); **(e)** IRD concentrations (*black*); (**f**) IRD percentages (*black*). All unpublished data from Dr Mark Chapman, University of East Anglia. Grey highlighted area: occurrence of 5e-Eem/RHY-I tephra (Davies et al. 2014). Please note breaks in panels (**d**) and (**f**).

In order to evaluate which of the two 5e-Eem/RHY-I ages is the more likely, we explored research which has suggested a correlation between mean sortable silt ($\overline{SS}$), flow speed and accumulation rate; for example by Ledbetter (1986) and McCave & Hall (2006). The $\overline{SS}$ from sedimentary core NEAP-18K, which is located close to U1304 (210 km southeast, see Figure 4.1), is lower during the early part of MIS 5e than at the later stages (Hall et al. 1998; Hodell et al. 2009) (Figure 4.9). The average over the $\overline{SS}$ in the early part of MIS 5e (i.e. before the tephra deposit) is about 13.9 ± 1.5 μm and after the 5e-Eem/RHY-I horizon it increases to 16.1 ± 1μm (Figure 4.9). These values suggest a current speed of less than 15cm/s (Ledbetter 1986, in their Figure 2). In such a slow speed $\overline{SS}$, flow speed and accumulation rate have a positive correlation (McCave & Hall 2006), i.e. a smaller $\overline{SS}$ suggests a slower flow speed and a lower sedimentation rate. Using the MD99-2253 5e-Eem/RHY-I age as an additional tie-point in the U1304 record would result in a higher/lower sedimentation rate (46.6/33.7 cm/kyr) in U1304 for the early/later part of MIS 5e (Figure 4.9, dashed black line), whereas assigning the U1304-Eem/RHY-I age to MD99-2253 would allow to a lower/higher sedimentation rate (18.3/25.13 cm/kyr) in MD99-2253 for the early/later part of MIS 5e (Figure 4.9, dashed orange line). Thus, we suggest adopting the U1304 5e-Eem/RHY-I age as an additional tie-point for MD99-2253, as the other scenario would lead to a higher sedimentation rate in the early part of MIS 5e in U1304, which contradicts the $\overline{SS}$ data available at this site. In order to achieve lower sedimentation rates during the early MIS 5e than the late MIS 5e, the U1304 5e-Eem/RHY-I age could be moved within the age uncertainties to make it even younger (120.99 ka). Even though this action would provide a better fit to the sedimentation rate pattern inferred by the $\overline{SS}$, it also would lead to a larger difference in the accumulation rate in MD99-2253 between early and late MIS 5e. Because of the latter observation, as well as the fact that the difference in average over the $\overline{SS}$ in NEAP-18K during early/late MIS 5e is not very large, it was felt that reducing the U1304 5e-Eem/RHY-I age would be a step too far. Based on the evidence currently available, we recommend an age of 121.99 ± 1ka be applied to the 5e-Eem/RHY-I isochron. Future work will be required to find data either supporting or

challenging this age estimate. It has to be noted that currently no direct transfer function between $\overline{SS}$ and sedimentation rate exists and the conclusion made above are based on the hypothetical model by McCave & Hall (2006 in their Figure 8). McCave & Hall (2006) point out that though their model assumes a positive correlation between $\overline{SS}$ flow speed and accumulation rate exists up to flow speeds of 15cm/s, depending on the specific environmental setting, the this correlation can already break down for slow flow speeds of 10cm/s (Gross & Williams III 1991). Therefore, optimal goal would be to derive an independent absolute age for 5e-Eem/RHY-I e.g. based on argon dating.

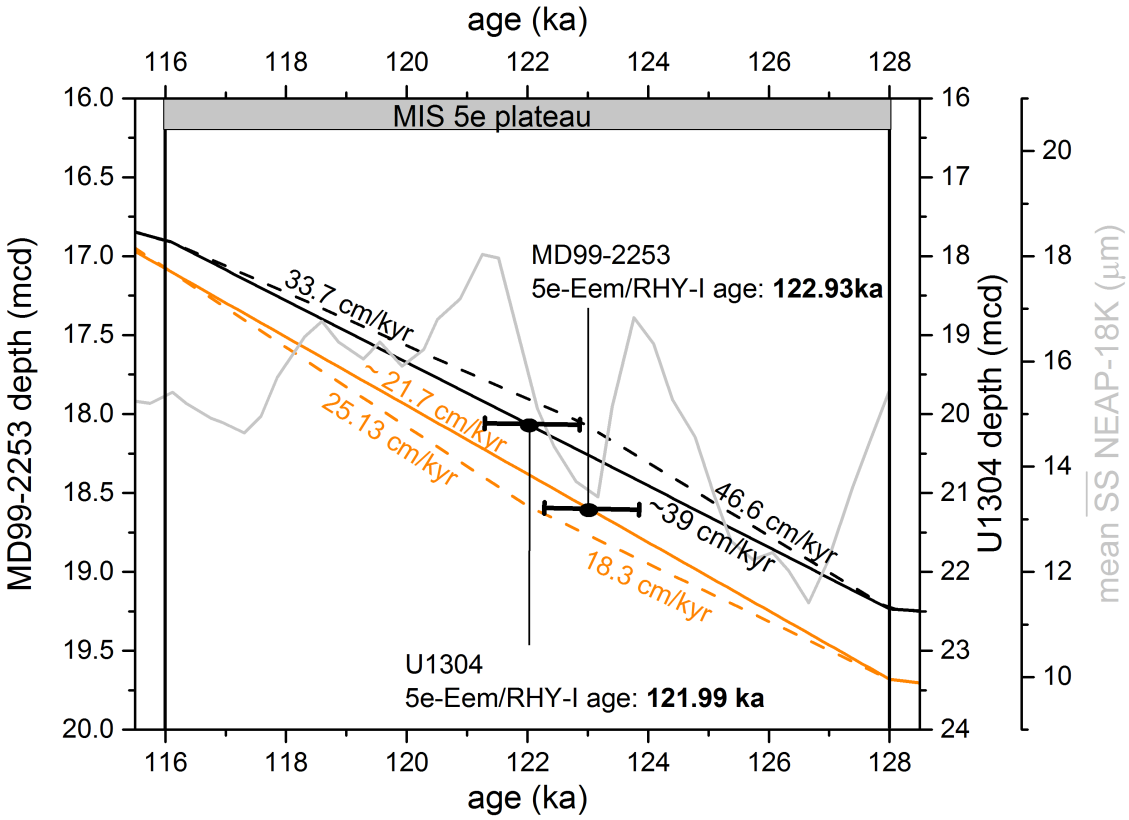

Figure 4.9: Age-depth model for U1304 (*black)* and MD99-2253 (*orange*) with U1304 5e-Eem/RHY-I age 121.99 ± 1 ka and MD99-2253 5e-Eem/RHY-I age 122.93 ± 1 ka. Sedimentation rates for MD99-2253 (*solid orange*) and U1304 (*solid black*) based linear interpolation between tie-points at start (128 ± 1 ka) and end (116.1 ± 0.9 ka) of MIS 5e benthic $\delta^{18}O$ plateau. Sedimentation rates for MD99-2253 (*dashed orange*) and U1304 (*dashed black*) based on linear interpolation using the 5e-Eem/RHY-I age from U1035/MD99-2253 as extra tie-point. Mean sortable silt ($\overline{SS}$) NEAP-18K (*grey*) (Hall et al. 1998; Hodell et al. 2009).

5e-Eem/RHY-I ages reported from other locations vary between 121-125ka (Sejrup et al. 1989; Fronval & Jansen 1996a; Fronval & Jansen 1997; Fronval et al. 1998; Rasmussen et al. 1999; Davies et al. 2014) (Table 4. 2). The age-models of the majority of these records are based on correlation to the orbitally tuned $\delta^{18}O$ stack SPECMAP (Sejrup et al. 1989; Fronval & Jansen 1996a; Fronval & Jansen 1997; Fronval et al. 1998; Rasmussen et al. 1999). Only the chronologies of the cores MD99-2253 and MD99-2289 are based on Greenland ice core ages (Brendryen et al. 2010; Davies et al. 2014). The age-uncertainties associated with the SPECMAP-chronology are about 3 ka and 6 ka (Imbrie et al. 1984; Martinson et al. 1987) for the MIS 5e start and end, respectively . Taking these uncertainties into account allow the older 5e-Eem/RH-I ages derived from orbital tuning allow a fit to the U1304 age of 121.99 ± 1 ka. As a matter of fact it is interesting that the majority of the 5e-Eem/RHY-I ages from other locations vary only between 121 and 122 ka, notably the Greenland ice core based ages from MD99-2289 (121.8 ka); (Brendryen et al. 2010) and MD99-2253 ~122 ka (Davies et al. 2014) match the U1304 age of 121.99 ± 1 ka very closely. The older ages are usually associated with inconsistency in the developed age-model. Fronval & Jansen (1996b; 1997) give 5e-Eem/RHY-I tephra ages between 121 and 122 ka for cores in the Nordic Sea, but in their subsequent paper (Fronval et al. 1998) the age changes to 125 ka for the same sedimentary cores. This discrepancy potentially originates from assigning different ages to the start/ end of MIS 5e and/or choosing different tie-points for their age-depth models.

Core	Latitude [°]	Longitude [°]	Depth [m]	Age [ka]	References
HM57-7	68.26	-13.52	1620	124 (118)[1]	(Sejrup et al. 1989)
				121-122	(Fronval & Jansen 1996b; Fronval & Jansen 1997)
				125	(Fronval et al. 1998)
HM71-19	69.29	-9.32	2210	121-122	(Fronval & Jansen 1996b; Fronval & Jansen 1997)
				125	(Fronval et al. 1998)
HM79-31	67.02	-7.57	1790	125	(Fronval et al. 1998)
Link16	62.36	-3.31	733	N/A	(Abbott et al. 2014)
MD95-2009	62.44	-3.59	1027	124[2]	(Rasmussen et al. 1999; Wastegård & Rasmussen 2001)
MD99-2253	56.21	-27.48	2840	~122	(Davies et al. 2014)
MD99-2289	64.39	4.12	1262	121.8	(Brendryen et al. 2010)
ODP644	66.40	4.34	1227	121-122	(Fronval & Jansen 1996b; Fronval & Jansen 1997)
				125	(Fronval et al. 1998)
U1304	53.03	-33.32	3082	121.99	(Hodell et al. 2009)
Klaksvík	Faroe Islands				(Wastegård et al. 2005)

Table 4.2: Locations and water depths of marine sediment cores as well as of the only lacustrine record bearing the 5e-Eem/RHY-I isochron.

4.5.3. Stratigraphic Sub-Division of MIS 5e

Due to the alignment on a common age-model (see above), the MD99-2253 and the U1304 proxy records, especially the stable $\delta^{13}C$ and $\delta^{18}O$ isotope records, are quite similar. In the U1304 and MD99-2253 records the transition from MIS 6 (glacial) to the MIS 5e (interglacial) can be clearly identified by the steep decrease in benthic $\delta^{18}O$ (Figure 4.2b & 4.8a), representing the change from high to low global ice volume (Termination II). This decay of the Northern Hemisphere Ice Sheets is further supported by the increase of IRD concentrations across the glacial termination (Figure 4.3f & 4.8e). Nearly simultaneously, the surface water became much warmer as the shift in $\delta^{18}O$ planktonic and *N. pachyderma* (s) % indicates (Figure 4.2 & 4.8).

[1] Two peaks in the tephra concentration
[2] Used the age from (Fronval et al. 1998)

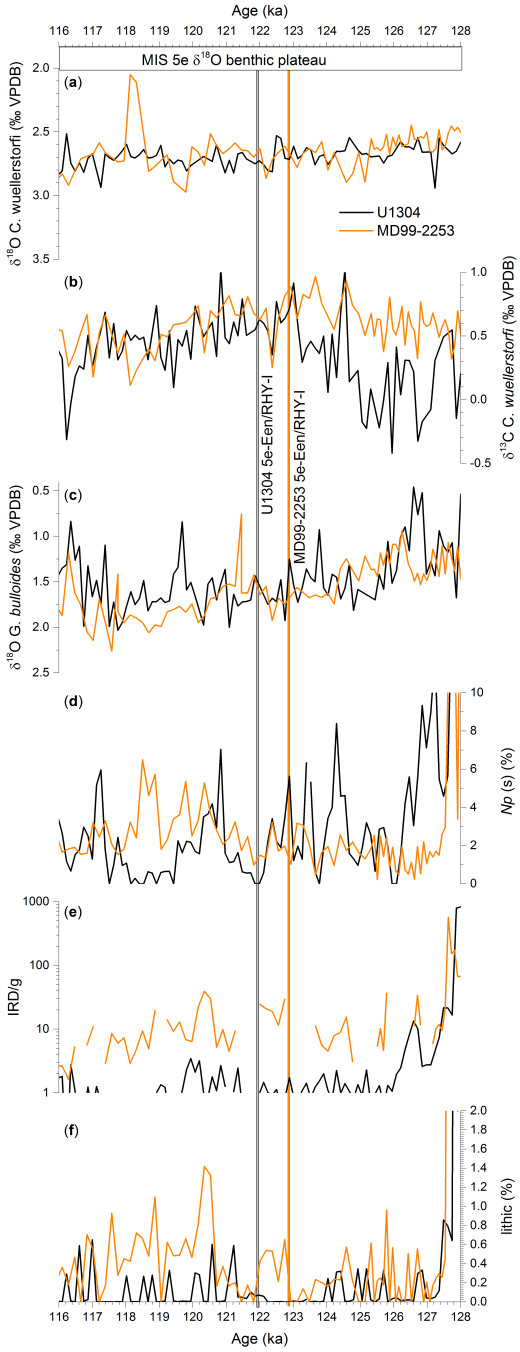

Figure 4.10: Proxy data from MD99-2253 (orange) and U1304 (black) on Shackleton timescale MIS 5e benthic $\delta^{18}O$ plateau (Shackleton et al. 2002; Shackleton et al. 2003) with start (128 ± 1 ka) and end (116.1 ± 0.9 ka) of MIS 5e benthic $\delta^{18}O$ plateau. MD99-2253 5e-Eem/RHY-I age: 122.93 ± 1 ka (highlighted orange) U1304 5e-Eem/RHY-I age121.99 ± 1 ka (highlighted grey). (**a**) $\delta^{18}O$ *C. wuellerstorfi*; (**b**) $\delta^{13}C$ *C. wuellerstorfi;* (**c**) *G. bulloides* $\delta^{18}O$; (**d**) percentage abundance of *Np* (s)*;* (**e**) IRD concentrations (*on log scale*); (**f**) lithic percentages.

In contrast to these marked changes described above, $\delta^{13}C$ benthic does not show any major changes during Termination II and continues to stay low during the first part of the MIS 5e $\delta^{18}O$ benthic plateau (Figure 4.2 & 4.8). A similar pattern can be observed in U1304 $CaCO_3$wt%. After a short and sharp decrease $CaCO_3$wt% reaches its 'glacial' values again at the start of the benthic $\delta^{18}O$ plateau and it remains very low during the early part of the MIS 5e until 20.12 mcd (Figure 4.3). This delayed increase of benthic $\delta^{13}C$ during MIS 5e is a widespread event across the North Atlantic during the early MIS 5e (Keigwin et al. 1994; Oppo et al. 1997; Hall et al. 1998; Hodell et al. 2009; Skinner & Shackleton 2006; Galaasen et al. 2014). The origin of the isotopically light $\delta^{13}C$ water mass is thought to be either a southerly source (Oppo et al. 1997; Hodell & Curtis 2008) or derived from water created by brine formation in the Nordic Sea (Raymo et al. 2004). The variation of benthic $\delta^{13}C$ is routinely used as an indicator of changes in deep-water formation and ocean ventilation. Oppo et al. (1997) and Hodell et al. (2009) have shown that during Termination II the Glacial North Atlantic Intermediate Water (GNAIW) was replaced by ^{13}C-depleted Antarctic Intermediate Water (AAIW) or Norwegian Sea Intermediate Water (NSIW) at water depths above 2000m. Southern Source Water (SSW) which occupied water depths below 2000m during MIS 6 were possibly pushed to depths below 2800m and replaced by Iceland-Scotland Overflow Water (ISOW) (Oppo et al. 1997; Hodell et al. 2009).

In both cores, MD99-2253 and U1304, the 5e-Eem/RHY-I was found close to the onset of the start of fully interglacial benthic $\delta^{13}C$ conditions and corresponding deep-ocean circulation regime at around 123 ka (Figure 4.10). The occurrence of the 5e-Eem/RHY-I tephra at this pronounced mid-MIS 5e transition can therefore be used as a marker for the onset of the fully-interglacial-type circulation in the eastern North Atlantic and can also provide a test whether or not the onset of fully-interglacial deep-ocean circulation was a synchronous event across the North Atlantic. Comparing the records of MD99-2253 and U1304, both on the Shackleton MIS 5e timescale, showed that the onset of fully interglacial benthic $\delta^{13}C$ occurred about 800 years earlier at the MD99-2253 site (123.8 ka) than at U1304 (123 ka) (Figure 4.10). However, using the 5e-Eem/RHY-I as

an additional tie-point in the age-models of these records suggests that the onset of the fully interglacial ventilation state seems to have been synchronous (within the ±1000 years uncertainty) (Figure 4.11).[1] This synchronicity is probably not surprising, taking the close proximity of U1304 and MD99-2253 and similar water depth into account. However, it would be interesting to know whether the onset of fully-interglacial ventilation occurred synchronously over the North Atlantic or whether there were temporal offsets between different areas during this transition.

The 5e-Eem/RHY-I tephra is not only found in the North Atlantic, but also in the Norwegian and Greenland Sea (Sejrup et al. 1989; Fronval & Jansen 1996a; Fronval & Jansen 1997; Fronval et al. 1998; Rasmussen et al. 1999; Davies et al. 2014). In order to test the potential synchronicity of the start of fully-interglacial type circulation during the mid-MIS 5e transition, all the records in which this tephra occur have to be set onto a common timescale, with an additional alignment of the onset of full interglacial conditions, indicated by the distinct maximum in benthic $\delta^{13}C$. The 5e-Eem/RHY-I tephra would not only provide an independent marker to assess the assumption of synchronicity, but also potential offsets between the onset of fully-interglacial conditions at different locations. Ultimately, this would give the advantage that even in cores without the 5e-Eem/RHY-I tephra correlation might be applied with greater confidence. The establishment of this extra tie-point during MIS 5e could give the opportunity to investigate the correlation of e.g. surface proxies of different regions and might lead to a better understanding of the evolution of the LIG and its decline. In particular, the investigation of Nordic Sea–North Atlantic connections is of major interest because of the Nordic Sea's important role of NADW formation.

[1] A further improvement of the MD99-2253-U1304 alignment is the closer match of the *G. bulloides* $\delta^{18}O$ record, especially the distinct peak $\delta^{18}O$ in the later MIS 5e (~ 119.8ka). Due to the additional tie-point the age different decrease from 1800 years to 1000 years.(Figure 4.10 & 4.11)

So far, the 5e-Eem/RHY-I tephra has not been found in any sediment cores from the western North Atlantic, which might be a result of the prevailing wind pattern at mid-latitudes and sea-ice trajectories. The Greenland Ice Sheet (GIS) and Laurentide Ice Sheet (LIS) almost certainly have an important role in the evolution of MIS 5e and the establishment of an event-stratigraphy would potentially give more detailed insights about the influence of ice-sheet growth/decline on the MIS 5e hydrology. For example, the MD03-2664 records from Erik Drift indicate apparently strong NADW anomalies during the early LIG (Galaasen et al. 2014), which were strongest during times of ice-melting. The argument has been made that, NADW ventilation was only stabilised after the major northern hemisphere ice-sheets had retreated (Galaasen et al. 2014). In the Labrador Sea, evidence for an 8.2 ka-like outburst flood and surface freshening event has been observed during early MIS 5e (Nicholl et al. 2012). This event is associated with a detrital layer, which was also found at the Erik Drift and is followed by the strongest of the NADW anomalies (~124.5 ka). Evidence for this outburst event might also be seen in U1304. The dominant IRD lithology around 124 ka is detrital carbonate (Figure 4.4), possibly derived from LIS; interestingly, after the detrital carbonate disappearance the NADW ventilation reached its fully- interglacial state (Nicholl et al. 2012; Galaasen et al. 2014). By means of the event-stratigraphy based sub-division of MIS 5e proposed in this study into early and late intervals, it would be possible to begin to evaluate the temporal relationship (i.e. lags/leads) between the events described above more precisely over a large area such as the North Atlantic and Nordic Seas.

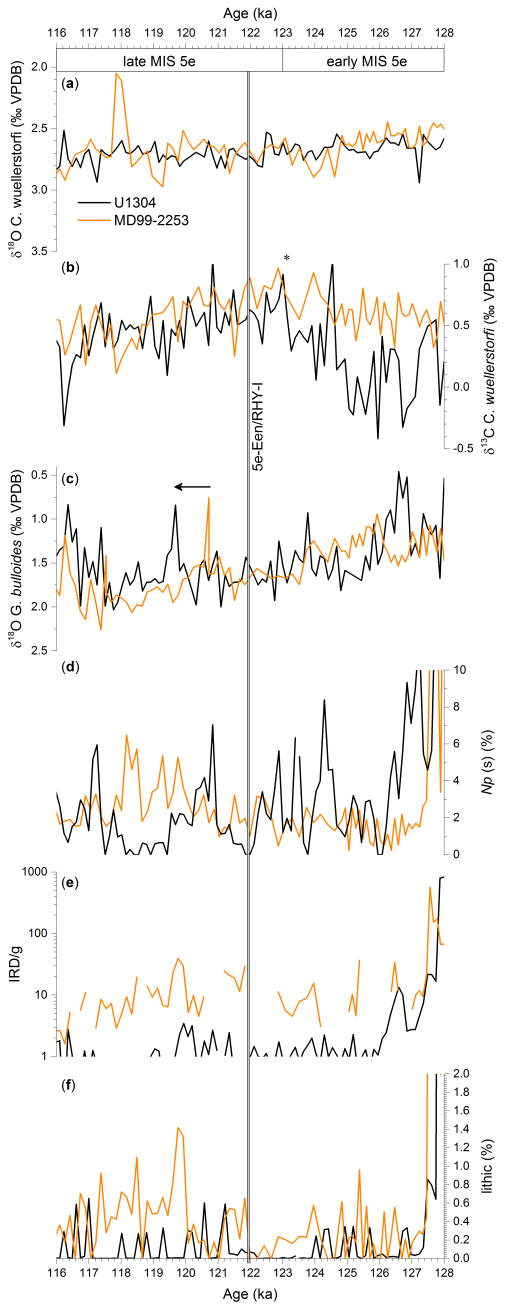

Figure 4.11 Proxy data v age from MD99-2253 (orange) and U1304 (black) on Shackleton timescale MIS 5e benthic $\delta^{18}O$ plateau (Shackleton et al. 2002; Shackleton et al. 2003) with start (128 ± 1 ka) and end (116.1 ± 0.9 ka) with the additional tie-point of the U1304 5e-Eem/RHY-I age121.99 ± 1 ka (highlighted grey). (**a**) $\delta^{18}O$ *C. wuellerstorfi*; (**b**) $\delta^{13}C$ *C. wuellerstorfi*; (**c**) *G. bulloides* $\delta^{18}O$; (**d**) percentage abundance of *Np* (s)*;* (**e**) IRD concentrations (*on log scale*); (**f**) lithic percentages. Improved alignment of $\delta^{13}C$ *C. wuellerstorfi* (*) and *G. bulloides* $\delta^{18}O$ (←). Onset of full interglacial $\delta^{13}C$ *C. wuellerstorfi* (b*) separates MIS 5e in to early MIS 5e and Late MIS 5e phase.

4.6. Conclusion

At present, core U1304 is the most southern and western marine record containing the 5e-Eem/RHY-I isochron. Based on the assigned age-depth model of U1304 we propose a revised 5e-Eem/RHY-I age of 121.99 ± 1 ka. The U1304 5e-Eem/RHY-I age is partly based on linear interpolation between well-established event-stratigraphy tie-points, constraints from sedimentation rates at the southern Gardar Drift and the associated age-uncertainties of the tie-points. The U1304 5e-Eem/RHY-I age of 121.99 ± 1 ka is in good agreement with previously published -Eem/RHY-I ages (Sejrup et al. 1989; Fronval & Jansen 1996a; Fronval et al. 1998; Rasmussen et al. 1999; Brendryen et al. 2010; Abbott et al. 2014; Davies et al. 2014). The unique position of the 5e-Eem/RHY-I isochron shortly after the onset of full-interglacial deep-ocean circulation provides an opportunity to develop a new event-stratigraphy in the North Atlantic region, which allows for the separation of MIS 5e into an early and late phase. Evidence provided by benthic $\delta^{13}C$ and $\overline{SS}$ suggest that during the early phase of MIS 5e deep-ocean ventilation was slower and sedimentation rates were lower, while during the late phase of MIS 5e the deep ocean became better ventilated and sedimentation rates increased. A mid-MIS 5e benthic $\delta^{13}C$ 'event' potentially provides the foundation for a systematic review of the MIS 5e stratigraphy of the North Atlantic and Nordic Seas. Based on the new proposed MIS 5e event-stratigraphy, other prominent short-term fluctuations of deep-ocean ventilation, such as those observed by e.g. Galaasen et al. (2014) and Hodell et al. (2009) during the late MIS 5e and changes in surface water conditions such as the cooling events described by McManus (1994) and Oppo et al. (2001), could be re-assessed and potentially lead to better understanding of the North Atlantic and Nordic Sea connections at this time. Furthermore, statistical treatments of the age-depth data, such as random walk models (e.g. Blaauw & Christeny 2011), should be the focus of future work. In particular, MIS 5e tie-point uncertainties as well as additional information to constrain potential accumulation rate changes should be included in the statistically developed age-depth models for the future; all of these would potentially lead to an improved MIS 5e chronology.

CHAPTER 5 Conclusion and future prospects

5.1. Conclusion

The aim of this thesis was to investigate the application of tephra related analyses in palaeoceanography as a tool to aid in the reconstruction of the climate during the penultimate glacial-interglacial cycle. To this end, the focus in Chapter 3 was on tephra deposits during the cold climates of the penultimate glacial (MIS 6), while Chapter 4 investigates tephra shards found during the warm interglacial (MIS 5e). The MIS 6 tephra highlight the potential of detailed shard analyses to help understand glacial ocean processes, while the MIS 5e tephra show considerable potential as chronostratigraphic markers which may allow the objective and reliable sub-division of the Last Interglacial in the North Atlantic region.

The key research questions related to the hydrology of the glacial North Atlantic and extent of the MIS 6 Icelandic Ice Sheet (IIS) (Q1 and Q2) have been addressed in Chapter 3. The detailed geochemical and shard size analyses, combined with the comparison of IIS flow models and reconstruction of glacial ocean surface circulation patterns suggested that the IIS extent and the surface ocean circulation during MIS 6 were broadly similar to the LGM. Geochemical analyses confirmed an Icelandic origin for all the tephra shards and comparison of these data with the published geochemistry of Holocene Icelandic volcanic systems allowed shards to be assigned to discrete volcanic sources. The heterogeneous composition, large shard size and IRD association of the U1304 tephra deposit found at the end of MIS 6 indicates that it was transported by iceberg-rafting processes. These detailed geochemical and shard size analyses, when combined with IIS flow models for the LGM suggest that the IIS had marine calving margins to both the north and south during the late MIS 6 and that icebergs could have been transported to Site U1304 by following surface ocean circulation patterns similar to those that prevailed during the LGM.

In Chapter 4, I investigated the possibility of an improved MIS 5e chronostratigraphy (Q3 and Q4). The analysis of tephra shards found in the MIS 5e interval of U1304 revealed that the rhyolitic shards can be associated with the 5e-Eem/RHY-I isochron. At the present time, core U1304 is the most southern and western marine record in the North Atlantic which has been shown to contain the 5e-Eem/RHY-I isochron. Based on the assigned age-depth model of U1304 we propose a revised 5e-Eem/RHY-I age of 121.99 ± 1 ka. We used this 5e-Eem/RHY-I age as an additional tie-point in Shackleton's MIS 5e age-model and applied it to the nearby MD99-2253. Comparing the climate proxy records in both cores, the U1304 and MD99-2553 data suggest that, at least in the southeast sector of the Gardar Drift, the onset of 'full' interglacial deep-ocean circulation was synchronous. The unique position of the 5e-Eem/RHY-I isochron, occurring shortly after the onset of 'full' interglacial deep-ocean circulation, provides an opportunity to develop a new event-stratigraphy in the North Atlantic region, which allows for the objective separation of MIS 5e into an early and late phase.

5.2. Future Prospects

5.2.1. Hydrology and Icelandic Ice Sheet Reconstruction

Moving beyond the simple 'Icelandic glass' descriptive concept to a quantitative characterisation assigning Icelandic tephra to potential volcanic sources would allow to test and improve established surface circulation models and would yield new information about the IIS during past glaciations. However, in order to test the validity of these glacial surface circulation models for the late MIS 6 period, more data will be required from different core sites across the North Atlantic. Some of the potential core sites from this region which are suitable for further study are identified in Chapter 3, Figure 3.9. Extending the tephra analyses described above towards application to MIS 2, a period with a tighter age-control as the MIS 6, established ISS and ocean circulation models, can potentially lead to a better understanding of ice-sheet dynamics and/or ocean surface circulation.

Using geochemical analyses and shard size analyses of tephra from different core locations in the North Atlantic would not only allow determining the mode of transport of the tephra and their source, but would also allow reconstructing the surface circulation which transported these tephra to their depositional location. The understanding of tephra transport mechanisms is of special importance for marine Quaternary research. During much of the Quaternary period, cold climate conditions prevailed over the North Atlantic and ice-rafting processes therefore represent a significant challenge for the detection of potential isochronous markers. These markers might help to establish and to improve regional tephrochronologies. However, iceberg-rafted tephra are an equally important tool in palaeoclimate studies and their potential to aid in the reconstruction of Icelandic Ice Sheets, their long-term dynamics and regional surface circulation has not been fully developed.

5.2.2. MIS 5e Chronology

A mid-MIS 5e benthic $\delta^{13}C$ 'event' potentially provides the foundation for a systematic review of the MIS 5e stratigraphy of the North Atlantic and Nordic Seas. Based on the new proposed MIS 5e event-stratigraphy, other prominent short-term fluctuations of deep-ocean ventilation, for example those observed by Galaasen et al. (2014) and Hodell et al. (2009) during the late MIS 5e, and also changes of surface water conditions within the cooling events described by McManus (1994) and Oppo et al. (2001), could be re-assessed and potentially lead to better understanding of the North Atlantic and Nordic Sea circulation at this time. Furthermore, statistical treatments of the age-depth data, such as random walk models (e.g. Blaauw & Christeny 2011), should be the focus of future work. In particular, MIS 5e tie-point uncertainties as well as additional information to constrain potential accumulation rate changes should be included in the statistically developed age-depth models of the future; all of these would potentially lead to an improved MIS 5e chronology.

CHAPTER 6 Appendix A

Probe	Si	Ti	Al	Fe	Mn	Mg	Ca	Na	K	P	S	F	Cl
TAU	Wollast-BL8	Rutile-BL8	BIR1G-BLG1	Fayalite	PuMn-BL8	Spinel-BL8	Wollast-BL8	Jadeite-BL7	Orthoclase-BL7	P K4	Pyrite-BL8	Fluorite	NaCl-BLOwn
FEEA	Quartz glass	Rutile	Corundum	Metallic Fe	Metallic Mn	Periclase	Wollastonite	Albite	Orthoclase	n.a.	n.a.	n.a.	n.a.

Table 6.1: Calibration Standard used at Tephrochronology Analytical Unit (TAU) at the Grant Institute, University of Edinburgh (Cameca SX100) and Facility of Earth & Environmental Analysis (FEEA) at the University of St Andrews (JEOL JXA 800).

Reference	SiO_2	TiO_2	Al_2O_3	FeO	MnO	MgO	CaO	Na_2O	K_2O	P_2O_5	SO_2	F	Cl	Total
a	74.03	0.08	12.72	1.75	0.08	0.00	0.72	4.06	5.18	0	n.d.	n.d.	n.d.	
b	73.72	n.d.	13.04	1.76	n.d.	0.03	0.76	4.06	5.06	n.d.	n.d.	n.d.	n.d.	

Table 6.2: Recommended values for secondary standard Lipari **a**) Sparks, R.S.J. (pers. comm. 1990) and **b**) Hunt & Hill (1996).

	SiO_2	TiO_2	Al_2O_3	FeO	MnO	MgO	CaO	Na_2O	K_2O	P_2O_5	Total
a) Recommendation	49.80	2.75	13.50	12.00	-	7.23	11.40	2.18	0.51	0.27	98.55
St Dev., σ	0.42	0.07	0.22	0.60	-	0.15	0.24	0.09	0.01	0.02	
b) Recommendation	49.30	2.78	13.60	11.3	0.17	7.13	11.4	2.40	0.51	0.29	99.00
St. Dev., σ	0.10	0.02	0.10	0.10	0.03	0.02	0.10	0.05	0.02	0.20	

Table 6.3: Recommended values and σ for the BHVO-2G(USGS) standard: **a**) USGS **b**) (Jochum et al. 2005).

	SiO_2	TiO_2	Al_2O_3	FeO	MnO	MgO	CaO	Na_2O	K_2O	P_2O_5	Total
Recommendation	54.1	2.26	13.5	12.41	n.d.	3.59	7.12	3.16	1.79	0.35	98.49
St. Dev.,σ	0.8	0.05	0.2	0.2	n.d.	0.05	0.11	0.11	0.05	0.02	

Table 6.4: Recommended values and σ for the BCR-2G (USGS) standard (Wilson 1997).

n	SiO_2	TiO_2	Al_2O_3	FeO	MnO	MgO	CaO	Na_2O	K_2O	P_2O_5	SO_2	F	Cl	Total
1	74.95	0.08	13.05	1.42	0.08	0.02	0.73	4.11	4.93	0.01	0.00	0.17	0.37	99.92
2	73.26	0.08	13.29	1.46	0.08	0.03	0.77	4.05	5.08	0.01	0.00	0.18	0.38	98.65
3	74.30	0.07	13.11	1.56	0.08	0.03	0.77	4.07	5.12	0.01	0.01	0.19	0.38	99.68
4	74.13	0.08	13.19	1.53	0.07	0.05	0.72	4.06	5.15	0.01	0.00	0.16	0.36	99.51
5	73.85	0.07	12.91	1.42	0.07	0.06	0.75	4.15	5.02	0.01	0.01	0.18	0.38	98.89
6	73.92	0.07	13.00	1.59	0.06	0.06	0.70	4.12	5.00	0.01	0.00	0.15	0.38	99.06
7	73.43	0.08	12.90	1.50	0.07	0.03	0.67	4.14	5.18	0.01	0.01	0.16	0.38	98.54
8	73.54	0.08	13.11	1.37	0.07	0.06	0.70	4.23	5.24	0.00	0.00	0.19	0.37	98.97
9	73.67	0.08	12.98	1.58	0.07	0.06	0.74	4.13	5.13	0.01	0.00	0.19	0.37	99.02
Mean	**73.89**	**0.08**	**13.06**	**1.49**	**0.07**	**0.04**	**0.73**	**4.12**	**5.09**	**0.01**	**0.00**	**0.17**	**0.37**	**99.14**
S.D.	**0.52**	**0.00**	**0.13**	**0.08**	**0.01**	**0.02**	**0.04**	**0.06**	**0.10**	**0.00**	**0.00**	**0.01**	**0.01**	

Table 6.5: Individual analyses of the secondary standard Lipari made throughout the analytical period in November 2010 at TAU (EMPA 1).

n	SiO_2	TiO_2	Al_2O_3	FeO	MnO	MgO	CaO	Na_2O	K_2O	P_2O_5	SO_2	F	Cl	Total
1	50.52	2.78	13.66	10.95	0.17	7.29	11.53	2.35	0.54	0.25	0.01	0.04	0.00	100.09
2	49.82	2.80	13.70	10.76	0.18	7.16	11.39	2.26	0.49	0.27	0.00	0.03	0.01	98.86
3	50.18	2.80	13.61	10.63	0.18	7.13	11.52	2.24	0.47	0.26	0.01	0.03	0.01	99.08
4	50.42	2.79	13.51	10.97	0.18	7.21	11.23	2.23	0.46	0.25	0.01	0.04	0.00	99.30
5	51.15	2.76	13.40	10.81	0.18	7.30	11.49	2.34	0.54	0.25	0.01	0.05	0.01	100.29
6	50.36	2.77	13.63	10.99	0.18	7.44	11.41	2.40	0.51	0.26	0.01	0.06	0.01	100.03
7	50.46	2.79	13.83	10.79	0.18	7.27	11.45	2.12	0.50	0.27	0.00	0.03	0.01	99.69
8	49.94	2.79	13.80	11.18	0.17	7.24	11.65	2.25	0.48	0.26	0.01	0.04	0.01	99.79
9	50.32	2.80	13.73	11.06	0.19	7.39	11.25	2.30	0.56	0.25	0.00	0.04	0.01	99.91
10	50.02	2.78	13.84	11.00	0.18	7.20	11.57	2.19	0.53	0.26	0.01	0.05	0.01	99.62
11	50.74	2.77	14.21	10.97	0.17	7.39	11.36	2.28	0.49	0.26	0.01	0.04	0.01	100.69
12	49.94	2.79	13.95	11.08	0.17	7.28	11.46	2.33	0.45	0.26	0.01	0.03	0.00	99.74
13	49.89	2.81	14.00	11.00	0.18	7.39	11.48	2.39	0.49	0.25	0.00	0.03	0.01	99.93
14	49.84	2.79	13.54	10.95	0.17	7.36	11.44	2.25	0.46	0.27	0.00	0.02	0.01	99.10
Mean	**50.26**	**2.79**	**13.74**	**10.94**	**0.18**	**7.29**	**11.44**	**2.28**	**0.50**	**0.26**	**0.01**	**0.04**	**0.01**	**99.72**
Median	**50.25**	**2.79**	**13.72**	**10.97**	**0.18**	**7.28**	**11.46**	**2.27**	**0.49**	**0.29**	**0.01**	**0.04**	**0.01**	**99.76**
St. Dev.	**0.39**	**0.01**	**0.22**	**0.14**	**0.01**	**0.09**	**0.11**	**0.08**	**0.03**	**0.01**	**0.00**	**0.01**	**0.00**	

Table 6.6: Individual analyses of the secondary standard BHVO-2G made throughout the analytical period in November 2010 at TAU (EMPA 1).

n	SiO_2	TiO_2	Al_2O_3	FeO	MnO	MgO	CaO	Na_2O	K_2O	Total
1	48.70	2.65	13.46	10.48	0.20	6.91	10.83	2.29	0.54	96.07
2	49.23	2.92	13.04	10.82	0.12	7.05	10.87	2.28	0.51	96.83
3	49.44	2.76	13.47	10.85	0.24	6.85	10.98	2.18	0.54	97.30
4	49.49	2.89	13.59	10.70	0.31	6.93	11.06	2.16	0.47	97.61
5	49.66	2.85	13.48	10.27	0.26	6.99	10.99	2.30	0.51	97.33
6	49.65	2.64	13.63	10.58	0.22	7.01	10.73	1.96	0.47	96.91
7	49.64	2.86	13.41	10.76	0.23	7.09	10.77	2.45	0.47	97.70
8	49.84	2.68	13.44	10.50	0.23	6.72	11.05	2.38	0.58	97.41
9	49.28	2.76	13.48	10.48	0.29	7.12	11.08	2.25	0.53	97.26
10	49.86	2.57	13.56	10.98	0.17	7.01	10.90	2.22	0.47	97.73
11	49.38	2.64	13.63	10.86	0.24	6.98	10.91	2.22	0.49	97.35
12	48.78	2.84	13.39	10.69	0.12	7.06	10.86	2.36	0.52	96.62
13	48.92	2.83	13.16	11.13	0.23	7.09	10.90	1.72	0.53	96.51
14	49.72	2.84	13.49	10.86	0.24	6.82	11.11	2.22	0.52	97.81
15	49.62	2.82	13.59	10.65	0.04	6.95	11.03	2.45	0.55	97.69
16	49.49	2.73	13.29	10.60	0.08	7.01	10.79	2.08	0.53	96.60
17	50.10	2.89	13.57	10.80	0.09	6.93	11.09	1.79	0.51	97.77
18	49.61	2.74	13.64	10.37	0.09	6.72	11.15	2.20	0.51	97.03
19	49.75	2.74	13.59	10.54	0.11	6.81	10.90	2.13	0.50	97.08
20	48.72	2.60	13.44	10.78	0.08	6.96	11.24	2.06	0.52	96.40
21	49.81	2.69	13.59	10.96	0.16	6.90	11.11	2.16	0.52	97.89
22	49.69	2.93	13.29	10.29	0.19	6.94	10.83	1.83	0.48	96.48
23	49.29	2.61	13.10	10.63	0.10	6.99	10.90	2.20	0.54	96.35
24	49.44	2.61	13.30	10.95	0.18	6.93	11.18	1.30	0.56	96.45
25	49.79	2.68	13.59	10.61	0.09	7.00	11.13	2.20	0.56	97.64
26	49.78	2.69	13.47	10.87	0.12	7.05	11.20	2.32	0.60	98.10
27	49.18	2.79	13.59	10.97	0.27	7.11	11.04	2.61	0.61	98.17
28	49.06	2.82	13.35	10.92	0.16	7.04	10.96	1.98	0.41	96.70
29	49.56	2.59	13.69	10.65	0.26	6.95	11.21	2.25	0.53	97.69
30	49.36	2.84	13.53	10.91	0.11	6.92	10.92	2.00	0.58	97.16
31	48.89	2.78	13.24	10.96	0.13	6.86	10.97	2.17	0.52	96.52
32	49.11	2.70	13.25	10.53	0.14	6.91	11.14	2.28	0.53	96.58
33	48.41	2.51	13.28	10.55	0.12	6.82	10.72	2.17	0.45	95.03
34	49.14	2.61	13.44	10.07	0.27	7.16	10.89	2.09	0.52	96.19
Mean	49.39	2.74	13.44	10.69	0.17	6.96	10.98	2.15	0.52	97.06
Median	49.47	2.74	13.47	10.70	0.17	6.95	10.98	2.20	0.52	97.12
St. Dev.	0.40	0.11	0.16	0.24	0.07	0.11	0.14	0.24	0.04	

Table 6.7: Individual analyses of the secondary standard BHVO-2G made throughout the analytical period in July 2011 at FEEA (EMPA 2).

n	SiO_2	TiO_2	Al_2O_3	FeO	MnO	MgO	CaO	Na_2O	K_2O	P_2O_5	Total
1	73.76	0.08	12.83	1.63	0.07	0.05	0.75	5.11	4.14	0.01	98.42
2	73.04	0.08	12.92	1.67	0.07	0.05	0.67	5.28	4.02	0.01	97.80
3	73.12	0.08	12.67	1.48	0.08	0.05	0.85	5.22	3.94	0.02	97.51
Mean	73.30	0.08	12.81	1.59	0.07	0.05	0.75	5.21	4.03	0.01	97.91
St. Dev.	0.32	0.00	0.11	0.08	0.00	0.00	0.07	0.07	0.08	0.00	

Table 6.8: Individual analyses of the secondary standard Lipari made throughout the analytical period in May 2012 at TAU (EMPA 3).

n	SiO_2	TiO_2	Al_2O_3	FeO	MnO	MgO	CaO	Na_2O	K_2O	P_2O_5	Total
1	54.30	2.25	13.12	3.60	1.85	6.88	0.20	3.30	12.25	0.34	98.11
2	53.12	2.27	13.83	3.63	1.78	6.94	0.21	3.21	12.47	0.35	97.80
3	54.65	2.30	13.22	3.63	1.82	7.11	0.21	3.20	12.61	0.35	99.08
Mean	54.02	2.27	13.39	3.62	1.82	6.98	0.20	3.24	12.44	0.34	98.33
St. Dev.	0.65	0.02	0.31	0.01	0.03	0.10	0.00	0.04	0.15	0.00	

Table 6.9: Individual analyses of the secondary standard BCR-2G made throughout the analytical period in May 2012 at TAU (EMPA 3).

n	SiO_2	TiO_2	Al_2O_3	FeO	MnO	MgO	CaO	Na_2O	K_2O	P_2O_5	Total
1	73.31	0.09	12.96	1.52	0.06	0.06	0.66	4.37	5.22	0.00	98.24
2	72.38	0.07	13.43	1.64	0.06	0.04	0.85	4.11	4.99	0.00	97.57
3	73.04	0.07	13.07	1.44	0.05	0.04	0.74	4.33	5.22	0.01	98.01
4	73.63	0.08	13.28	1.59	0.07	0.05	0.82	4.09	5.18	0.00	98.78
5	72.67	0.08	12.94	1.40	0.06	0.06	0.69	4.41	5.05	0.01	97.38
6	73.37	0.07	12.99	1.42	0.06	0.02	0.79	4.40	5.13	0.01	98.27
7	72.53	0.08	13.08	1.52	0.08	0.06	0.80	4.24	5.28	0.01	97.67
8	72.66	0.09	13.31	1.56	0.06	0.03	0.72	4.30	5.11	0.01	97.84
9	73.63	0.08	12.83	1.45	0.08	0.04	0.74	4.27	4.98	0.01	98.10
10	73.74	0.08	13.24	1.43	0.07	0.05	0.68	4.44	5.24	0.01	98.98
11	73.14	0.07	13.16	1.65	0.07	0.05	0.75	4.41	5.10	0.00	98.39
12	73.58	0.08	13.08	1.49	0.08	0.04	0.71	4.42	5.30	0.00	98.78
Mean	73.14	0.08	13.12	1.51	0.07	0.05	0.75	4.31	5.15	0.01	98.17
St. Dev.	0.46	0.00	0.17	0.08	0.01	0.01	0.06	0.11	0.10	0.00	

Table 6.10: Individual analyses of the secondary standard Lipari made throughout the analytical period in June 2012 at TAU (EMPA 4).

n	SiO_2	TiO_2	Al_2O_3	FeO	MnO	MgO	CaO	Na_2O	K_2O	P_2O_5	Total
1	53.18	2.25	13.72	12.35	0.19	3.57	7.22	3.48	1.75	0.29	98.00
2	53.37	2.25	13.84	12.60	0.19	3.65	7.23	3.39	1.81	0.29	98.61
3	53.29	2.28	13.65	12.46	0.19	3.67	7.26	3.62	1.77	0.28	98.46
4	53.99	2.30	13.84	12.32	0.20	3.54	7.52	3.65	1.72	0.29	99.38
5	53.36	2.28	13.69	12.22	0.19	3.54	7.61	3.52	1.81	0.27	98.48
6	53.29	2.30	14.21	12.83	0.20	3.58	7.48	3.50	1.85	0.27	99.51
7	54.31	2.28	13.40	12.24	0.19	3.58	7.52	3.54	1.85	0.26	99.17
8	53.67	2.27	13.44	12.13	0.20	3.50	7.29	3.62	1.85	0.26	98.23
Mean	53.56	2.28	13.72	12.39	0.19	3.58	7.39	3.54	1.80	0.28	98.73
St. Dev.	0.37	0.02	0.24	0.21	0.00	0.05	0.15	0.08	0.05	0.01	

Table 6.11: Individual analyses of the secondary standard BCR-2G made throughout the analytical period in June 2012 at TAU (EMPA 4).

n	SiO_2	TiO_2	Al_2O_3	FeO	MnO	MgO	CaO	Na_2O	K_2O	P_2O_5	Total
1	73.91	0.08	12.86	1.72	0.07	0.05	0.72	4.16	5.16	0.00	98.72
2	74.18	0.08	13.03	1.50	0.07	0.04	0.75	4.25	5.09	0.01	99.00
3	74.26	0.08	12.87	1.61	0.07	0.04	0.67	4.05	5.26	0.01	98.91
4	74.30	0.08	13.20	1.46	0.07	0.05	0.69	4.18	5.13	0.01	99.18
5	74.74	0.08	13.05	1.70	0.07	0.02	0.75	4.11	5.23	0.01	99.78
6	74.74	0.08	12.75	1.47	0.07	0.03	0.72	4.18	5.29	-0.01	99.31
7	73.76	0.07	13.00	1.57	0.06	0.07	0.71	4.15	5.31	0.01	98.71
8	75.50	0.09	12.82	1.60	0.06	0.05	0.78	4.10	5.23	0.00	100.22
9	74.30	0.08	13.31	1.55	0.07	0.05	0.74	4.03	4.98	0.00	99.11
10	74.22	0.07	13.37	1.63	0.06	0.05	0.74	4.14	5.24	0.01	99.54
Mean	74.39	0.08	13.03	1.58	0.07	0.04	0.73	4.13	5.19	0.01	99.25
St. Dev.	0.47	0.00	0.20	0.09	0.00	0.01	0.03	0.06	0.10	0.01	

Table 6.12: Individual analyses of the secondary standard Lipari made throughout the analytical period in March 2015 at TAU (EMPA 5).

n	SiO_2	TiO_2	Al_2O_3	FeO	MnO	MgO	CaO	Na_2O	K_2O	P_2O_5	Total
1	49.68	2.72	13.39	11.12	0.18	7.27	11.75	2.32	0.52	0.28	99.21
2	50.18	2.71	13.27	11.21	0.16	7.38	11.33	2.37	0.52	0.27	99.41
3	49.90	2.70	13.49	10.86	0.16	7.23	11.75	2.23	0.49	0.26	99.08
4	49.80	2.71	13.10	10.92	0.16	7.25	11.39	2.34	0.56	0.27	98.49
5	50.14	2.71	13.31	11.20	0.17	7.31	11.58	2.45	0.54	0.27	99.68
6	50.19	2.69	13.34	11.40	0.18	7.32	11.55	2.28	0.51	0.28	99.72
7	49.98	2.71	13.50	11.48	0.15	7.32	11.36	2.34	0.56	0.27	99.67
8	49.26	2.72	13.57	11.18	0.18	7.33	11.44	2.26	0.53	0.28	98.74
9	49.80	2.72	13.83	10.97	0.17	7.19	11.56	2.33	0.55	0.27	99.40
10	50.18	2.72	13.44	11.09	0.16	7.29	11.48	2.26	0.54	0.26	99.41
Mean	49.91	2.71	13.43	11.14	0.17	7.29	11.52	2.32	0.53	0.27	99.28
St. Dev.	0.28	0.01	0.19	0.19	0.01	0.05	0.14	0.06	0.02	0.01	

Table 6.13: Individual analyses of the secondary standard BHVO-2G made throughout the analytical period in March 2015 at TAU (EMPA 5).

n	SiO_2	TiO_2	Al_2O_3	FeO	MnO	MgO	CaO	Na_2O	K_2O	P_2O_5	Total
1	53.85	2.24	13.41	12.99	0.20	3.68	7.13	3.31	1.81	0.36	98.98
2	52.96	2.25	12.87	12.91	0.21	3.62	7.19	3.45	1.73	0.39	97.58
3	53.65	2.26	13.21	12.41	0.20	3.63	7.12	3.42	1.78	0.35	98.03
4	52.69	2.25	13.27	12.76	0.22	3.51	7.04	3.31	1.85	0.37	97.27
5	53.46	2.26	12.82	12.34	0.19	3.59	7.21	3.35	1.86	0.37	97.44
6	53.35	2.25	13.03	12.75	0.21	3.69	7.03	3.35	1.88	0.34	97.87
7	54.21	2.27	13.16	12.32	0.20	3.53	7.07	3.45	1.94	0.37	98.53
8	54.24	2.27	12.97	12.24	0.20	3.68	7.08	3.31	1.80	0.37	98.16
9	54.42	2.28	13.36	12.49	0.20	3.78	6.88	3.26	1.83	0.36	98.86
10	54.87	2.29	13.43	12.55	0.20	3.51	7.05	3.29	1.82	0.37	99.38
Mean	53.77	2.26	13.15	12.58	0.20	3.62	7.08	3.35	1.83	0.37	98.21
St. Dev.	0.65	0.02	0.21	0.25	0.01	0.08	0.09	0.06	0.06	0.01	

Table 6.14: Individual analyses of the secondary standard BCR-2G made throughout the analytical period in March 2015 at TAU (EMPA 5).

6.1. Accuracy of the Wavelength Dispersive Spectrometers

----------This material is unavailable due to copyright restrictions----------

	JEOL JXA 800	USGS	Cameca SX100
JEOL JXA 800	1.00	0.98	0.96
USGS		1.00	0.99
Cameca SX100			1.00

Table 6.15: Similarity coefficient between electron microprobe Cameca SX100, JEOL JXA 800 and recommended values for BHVO-2G on the basis of seven oxides with a weight % greater than 1 (SiO_2, TiO_2, Al_2O_3, FeO, TiO, MgO, CaO, Na_2O).

	JEOL JXA 800	USGS	Cameca SX100
JEOL JXA 800	0.00	5.14	16.72
USGS		0.00	2.52
Cameca SX100			0.00

Table 6.16: Calculated D2 of statistical distance function between electron microprobe Cameca SX100, JEOL JXA 800 and recommended values from the USGS for BHVO-2G on the basis of oxide mean and standard deviation. Eight oxides (SiO_2, TiO_2, Al_2O_3, FeO, TiO, MgO, CaO, Na_2O, K_2O) with a weight % greater than 0.1 were used, which gives a D^2 critical of 20.09 (99 % confidence level)

CHAPTER 7 Appendix B

	2317A	2317B	2317C	2322A	2322B	2322C	2322D	2327A	2327B	2327C	2327D	2327F	2332A	2332B	2332C	2332D	2332E	2332F	2332G
2317A	0.00	78.24	100.39	3.79	118.49	160.20	40.63	99.25	726.09	240.3	131.49	57.56	3.08	32.79	312.39	224.59	532.1	553.73	522.57
2317B		0.00	90.92	82.45	218.69	270.41	128.46	224.11	921.75	390.25	252.48	23.83	95.53	140.09	553.07	367.23	817.82	680.21	651.99
2317C			0.00	92.34	82.37	155.30	43.07	96.45	575.72	182.44	156.66	59.99	116.25	104.87	222.72	166.80	315.21	482.93	410.92
2322A				0.00	94.59	130.1	34.01	82.37	625.21	210.40	116.16	57.84	1.02	21.89	209.37	176.18	376.17	468.59	405.38
2322B					0.00	19.72	16.92	&1.20	189.48	36.77	14.38	113.93	132.96	16.90	2.46	26.49	61.04	131.5	91.09
2322C						0.00	43.28	16.78	35.98	2.56	1.37	146.12	148.56	72.29	24.30	3.71	4.02	31.09	8.10
2322D							0.00	15.05	274.14	75.77	36.19	83.25	44.16	2.00	31.45	68.31	124.33	193.18	151.15
2327A								0.00	136.10	25.82	12.34	116.23	111.86	18.87	1.64	22.62	49.85	122.60	72.91
2327B									0.00	28.50	52.54	272.51	762.27	373.65	313.47	86.23	64.13	&1.52	26.35
2327C										0.00	6.22	173.81	219.88	90.25	45.76	15.64	6.00	24.66	4.29
2327D											0.00	145.39	132.12	53.92	15.78	1.70	6.76	46.96	16.80
2317F												0.00	60.32	76.34	137.28	157.64	196.63	260.11	221.79
2332A													0.00	29.65	339.41	231.96	442.73	602.10	565.95
2332B														0.00	99.79	61.9	190.13	365.40	291.04
2332C															0.00	31.07	130.23	229.84	152.73
2332D																0.00	15.35	63.04	34.89
2332E																	0.00	47.43	19.96
2332F																		0.00	22.7
2332G																			0.00

Table 7.1: Table shows the result of the statistical distance function for each sample depth. The D^2 values were calculated from nine oxides (SiO_2, TiO_2, Al_2O_3, FeO, MnO, MgO, CaO, Na_2O, K_2O), which gives a D^2 critical from 21.67 (99 % confidence level). Only populations comprising more than two shards were included in this test. Intra-depth comparison shows that none of the populations found in these same depth are identical (see Chapter 3).

	2317A	2317B	2317C	2322A	2322B	2322C	2322D	2327A	2327B	2327C	2327D	2327F	2332A	2332B	2332C	2332D	2332E	2332F	2332G
2317A	1.00	0.98	0.94	0.99	0.90	0.87	0.95	0.91	0.80	0.85	0.88	0.92	0.99	0.95	0.90	0.88	0.85	0.80	0.83
2317B		1.00	0.93	0.98	0.89	0.85	0.93	0.90	0.79	0.84	0.86	0.93	0.97	0.93	0.88	0.86	0.84	0.79	0.82
2317C			1.00	0.94	0.95	0.91	0.98	0.96	0.84	0.89	0.92	0.87	0.94	0.96	0.94	0.92	0.90	0.84	0.87
2322A				1.00	0.90	0.87	0.95	0.91	0.80	0.85	0.88	0.91	0.99	0.95	0.90	0.88	0.85	0.80	0.83
2322B					1.00	0.95	0.95	0.98	0.88	0.94	0.96	0.83	0.91	0.95	0.99	0.97	0.94	0.88	0.92
2322C						1.001	0.91	0.95	0.92	0.98	0.99	0.80	0.87	0.91	0.96	0.98	0.98	0.92	0.96
2322D							1.00	0.96	0.84	0.90	0.92	0.87	0.95	0.99	0.95	0.93	0.90	0.84	0.87
2327A								1.00	0.87	0.93	0.96	0.84	0.92	0.96	0.98	0.96	0.93	0.87	0.91
2327B									1.00	0.94	0.91	0.74	0.80	0.84	0.88	0.91	0.93	0.99	0.96
2327C										1.00	0.97	0.78	0.85	0.89	0.94	0.96	0.98	0.94	0.97
2327D											1.00	0.81	0.88	0.92	0.97	0.99	0.97	0.91	0.95
2317F												1.00	0.91	0.87	0.83	0.81	0.79	0.74	0.77
2332A													1.00	0.95	0.91	0.88	0.86	0.80	0.83
2332B														1.00	0.95	0.92	0.90	0.84	0.87
2332C															1.00	0.97	0.94	0.89	0.92
2332D																1.00	0.97	0.91	0.95
2332E																	1.00	0.94	0.97
2332F																		1.00	0.96
2332G																			1.00

Table 7.2: Similarity coefficient (SC) for populations found in different sample depths. Six oxides were used to calculate the SC and only populations consisting of at least two shards were included. Even though, the SC between different populations is very high, i.e. larger than 0.95, they are not considered to be similar as the statistical distance function (Table 7.1) rejects the null-hypothesis that they are identical (Chapter 2 Statistical Tests). Only oxides with a weight % greater than 1 were used (SiO_2, Al_2O_3, FeO, MgO, CaO, Na_2O).

SiO_2	TiO_2	Al_2O_3	FeO	MnO	MgO	CaO	Na_2O	K_2O	P_2O_5	SO_2	F	Cl	Total	Probe	Source	n
51.76	2.03	13.23	14.27	0.27	5.57	9.80	2.80	0.27	n.a	n.a	n.a	n.a	100	FEEA	KVS	2
51.20	1.98	13.36	14.31	0.27	5.80	10.02	2.73	0.33	n.a	n.a	n.a	n.a	100	FEEA	KVS	1
51.35	1.93	13.39	14.63	0.35	5.79	9.87	2.38	0.32	n.a	n.a	n.a	n.a	100	FEEA	KVS	1
50.43	2.10	13.08	14.42	0.25	5.79	10.25	2.77	0.33	0.23	0.24	0.04	0.06	100	TAU	KVS	1
50.90	2.08	13.35	14.14	0.24	5.58	10.13	2.73	0.32	0.22	0.22	0.04	0.06	100	TAU	KVS	1
50.76	2.06	13.24	14.22	0.24	5.88	10.09	2.67	0.30	0.23	0.22	0.04	0.06	100	TAU	KVS	1
50.97	2.08	13.36	14.42	0.25	5.60	10.02	2.51	0.29	0.22	0.19	0.05	0.05	100	TAU	KVS	1
50.61	3.11	13.26	14.37	0.25	5.45	9.69	2.87	0.39	n.a.	n.a.	n.a.	n.a.	100	FEEA	GVS	1
50.64	3.26	13.16	14.04	0.18	5.63	9.89	2.74	0.46	n.a.	n.a.	n.a.	n.a.	100	FEEA	GVS	4
51.11	3.38	13.11	14.15	0.21	5.28	9.73	2.63	0.40	n.a.	n.a.	n.a.	n.a.	100	FEEA	GVS	1
50.47	2.81	13.92	12.66	0.20	6.16	10.67	2.74	0.38	n.a	n.a	n.a	n.a	100	FEEA	GVS	1
50.71	2.77	14.06	12.23	0.21	6.31	10.74	2.61	0.36	n.a	n.a	n.a	n.a	100	FEEA	GVS	2
50.58	2.58	13.94	12.36	0.24	6.29	10.75	2.90	0.35	n.a	n.a	n.a	n.a	100	FEEA	GVS	1
50.39	2.71	13.89	12.61	0.34	6.24	10.75	2.61	0.46	n.a	n.a	n.a	n.a	100	FEEA	GVS	1
50.32	2.85	13.69	13.34	0.22	6.11	10.29	2.81	0.37	n.a	n.a	n.a	n.a	100	FEEA	GVS	4
50.78	2.72	13.84	12.44	0.19	6.24	10.79	2.62	0.38	n.a	n.a	n.a	n.a	100	FEEA	GVS	3
49.71	2.70	13.95	12.78	0.23	6.35	10.81	2.65	0.35	0.29	0.14	0.03	0.01	100	TAU	GVS	1
46.84	5.02	12.61	14.89	0.32	6.92	9.64	3.10	0.66	n.a	n.a	n.a	n.a	100	FEEA	Trans	3
51.95	2.10	13.49	13.83	0.21	5.64	9.86	2.64	0.30	n.a.	n.a.	n.a.	n.a.	100	FEEA	KVS	5
51.84	2.11	13.31	14.76	0.20	5.41	9.49	2.57	0.30	n.a.	n.a.	n.a.	n.a.	100	FEEA	KVS	1
51.66	1.99	13.48	13.82	0.33	5.71	9.85	2.88	0.28	n.a.	n.a.	n.a.	n.a.	100	FEEA	KVS	5

Table 7.3: Mean major oxide concentrations of U1304 tephra shards found in the sample depth: 23.17 mcd, 23.22 mcd, 23.27 mcd and 23.32 mcd. (Normalised to 100 weight %). n: number of analysed points which are used to calculate the mean concentration of a certain shard. Probe: Tephrochronology Analytical Unit (TAU) at the Grant Institute, University of Edinburgh (Cameca SX100) and Facility of Earth & Environmental Analysis (FEEA) at the University of St Andrews (JEOL JXA 800). Source: Krafla volcano system (KVS), Grímsvötn volcano system (GVS), Veidivötn-Bárdarbunga volcano system (VBVS), Western volcanic zone (WVZ), Trans: shards belong to the Transitional-alkalic series; no further investigation regarding volcanic source were made. All oxides are presented as weight %.

z	TiO_2	Al_2O_3	FeO	MnO	MgO	CaO	Na_2O	K_2O	P_2O_5	SO_2	F	Cl	Total	Probe	Source	n
99	2.00	13.31	14.11	0.51	5.61	9.78	2.38	0.32	n.a.	n.a.	n.a.	n.a.	100	FEEA	KVS	1
80	2.07	13.52	13.76	0.24	5.55	9.89	2.90	0.28	n.a.	n.a.	n.a.	n.a.	100	FEEA	KVS	5
90	2.14	13.46	13.87	0.19	5.79	9.79	2.57	0.29	n.a.	n.a.	n.a.	n.a.	100	FEEA	KVS	1
93	2.02	13.49	14.07	0.20	5.60	9.97	2.51	0.22	n.a.	n.a.	n.a.	n.a.	100	FEEA	KVS	1
66	2.02	13.32	14.18	0.24	5.89	10.30	2.65	0.27	0.22	0.17	0.03	0.06	100	TAU	KVS	1
51	1.50	14.22	12.35	0.25	6.82	11.16	1.97	0.22	n.a.	n.a.	n.a.	n.a.	100	FEEA	VBVS	1
19	1.57	13.94	12.70	0.23	6.64	10.86	2.61	0.27	n.a.	n.a.	n.a.	n.a.	100	FEEA	VBVS	1
37	1.42	13.98	13.01	0.23	6.73	11.11	1.96	0.19	n.a.	n.a.	n.a.	n.a.	100	FEEA	VBVS	1
54	1.76	14.08	12.71	0.25	6.90	11.32	2.24	0.21	n.a.	n.a.	n.a.	n.a.	100	FEEA	VBVS	1
03	1.82	13.89	12.85	0.15	6.70	11.08	2.26	0.21	n.a.	n.a.	n.a.	n.a.	100	FEEA	VBVS	1
50	1.57	13.95	12.50	0.23	6.76	11.00	2.29	0.21	n.a.	n.a.	n.a.	n.a.	100	FEEA	VBVS	5
93	1.70	14.20	11.89	0.24	6.74	10.73	2.35	0.23	n.a.	n.a.	n.a.	n.a.	100	FEEA	VBVS	1
97	1.52	14.02	11.79	0.10	7.16	12.06	2.23	0.15	n.a.	n.a.	n.a.	n.a.	100	FEEA	VBVS	1
00	1.18	13.95	12.08	0.18	7.25	11.54	2.65	0.17	n.a.	n.a.	n.a.	n.a.	100	FEEA	VBVS	1
56	1.42	13.84	11.65	0.20	7.08	11.63	2.49	0.14	n.a.	n.a.	n.a.	n.a.	100	FEEA	VBVS	1
01	1.33	14.43	11.19	0.25	7.50	11.97	2.18	0.14	n.a.	n.a.	n.a.	n.a.	100	FEEA	VBVS	5
43	1.31	14.50	11.39	0.21	7.50	11.98	2.12	0.19	0.16	0.16	0.02	0.03	100	TAU	VBVS	1
12	1.25	14.46	10.77	0.20	7.90	12.71	2.08	0.16	0.12	0.18	0.02	0.02	100	TAU	VBVS	1
52	1.84	13.79	13.11	0.27	6.32	10.35	2.53	0.28	n.a.	n.a.	n.a.	n.a.	100	FEEA	VBVS	5
52	1.90	13.56	12.69	0.34	6.36	10.77	2.66	0.22	n.a.	n.a.	n.a.	n.a.	100	FEEA	VBVS	1
71	1.97	13.79	12.67	0.17	6.25	10.59	2.58	0.27	n.a.	n.a.	n.a.	n.a.	100	FEEA	VBVS	1
00	1.78	13.90	12.93	0.24	6.33	10.72	2.86	0.24	n.a.	n.a.	n.a.	n.a.	100	FEEA	VBVS	1
42	1.86	13.79	13.47	0.24	6.42	10.46	2.14	0.20	n.a.	n.a.	n.a.	n.a.	100	FEEA	VBVS	1
52	1.57	13.97	12.84	0.23	6.27	10.72	2.67	0.22	n.a.	n.a.	n.a.	n.a.	100	FEEA	VBVS	1

Table 7.3 continued

SiO_2	TiO_2	Al_2O_3	FeO	MnO	MgO	CaO	Na_2O	K_2O	P_2O_5	SO_2	F	Cl	Total	Probe	Source	n
51.96	1.56	13.94	12.37	0.05	6.48	10.86	2.51	0.26	n.a.	n.a.	n.a.	n.a.	100	FEEA	VBVS	1
50.03	1.82	13.73	13.75	0.24	6.42	10.84	2.47	0.22	0.19	0.20	0.04	0.06	100	TAU	VBVS	1
50.38	1.90	13.64	13.94	0.24	6.14	10.54	2.45	0.27	0.20	0.22	0.04	0.04	100	TAU	VBVS	1
50.04	1.86	13.72	13.83	0.24	6.44	10.66	2.46	0.29	0.21	0.20	0.01	0.04	100	TAU	VBVS	1
48.01	5.14	12.74	15.11	0.20	5.17	10.18	2.90	0.56	n.a.	n.a.	n.a.	n.a.	100	FEEA	Trans	1
47.78	4.98	13.03	14.60	0.32	5.23	10.08	3.30	0.68	n.a.	n.a.	n.a.	n.a.	100	FEEA	Trans	1
50.68	3.26	13.12	14.90	0.16	5.29	9.45	2.69	0.45	n.a.	n.a.	n.a.	n.a.	100	FEEA	GVS	1
49.45	2.96	13.63	13.31	0.23	6.15	10.77	2.60	0.38	0.30	0.16	0.05	0.02	100	TAU	GVS	1
51.36	1.63	14.23	12.14	0.19	6.88	11.02	2.32	0.23	n.a.	n.a.	n.a.	n.a.	100	FEEA	VBVS	2
51.34	1.49	14.16	12.56	0.07	6.73	11.21	2.21	0.23	n.a.	n.a.	n.a.	n.a.	100	FEEA	VBVS	1
51.28	1.56	14.00	12.24	0.24	6.76	11.10	2.58	0.24	n.a.	n.a.	n.a.	n.a.	100	FEEA	VBVS	3
51.49	1.53	14.02	11.96	0.23	6.78	11.05	2.71	0.22	n.a.	n.a.	n.a.	n.a.	100	FEEA	VBVS	5
51.41	1.48	14.25	11.83	0.21	6.94	11.12	2.53	0.23	n.a.	n.a.	n.a.	n.a.	100	FEEA	VBVS	2
51.41	1.47	14.11	11.94	0.30	6.92	11.05	2.59	0.22	n.a.	n.a.	n.a.	n.a.	100	FEEA	VBVS	2
51.46	1.54	14.02	12.04	0.16	6.94	11.09	2.55	0.19	n.a.	n.a.	n.a.	n.a.	100	FEEA	VBVS	3
51.22	1.76	14.12	12.48	0.19	6.60	10.83	2.55	0.26	n.a.	n.a.	n.a.	n.a.	100	FEEA	VBVS	3
51.53	1.42	14.19	11.72	0.23	6.98	11.40	2.32	0.21	n.a.	n.a.	n.a.	n.a.	100	FEEA	VBVS	2
51.57	1.38	14.13	11.92	0.27	6.86	11.23	2.43	0.21	n.a.	n.a.	n.a.	n.a.	100	FEEA	VBVS	2
50.67	1.63	13.63	12.77	0.22	6.58	11.35	2.46	0.26	0.18	0.16	0.04	0.04	100	TAU	VBVS	1
50.64	1.77	13.46	13.06	0.23	6.81	11.11	2.26	0.25	0.20	0.12	0.03	0.06	100	TAU	VBVS	1
50.15	1.66	13.78	13.39	0.22	6.53	11.16	2.47	0.24	0.19	0.14	0.04	0.04	100	TAU	VBVS	1
51.20	1.57	13.27	12.90	0.23	6.87	11.12	2.25	0.19	0.18	0.16	0.03	0.04	100	TAU	VBVS	1
51.24	0.85	14.68	9.54	0.26	8.27	13.40	1.70	0.05	n.a.	n.a.	n.a.	n.a.	100	FEEA	WVZ	2
50.82	0.89	14.85	10.05	0.16	8.31	12.84	1.98	0.10	n.a.	n.a.	n.a.	n.a.	100	FEEA	WVZ	2

Table 7.3 continued

SiO_2	TiO_2	Al_2O_3	FeO	MnO	MgO	CaO	Na_2O	K_2O	P_2O_5	SO_2	F	Cl	Total	Probe	Source	n
50.94	0.96	14.70	10.16	0.25	8.03	12.74	2.07	0.13	n.a.	n.a.	n.a.	n.a.	100	FEEA	WVZ	2
51.02	1.00	14.72	10.06	0.19	8.09	12.76	2.04	0.12	n.a.	n.a.	n.a.	n.a.	100	FEEA	WVZ	3
50.96	1.22	14.39	10.76	0.17	7.92	12.25	2.14	0.19	n.a.	n.a.	n.a.	n.a.	100	FEEA	VBVS	2
50.98	1.49	14.53	11.23	0.11	7.33	11.65	2.44	0.23	n.a.	n.a.	n.a.	n.a.	100	FEEA	VBVS	3
51.20	1.22	14.37	11.33	0.31	7.43	11.80	2.18	0.15	n.a.	n.a.	n.a.	n.a.	100	FEEA	VBVS	2
51.34	1.21	14.63	10.34	0.20	7.62	12.40	2.06	0.20	n.a.	n.a.	n.a.	n.a.	100	FEEA	VBVS	2
51.22	1.35	14.56	11.13	0.17	7.49	11.76	2.18	0.14	n.a.	n.a.	n.a.	n.a.	100	FEEA	VBVS	2
51.05	1.40	14.04	12.39	0.19	7.24	11.41	2.15	0.14	n.a.	n.a.	n.a.	n.a.	100	FEEA	VBVS	2
50.96	1.43	14.25	11.98	0.10	7.17	11.65	2.27	0.19	n.a.	n.a.	n.a.	n.a.	100	FEEA	VBVS	2
51.42	1.31	13.41	11.32	0.22	7.81	12.02	2.38	0.11	n.a.	n.a.	n.a.	n.a.	100	FEEA	VBVS	3
50.07	1.54	13.98	11.84	0.22	7.45	12.07	2.25	0.19	0.16	0.17	0.02	0.03	100	TAU	VBVS	1
48.31	4.98	13.17	14.52	0.30	5.06	9.80	3.19	0.67	n.a.	n.a.	n.a.	n.a.	100	FEEA	Trans	5
50.30	4.14	13.71	13.80	0.17	4.31	8.98	3.63	0.96	n.a.	n.a.	n.a.	n.a.	100	FEEA	Trans	2
48.77	4.78	12.87	15.22	0.20	4.89	9.40	3.22	0.65	n.a.	n.a.	n.a.	n.a.	100	FEEA	Trans	1
46.99	4.67	13.06	15.05	0.26	4.86	9.57	3.38	0.77	0.88	0.33	0.14	0.04	100	TAU	Trans	1
50.44	3.14	13.01	14.83	0.22	5.37	9.62	2.94	0.42	n.a.	n.a.	n.a.	n.a.	100	FEEA	-	2
51.61	2.17	13.27	14.13	0.27	5.63	9.79	2.86	0.28	n.a.	n.a.	n.a.	n.a.	100	FEEA	-	2
51.15	2.05	13.19	14.17	0.25	5.75	10.11	2.50	0.28	0.22	0.23	0.05	0.06	100	TAU	-	1
51.56	1.97	13.43	14.73	0.34	5.62	9.69	2.36	0.31	n.a.	n.a.	n.a.	n.a.	100	FEEA	KVS	1
51.86	2.02	13.52	13.77	0.19	5.68	9.91	2.72	0.32	n.a.	n.a.	n.a.	n.a.	100	FEEA	KVS	5
51.41	2.04	13.45	14.22	0.34	5.74	9.94	2.54	0.32	n.a.	n.a.	n.a.	n.a.	100	FEEA	KVS	3
51.86	2.01	13.53	14.12	0.25	5.65	9.84	2.40	0.33	n.a.	n.a.	n.a.	n.a.	100	FEEA	KVS	2

Table 7.3 continued

Table 7.3 continued

SiO_2	TiO_2	Al_2O_3	FeO	MnO	MgO	CaO	Na_2O	K_2O	P_2O_5	SO_2	F	Cl	Total	Probe	Source	n
51.85	2.03	13.30	13.75	0.25	5.77	10.00	2.76	0.29	n.a.	n.a.	n.a.	n.a.	100	FEEA	KVS	1
51.95	2.05	13.50	13.87	0.32	5.86	9.65	2.49	0.30	n.a.	n.a.	n.a.	n.a.	100	FEEA	KVS	1
50.65	2.06	13.43	14.23	0.24	5.82	10.05	2.76	0.27	0.21	0.20	0.02	0.06	100	TAU	KVS	1
50.71	2.04	13.65	14.25	0.24	5.66	9.93	2.74	0.27	0.23	0.18	0.03	0.06	100	TAU	KVS	1
51.36	1.87	13.83	13.28	0.21	6.36	10.37	2.45	0.28	n.a.	n.a.	n.a.	n.a.	100	FEEA	KVS	5
51.14	1.89	13.82	13.22	0.13	6.86	9.90	2.75	0.29	n.a.	n.a.	n.a.	n.a.	100	FEEA	KVS	1
51.78	1.85	13.82	13.39	0.16	6.25	10.19	2.31	0.25	n.a.	n.a.	n.a.	n.a.	100	FEEA	KVS	1
50.37	1.91	13.48	13.70	0.23	6.27	10.81	2.44	0.27	0.21	0.25	0.02	0.04	100	TAU	KVS	1
51.45	1.60	14.04	12.12	0.23	6.84	11.20	2.26	0.25	n.a.	n.a.	n.a.	n.a.	100	FEEA	VBVS	3
51.50	1.59	14.11	12.16	0.28	6.77	11.05	2.29	0.26	n.a.	n.a.	n.a.	n.a.	100	FEEA	VBVS	3
51.22	1.55	14.04	12.32	0.19	6.95	11.13	2.37	0.22	n.a.	n.a.	n.a.	n.a.	100	FEEA	VBVS	3
51.18	1.24	13.95	12.39	0.22	7.12	11.68	2.11	0.11	n.a.	n.a.	n.a.	n.a.	100	FEEA	VBVS	1
51.24	1.12	14.17	11.95	0.34	7.40	11.75	1.96	0.08	n.a.	n.a.	n.a.	n.a.	100	FEEA	VBVS	5
51.31	1.35	14.17	11.49	0.20	7.25	11.88	2.18	0.16	n.a.	n.a.	n.a.	n.a.	100	FEEA	VBVS	2
51.25	1.23	14.01	11.97	0.22	7.12	11.52	2.56	0.11	n.a.	n.a.	n.a.	n.a.	100	FEEA	VBVS	3
50.64	1.48	14.09	12.38	0.27	7.25	11.54	2.17	0.18	n.a.	n.a.	n.a.	n.a.	100	FEEA	VBVS	2
50.87	1.33	13.96	12.29	0.20	7.37	11.64	2.21	0.13	n.a.	n.a.	n.a.	n.a.	100	FEEA	VBVS	2
50.49	1.19	13.67	12.29	0.23	7.54	12.00	2.14	0.07	0.10	0.21	0.04	0.03	100	TAU	VBVS	1
50.34	1.35	13.95	12.32	0.22	7.36	11.86	2.15	0.11	0.14	0.15	0.02	0.03	100	TAU	VBVS	1
50.09	1.41	13.72	12.36	0.21	7.56	11.84	2.30	0.14	0.13	0.17	0.03	0.03	100	TAU	VBVS	1
49.10	1.53	13.97	12.36	0.21	7.43	11.85	2.58	0.20	0.16	0.20	0.04	0.38	100	TAU	VBVS	1
50.84	1.29	14.41	11.41	0.27	7.81	11.73	2.14	0.10	n.a.	n.a.	n.a.	n.a.	100	FEEA	VBVS	3
50.92	1.29	14.46	11.55	0.17	7.49	11.81	2.19	0.13	n.a.	n.a.	n.a.	n.a.	100	FEEA	VBVS	1
51.02	1.36	14.50	11.40	0.24	7.42	11.73	2.17	0.17	n.a.	n.a.	n.a.	n.a.	100	FEEA	VBVS	3

SiO_2	TiO_2	Al_2O_3	FeO	MnO	MgO	CaO	Na_2O	K_2O	P_2O_5	SO_2	F	Cl	Total	Probe	Source	n
50.69	1.25	14.46	11.72	0.05	7.87	11.66	2.18	0.13	n.a.	n.a.	n.a.	n.a.	100	FEEA	VBVS	1
50.68	1.24	14.47	11.42	0.14	7.90	11.73	2.29	0.13	n.a.	n.a.	n.a.	n.a.	100	FEEA	VBVS	3
50.46	1.12	14.50	11.67	0.29	7.89	11.92	2.03	0.13	n.a.	n.a.	n.a.	n.a.	100	FEEA	VBVS	1
50.08	1.28	14.37	11.51	0.23	7.89	12.04	2.07	0.11	0.13	0.24	0.03	0.02	100	TAU	VBVS	1
51.04	0.92	14.59	10.24	0.33	8.14	12.78	1.85	0.12	n.a.	n.a.	n.a.	n.a.	100	FEEA	WVZ	2
51.04	0.80	15.01	9.68	0.13	8.64	13.07	1.55	0.08	n.a.	n.a.	n.a.	n.a.	100	FEEA	WVZ	2
51.04	1.05	14.65	10.21	0.22	7.96	12.88	1.88	0.11	n.a.	n.a.	n.a.	n.a.	100	FEEA	WVZ	3
51.44	0.99	14.53	10.66	0.15	7.81	12.31	2.00	0.12	n.a.	n.a.	n.a.	n.a.	100	FEEA	WVZ	3
51.02	1.01	14.73	9.86	0.22	7.95	13.00	2.07	0.13	n.a.	n.a.	n.a.	n.a.	100	FEEA	WVZ	1
50.60	0.92	14.60	10.12	0.39	8.22	12.77	2.28	0.10	n.a.	n.a.	n.a.	n.a.	100	FEEA	WVZ	1
50.82	1.00	14.69	9.90	0.23	8.26	12.92	2.08	0.11	n.a.	n.a.	n.a.	n.a.	100	FEEA	WVZ	5
50.68	1.07	15.16	9.43	0.24	8.18	12.95	2.13	0.17	n.a.	n.a.	n.a.	n.a.	100	FEEA	WVZ	1
50.05	0.99	14.58	10.16	0.19	8.32	13.42	1.89	0.12	0.08	0.16	0.02	0.02	100	TAU	WVZ	1
49.79	0.98	14.74	10.57	0.20	8.33	13.08	1.98	0.07	0.08	0.16	0.01	0.02	100	TAU	WVZ	1
50.24	0.96	14.34	10.40	0.19	8.22	13.31	1.98	0.11	0.09	0.14	0.01	0.02	100	TAU	WVZ	1
50.16	0.95	14.19	10.21	0.19	8.67	13.22	2.04	0.09	0.09	0.18	-0.01	0.02	100	TAU	WVZ	1
50.08	0.95	14.73	10.27	0.19	8.39	13.20	1.84	0.10	0.08	0.17	-0.01	0.02	100	TAU	WVZ	1
49.83	0.97	14.92	10.27	0.17	8.54	13.10	1.86	0.09	0.09	0.14	0.00	0.02	100	TAU	WVZ	1
50.39	0.99	14.58	10.18	0.19	8.21	13.14	1.91	0.13	0.10	0.15	0.01	0.02	100	TAU	WVZ	1
50.41	0.95	14.27	10.09	0.19	8.37	13.31	2.06	0.08	0.09	0.16	0.00	0.02	100	TAU	WVZ	1
51.22	1.29	14.56	10.31	0.25	7.65	12.42	2.16	0.16	n.a.	n.a.	n.a.	n.a.	100	FEEA	VBVS	3
50.95	1.23	14.82	10.67	0.16	7.99	12.18	1.85	0.15	n.a.	n.a.	n.a.	n.a.	100	FEEA	VBVS	1
51.08	1.29	14.54	10.51	0.21	7.64	12.25	2.31	0.18	n.a.	n.a.	n.a.	n.a.	100	FEEA	VBVS	3
50.27	1.25	14.26	10.94	0.20	7.90	12.55	2.14	0.17	0.14	0.17	0.00	0.02	100	TAU	VBVS	1
49.90	1.19	14.51	10.83	0.20	8.02	12.70	2.15	0.21	0.12	0.14	0.01	0.02	100	TAU	VBVS	1
50.67	1.19	14.27	10.58	0.20	7.89	12.70	2.07	0.15	0.13	0.12	0.01	0.02	100	TAU	VBVS	1

Table 7.3 continued

MgO	CaO	Na_2O	K_2O	P_2O_5	SO_2	F	Cl	Total	Probe	Source	n
6.58	10.97	2.65	0.33	n.a.	n.a.	n.a.	n.a.	100	FEEA	-	2
9.47	13.81	1.69	0.04	n.a.	n.a.	n.a.	n.a.	100	FEEA	-	2
9.56	13.83	1.75	0.02	0.05	0.10	0.02	0.01	100	TAU	-	1

Table 7.3 continued

CHAPTER 8 Appendix C

	U1304	MD95-2289	MD95-2009	HM71-19	HM57-7	Link16	MD99-2253
U1304	1.00	0.97	0.94	0.91	0.82	0.98	0.97
MD95-2289		1.00	0.93	0.90	0.80	0.96	0.96
MD95-2009			1.00	0.95	0.83	0.95	0.96
HM71-19				1.00	0.85	0.92	0.92
HM57-7					1.00	0.83	0.82
Link16						1.00	0.98
MD99-2253							1.00

Table 8.1: Similarity coefficient (SC) for 5e-Eem/RHY-1 geochemistry found in different location compared to the tephra shards found in the interval 19.27-19.62 mcd of U1304. Six oxides with a weight % greater than 1 were used: SiO_2, Al_2O_3, FeO, MgO, CaO, Na_2O.

	U1304	MD95-2289	HM71-19	HM57-7	LINK16	MD99-2253
U1304	0.00	4.64	10.83	54.25	2.56	1.23
MD95-2289		0.00	9.41	41.82	4.15	3.76
HM71-19			**0.00**	19.55	11.59	15.13
HM57-7				0.00	115.96	106.10
LINK16					0.00	2.35
MD99-2253					2.35	0.00

Table 8.2: Table shows the result of the statistical distance function for 5e-Eem/RHY-1 geochemistry found in different location compared to the tephra shards found in the interval 19.27-19.62 mcd of U1304. The D^2 values were calculated from seven (SiO_2, TiO_2, Al_2O_3, FeO, CaO, Na_2O, K_2O), which gives a D^2 critical from 18.48 (99 % confidence level).

	U1304 *2012*	U1304 *2017*	U1304 *1992*	MD95-2289	MD95-2009	HM71-19	HM57-7	Link16	MD99-2253
U1304 *2012*	1.00	0.99	0.99	0.97	0.94	0.92	0.85	0.98	0.98
U1304 *2017*		1.00	0.99	0.97	0.94	0.91	0.85	0.98	0.98
U1304 *1992*			1.00	0.97	0.95	0.92	0.85	0.98	0.99
MD95-2289				1.00	0.93	0.91	0.83	0.96	0.97
MD95-2009					1.00	0.95	0.84	0.95	0.95
HM71-19						1.00	0.86	0.93	0.92
HM57-7							1.00	0.85	0.85
Link16								1.00	0.98
MD99-2253									1.00

Table 8.3: Similarity coefficient (SC) for 5e-Eem/RHY-1 geochemistry found in different location compared to the tephra shards found in the sample depth 19.92 mcd, 20.12 mcd, 20.17 mcd of U1304. Six oxides with a weight % greater than 1 were used: SiO_2, Al_2O_3, FeO, MgO, CaO, Na_2O.

	U1304 *2012*	MD95-2289	HM71-19	HM57-7	MD99-2253	Link 16	U1304 *2017*	U1304 *1992*
U1304 *2012*	0.00	0.85	16.71	118.96	1.97	3.30	0.32	0.36
MD95-2289		0.00	14.55	83.36	2.92	2.65	1.07	1.10
HM71-19			0.00	19.55	15.13	11.59	21.66	19.55
HM57-7				0.00	106.10	115.96	133.64	129.83
MD99-2253					0.00	2.35	3.18	1.30
Link16						0.00	6.77	3.35
U1304 *2017*							0.00	1.39
U1304 *1992*								0.00

Table 8.4: Table shows the result of the statistical distance function for 5e-Eem/RHY-1 geochemistry found in different location compared to the tephra shards found in sample depth 19.92 mcd, 20.12 mcd, 20.17 mcd of U1304. The D^2 values were calculated from seven (SiO_2, TiO_2, Al_2O_3, FeO, CaO, Na_2O, K_2O), which gives a D^2 critical from 18.48 (99 % confidence level).

SiO_2	TiO_2	Al_2O_3	FeO	MnO	MgO	CaO	Na_2O	K_2O	P_2O_5	Total	VZ/VS	EPMA Period
9.49	2.82	12.62	13.91	0.24	5.66	10.35	2.77	0.35	0.30	98.51	Grimsvötn	5
8.18	2.00	14.21	11.77	0.20	7.72	12.11	1.95	0.21	0.23	98.60	WVZ?	5
6.19	3.90	12.56	14.05	0.21	5.67	10.55	2.90	0.55	0.39	96.96	-	5
7.61	1.41	15.51	12.15	0.20	7.66	11.80	2.94	0.13	0.10	99.53	Reykjanes	3
7.52	4.33	12.69	14.92	0.24	4.88	9.91	3.21	0.73	0.53	98.96	-	3
9.29	2.46	13.10		0.21	6.21	10.75	2.72	0.34	0.25	98.50	Grimsvötn	3
9.14	1.95	13.80	11.77	0.20	7.26	11.56	2.28	0.24	0.23	98.43	WVZ?	3
9.68	2.45	13.88	12.88	0.21	6.45	10.68	2.58	0.36	0.24	99.40	Grimsvötn	3
9.26	2.89	12.95	13.57	0.21	5.97	10.27	2.50	0.44	0.27	98.34	Grimsvötn	3
9.58	1.89	13.54	13.18	0.24	6.75	10.98	2.13	0.24	0.20	98.74	Krafla?	3
8.72	1.64	14.15	11.90	0.21	7.19	11.53	2.05	0.23	0.15	97.76	WVZ?	3
8.25	2.27	14.02	11.80	0.21	6.96	11.25	2.47	0.37	0.21	97.82	WVZ?	3
9.72	2.00	12.75	14.31	0.23	5.52	10.01	2.74	0.28	0.18	97.76	Krafla	4
9.37	2.75	13.18	13.74	0.23	6.36	10.53	2.59	0.46	0.25	99.46	Grimsvötn	3
0.69	1.06	14.05	10.98	0.19	7.60	12.32	2.18	0.07	0.09	99.23		5
7.37	*1.40*	*15.29*	*11.76*	*0.19*	*7.76*	*11.97*	*2.91*	*0.11*	*0.09*	*98.85*		*5*
0.43	*1.65*	*14.04*	*12.33*	*0.19*	*7.52*	*11.47*	*2.06*	*0.16*	*0.17*	*100.03*		*3*

Table 8.5: Major oxide concentrations of basaltic shards found in the three sample intervals: 19.92-20.17 mcd, 19.27-19.62 mcd and 18.02-18.22 mcd from the Site U1304. WVZ: Western volcanic zone. Trans: shards potentially originate from the Transitional-alkalic series of Iceland. All oxides are presented as weight %.

ber	SiO_2	TiO_2	Al_2O_3	FeO	MnO	MgO	CaO	Na_2O	K_2O	P_2O_5	Total	Comment	EPMA Period
802	72.24	0.25	13.24	2.57	0.06	0.25	1.31	4.70	3.85	0.03	98.52	Trans	5
7_1	71.06	0.27	13.49	2.45	0.05	0.26	1.32	4.53	3.71	0.03	97.17	Trans	5
2_1	72.80	0.19	11.17	2.99	0.09	0.05	1.37	4.28	3.06	0.01	96.01	Trans	3
7_1	72.47	0.19	10.68	2.74	0.08	0.01	1.54	4.71	1.87	0.01	94.30	5e-Eem/RHY-I	4
2_1	75.97	0.19	11.34	3.16	0.08	0.02	1.51	3.96	1.93	0.01	98.17	5e-Eem/RHY-I	3
2_2	76.55	0.20	12.16	3.00	0.09	0.04	1.56	4.30	1.87	0.00	99.77	5e-Eem/RHY-I	3
2_21	73.35	0.19	10.05	2.71	0.08	0.00	1.32	4.41	1.87	0.03	93.99	5e-Eem/RHY-I	4
7_2	73.84	0.21	11.11	3.27	0.11	0.06	1.80	4.65	1.90	0.03	96.98	5e-Eem/RHY-I	4
2_2	74.77	0.19	10.96	2.51	0.08	0.03	1.38	3.83	2.12	0.01	95.89	5e-Eem/RHY-I	3
7_1	73.47	0.19	10.86	3.07	0.09	0.04	1.56	4.90	1.88	0.01	96.06	5e-Eem/RHY-I	4
2_1	74.50	0.19	10.69	2.82	0.09	0.05	1.60	4.65	1.90	0.01	96.50	5e-Eem/RHY-I	4
_A4	75.55	0.20	10.81	2.68	0.10	0.03	1.45	4.26	1.77	0.01	96.86	5e-Eem/RHY-I	5
_B1	75.57	0.20	11.25	2.98	0.09	0.05	1.60	4.40	1.89	0.02	98.04	5e-Eem/RHY-I	5
_B5	74.72	0.20	10.84	2.80	0.09	0.02	1.58	4.39	1.84	0.02	96.50	5e-Eem/RHY-I	5
_B6	74.73	0.19	10.76	3.05	0.09	0.02	1.54	4.27	1.91	0.02	96.59	5e-Eem/RHY-I	5
_A1	76.68	0.19	11.38	2.89	0.09	0.00	1.54	4.29	1.76	0.02	98.85	5e-Eem/RHY-I	5
_A2	76.34	0.21	11.28	3.09	0.11	0.04	1.65	4.23	2.00	0.01	98.95	5e-Eem/RHY-I	5
_A3	75.02	0.19	10.96	3.14	0.10	0.01	1.48	4.29	1.86	0.01	97.05	5e-Eem/RHY-I	5
_B2	75.20	0.20	11.16	3.07	0.09	0.02	1.55	4.24	1.83	0.01	97.35	5e-Eem/RHY-I	5
_B3	74.33	0.19	10.92	2.82	0.09	0.00	1.42	4.32	1.87	0.01	95.96	5e-Eem/RHY-I	5
_B4	74.55	0.20	10.84	2.73	0.10	0.01	1.70	4.27	1.87	0.01	96.29	5e-Eem/RHY-I	5
_A2	75.27	0.19	10.87	2.98	0.09	0.03	1.53	4.29	1.92	0.01	97.17	5e-Eem/RHY-I	5
_A3	74.26	0.20	10.68	3.18	0.09	0.02	1.55	4.52	1.70	0.01	96.20	5e-Eem/RHY-I	5
_A4	74.41	0.19	10.58	2.89	0.09	0.01	1.48	4.26	1.74	0.01	95.66	5e-Eem/RHY-I	5
A10	76.06	0.20	10.84	3.05	0.10	0.04	1.56	4.56	1.78	0.02	98.20	5e-Eem/RHY-I	5

Table 8.6: Major oxide concentrations of rhyolitic shards found in the three sample intervals: 19.92-20.17 mcd, 19.27-19.62 mcd and 18.02-18.22mcd from the Site U1304 volcanic zone.

ber	SiO_2	TiO_2	Al_2O_3	FeO	MnO	MgO	CaO	Na_2O	K_2O	P_2O_5	Total	Comment	EPMA Period
_B3	76.87	0.19	11.27	2.81	0.09	0.03	1.49	4.27	1.85	0.01	98.87	5e-Eem/RHY-I	5
_B4	74.43	0.20	11.12	3.10	0.10	0.04	1.68	4.37	1.78	0.02	96.85	5e-Eem/RHY-I	5
_A1	74.14	0.20	11.05	3.01	0.10	0.02	1.55	4.13	1.81	0.01	96.02	5e-Eem/RHY-I	5
_A5	76.09	0.19	11.10	3.07	0.10	0.02	1.52	4.43	1.86	0.01	98.39	5e-Eem/RHY-I	5
_A6	74.49	0.20	10.63	2.82	0.09	0.05	1.57	4.37	1.88	0.01	96.11	5e-Eem/RHY-I	5
_A7	75.04	0.22	10.84	3.16	0.08	0.03	1.64	4.26	1.81	0.02	97.10	5e-Eem/RHY-I	5
_A8	74.31	0.20	10.79	2.92	0.10	0.01	1.46	4.55	1.85	0.02	96.20	5e-Eem/RHY-I	5
_A9	74.83	0.19	10.56	2.52	0.09	0.04	1.35	4.34	2.03	0.01	95.96	5e-Eem/RHY-I	5
A11	74.22	0.19	10.69	3.01	0.10	0.01	1.46	4.30	1.87	0.01	95.86	5e-Eem/RHY-I	5
A12	75.06	0.20	11.46	2.91	0.10	0.03	1.59	4.54	1.88	0.01	97.79	5e-Eem/RHY-I	5
_C1	74.77	0.20	11.28	3.04	0.10	0.01	1.62	4.44	1.84	0.01	97.31	5e-Eem/RHY-I	5
_B1	75.02	0.20	10.80	2.82	0.09	0.04	1.53	4.25	1.69	0.01	96.46	5e-Eem/RHY-I	5
_B2	75.53	0.19	11.09	2.69	0.10	0.02	1.53	4.40	1.83	0.01	97.39	5e-Eem/RHY-I	5
_B5	76.08	0.19	10.68	2.69	0.10	0.04	1.57	4.39	1.83	0.01	97.59	5e-Eem/RHY-I	5
_B6	75.53	0.19	10.78	3.07	0.10	0.03	1.58	4.25	1.89	0.01	97.44	5e-Eem/RHY-I	5
_B7	74.60	0.19	11.15	2.87	0.08	0.00	1.58	4.17	1.86	0.01	96.51	5e-Eem/RHY-I	5
_B8	74.40	0.21	10.79	3.08	0.10	0.01	1.48	4.17	1.90	0.01	96.16	5e-Eem/RHY-I	5
7B1	75.01	0.19	10.74	2.87	0.09	-0.01	1.54	4.31	1.86	0.00	96.61	5e-Eem/RHY-I	5
7B1	73.55	0.19	10.52	2.55	0.09	0.03	1.40	4.37	1.73	0.01	94.43	5e-Eem/RHY-I	5
7B1	73.37	0.20	10.66	2.83	0.09	0.04	1.50	4.42	1.70	0.01	94.80	5e-Eem/RHY-I	5
_B2	76.40	0.20	11.01	2.92	0.09	0.02	1.56	4.48	1.79	0.01	98.48	5e-Eem/RHY-I	5
_A1	76.30	0.19	11.38	2.91	0.10	-0.01	1.58	4.48	1.75	0.01	98.68	5e-Eem/RHY-I	5
_A3	75.27	0.21	11.02	3.36	0.11	0.03	1.71	4.53	1.74	0.01	97.97	5e-Eem/RHY-I	5
_A4	73.71	0.21	11.17	2.95	0.10	0.02	1.52	4.34	1.90	0.01	95.91	5e-Eem/RHY-I	5
_A6	75.56	0.19	10.94	3.01	0.11	0.04	1.57	4.30	1.79	0.01	97.51	5e-Eem/RHY-I	5
_A7	76.07	0.19	11.09	3.13	0.09	0.05	1.63	4.42	1.89	0.02	98.58	5e-Eem/RHY-I	5
_A8	74.98	0.19	10.72	2.70	0.08	0.02	1.42	4.44	1.93	0.00	96.49	5e-Eem/RHY-I	5
_A9	74.89	0.19	10.81	2.81	0.08	0.02	1.53	4.26	1.88	0.02	96.47	5e-Eem/RHY-I	5
A10	73.78	0.20	10.60	2.67	0.09	0.05	1.51	4.52	1.81	0.02	95.25	5e-Eem/RHY-I	5
A11	75.13	0.20	11.02	3.06	0.08	0.01	1.50	4.35	1.78	0.02	97.15	5e-Eem/RHY-I	5
A12	75.32	0.19	10.59	2.91	0.09	0.02	1.51	4.59	1.90	0.01	97.14	5e-Eem/RHY-I	5
A13	74.51	0.19	10.74	2.80	0.09	0.02	1.54	4.44	1.84	0.01	96.19	5e-Eem/RHY-I	5
A14	74.23	0.20	10.74	2.78	0.08	0.01	1.60	4.45	1.83	0.01	95.94	5e-Eem/RHY-I	5
A15	74.62	0.19	10.84	2.90	0.08	0.01	1.43	4.69	1.80	0.01	96.58	5e-Eem/RHY-I	5

Table 8.6 continued

O_3	FeO	MnO	MgO	CaO	Na_2O	K_2O	P_2O_5	Total	Comment	EPMA Period
1.04	2.97	0.09	0.00	1.48	4.35	1.80	0.01	96.89	Sa-Eam/RHY-1	5
0.88	2.80	0.09	0.01	1.62	4.43	1.88	0.00	97.45	Sa-Eam/RHY-1	5
0.69	2.75	0.09	0.03	1.39	4.38	1.85	0.01	96.20	Sa-Eam/RHY-1	5
0.90	2.83	0.09	0.00	1.51	4.44	1.88	0.02	98.10	Sa-Eam/RHY-1	5
1.15	2.96	0.09	0.03	1.54	4.39	1.85	0.01	97.61	Sa-Eam/RHY-1	5
0.69	*2.71*	*0.09*	*0.01*	*1.61*	*2.66*	*1.87*	*0.01*	*93.42*	*lower total*	4
1.20	*2.81*	*0.07*	*0.02*	*1.50*	*3.99*	*1.83*	*0.01*	*97.55*	*lower total*	3
0.45	*2.76*	*0.09*	*0.01*	*1.40*	*4.31*	*2.02*	*0.01*	*94.34*	*lower total*	3
1.53	*2.35*	*0.07*	*0.04*	*0.66*	*4.92*	*4.00*	*0.00*	*93.81*	*outlier*	4
0.76	*2.86*	*0.10*	*0.17*	*1.50*	*4.60*	*1.85*	*0.01*	*94.57*	*outlier*	4
1.60	*2.62*	*0.09*	*0.06*	*1.10*	*4.25*	*2.89*	*0.02*	*95.92*	*outlier*	5
1.44	*2.88*	*0.10*	*0.08*	*1.33*	*4.32*	*2.86*	*0.01*	*94.95*	*outlier*	5

Table 8.6 continued

References

Abbott, P.M. et al., 2012. A detailed framework of Marine Isotope Stages 4 and 5 volcanic events recorded in two Greenland ice-cores. *Quaternary Science Reviews*, 36, pp.59–77.

Abbott, P.M. et al., 2011. Identification of cryptotephra horizons in a North East Atlantic marine record spanning marine isotope stages 4 and 5a (~ 60,000–82,000 a b2k). *Quaternary International*, 246(1-2), pp.177–189.

Abbott, P.M. et al., 2014. Re-evaluation and extension of the Marine Isotope Stage 5 tephrostratigraphy of the Faroe Islands region: The cryptotephra record. *Palaeogeography, Palaeoclimatology, Palaeoecology*, 409(0), pp.153–168.

Andersen, K.K. et al., 2006. The Greenland Ice Core Chronology 2005, 15–42ka. Part 1: constructing the time scale. *Quaternary Science Reviews*, 25(23-24), pp.3246–3257.

Andrews, J.T., 2000. Icebergs and iceberg rafted detritus (IRD) in the North Atlantic: facts and assumptions. *Oceanography*, 13(3), pp.100–108.

Andrews, J.T. & Tedesco, K., 1992. Detrial carbonate-rich sediments, northwestern Labrador Sea: Implcations for ice-sheet dynamics and iceberg rafting (Heinrich) events in teh North Atlantic. *Geology*, 20(10), pp.1087–1090.

Augustin, L. et al., 2004. Eight glacial cycles from an Antarctic ice core. *Nature*, 429(6992), pp.623–8.

Austin, W.E.N. et al., 1995. The 14C age of the Icelandic Vedde Ash: implications for Younger Dryas marine reservoir age corrections. *Radiocarbon*, 37(1), pp.53–62.

Austin, W.E.N. & Hibbert, F.D., 2012. Tracing time in the ocean: a brief review of chronological constraints (60 -8 kyr) on North Atlantic marine event-based stratigraphies. *Quaternary Science Reviews*, 36(0), pp.28–37.

Austin, W.E.N., Wilson, L.J. & Hunt, J.B., 2004. The age and chronostratigraphical significance of North Atlantic Ash zone II. *Journal of Quaternary Science*, 19(2), pp.137–146.

Barker, S. et al., 2005. Planktonic foraminiferal Mg/Ca as a proxy for past oceanic temperatures: a methodological overview and data compilation for the Last Glacial Maximum. *Quaternary Science Reviews*, 24(7–9), pp.821–834.

Bas, M. Le & Maitre, R. Le, 1986. A chemical classification of volcanic rocks based on the total alkali-silica diagram. *Journal of Petrology*, 27(1984), pp.745–750.

Bauch, H. a. & Kandiano, E.S., 2007. Evidence for early warming and cooling in North Atlantic surface waters during the last interglacial. *Paleoceanography*, 22(1), pp.1–11.

Bauch, H. a., Kandiano, E.S. & Helmke, J.P., 2012. Contrasting ocean changes between the subpolar and polar North Atlantic during the past 135 ka. *Geophysical Research Letters*, 39(11), pp.1–7.

Begét, J. et al., 1992. Age, extent and climatic significance of the c. 3400 BP Aniakchak tephra, western Alaska, USA. *The Holocene*, 2(1), pp.51–56.

Bianchi, G.G. & McCave, I.N., 2000. Hydrography and sedimentation under the deep western boundary current on Bjorn and Gardar Drifts, Iceland Basin. *Marine Geology*, 165, pp.137–169.

Blaauw, M., 2012. Out of tune: the dangers of aligning proxy archives. *Quaternary Science Reviews*, 36, pp.38–49.

Blaauw, M. & Christeny, J.A., 2011. Flexible paleoclimate age-depth models using an autoregressive gamma process. *Bayesian Analysis*, 6(3), pp.457–474.

Blockley, S.P.E. et al., 2007. Evidence for the presence of the Vedde Ash in Central Europe. *Quaternary Science Reviews*, 26(25-28), pp.3030–3036.

Blunier, T. et al., 2007. Synchronization of ice core records via atmospheric gases. *Climate of the Past Discussions*, 3(1), pp.365–381.

Blunier, T. & Brook, E.J., 2001. Timing of millennial-scale climate change in Antarctica and Greenland during the last glacial period. *Science (New York, N.Y.)*, 291(5501), pp.109–12.

Bodén, P. et al., 1996. A laminated sediment sequence from the northern North Atlantic Ocean and its climatic record. *Geology*, 24(6), pp.507–510.

Bond, G., 1997. A Pervasive Millennial-Scale Cycle in North Atlantic Holocene and Glacial Climates. *Science*, 278(5341), pp.1257–1266.

Bond, G. et al., 1993. Correlations between climate records from North Atlantic sediments and Greenland ice. *Nature*, 365(6442), pp.143–147.

Bond, G. et al., 1992. Evidence for massive discharges of icebergs into the North Atlantic ocean during the last glacial period. *Nature*, 360(6401), pp.245–249.

Bond, G.C. & Lotti, R., 1995. Iceberg discharges into the north atlantic on millennial time scales during the last glaciation. *Science*, 267(5200), pp.1005–10.

Borchardt, G.A. et al., 1972. Correlation of the Bishop ash, a Pleistocene marker bed, using instrumental neutron activation analysis. *Journal of Sedimentary Research*, 42(2), pp.301–306.

Borchardt, G.A., Harward, M.E. & Schmitt, R.A., 1971. Correlation of volcanic ash deposits by activation analysis of glass separates. *Quaternary Research*, 1(2), pp.247–260.

Bosch, J.H. a, Cleveringa, P. & Meijer, T., 2000. The Eemian stage in the Netherlands: History, character and new research. *Geologie en Mijnbouw/Netherlands Journal of Geosciences*, 79(2-3), pp.135–145.

Bourgeois, O. et al., 2000. Geothermal control on flow patterns in the last glacial maximum ice sheet of Iceland. *Earth Surface Processes and Landforms*, 25(1), pp.59–76.

Brendryen, J., Haflidason, H. & Sejrup, H.P., 2010. Norwegian Sea tephrostratigraphy

of marine isotope stages 4 and 5: Prospects and problems for tephrochronology in the North Atlantic region. *Quaternary Science Reviews*, 29(7-8), pp.847–864.

Broecker, W.S. et al., 1990. A salt oscillator in the glacial Atlantic? 1. The concept. *Paleoceanography*, 5(4), pp.469–477.

Broecker, W.S., 1998. Paleocean circulation during the Last Deglaciation: A bipolar seesaw? *Paleoceanography*, 13(2), pp.119–121.

Broecker, W.S. & van Donk, J., 1970. Insolation changes, ice volumes, and the O 18 record in deep-sea cores. *Reviews of Geophysics and Space Physics*, 8(1), pp.169–198.

Carlson, A.E. et al., 2008. Subtropical Atlantic salinity variability and Atlantic meridional circulation during the last deglaciation. *Geology*, 36(12), pp.991–994.

Chapman, M., 2012. Climate Variability In The Mid-Latitude North Atlantic During The Previous Two Interglacials. *Quaternary International*, 279-280(2012), p.84.

Chappellaz, J. et al., 1997. CH4 and δ18O of O2 records from Antarctic and Greenland ice: A clue for stratigraphic disturbance in the bottom part of the Greenland Ice Core Project and the Greenland Ice Sheet Project 2 ice cores. *Journal of Geophysical Research: Oceans*, 102(C12), pp.26547–26557.

Clark, P.U. et al., 2001. Freshwater forcing of abrupt climate change during the last glaciation. *Science (New York, N.Y.)*, 293(5528), pp.283–287.

Cleveringa, P. et al., 2000. The Eemian stratotype locality at Amersfoort in the central Netherlands: A re-evaluation of old and new data. *Geologie en Mijnbouw/Netherlands Journal of Geosciences*, 79(2-3), pp.197–216.

CLIMAP Project Members, 1976. CLIMAP1976. *Science*, 191, pp.1131 – 1137.

Dansgaard, W. et al., 1982. A New Greenland Deep Ice Core. *Science*, 218(4579), pp.1273–1277.

Dansgaard, W. et al., 1993. Evidence for general instability of past climate from a 250-kyr ice-core record. *Nature*, 364(6434), pp.218–220.

Davies, S. et al., 2005. Detection of Lateglacial distal tephra layers in the Netherlands. *Boreas*, 34(2), pp.123–135.

Davies, S.M. et al., 2014. A North Atlantic tephrostratigraphical framework for 130–60 ka b2k: new tephra discoveries, marine-based correlations, and future challenges. *Quaternary Science Reviews*, 106, pp.101–121.

Davies, S.M. et al., 2012. Integrating the INTIMATE records using tephrochronology: rising to the challenge. *Quaternary Science Reviews*, 36, pp.11–27.

Davies, S.M. et al., 2004. Were there two Borrobol Tephras during the early Lateglacial period: implications for tephrochronology? *Quaternary Science Reviews*, 23(5-6), pp.581–589.

Dokken, T.M. et al., 2013. Dansgaard-Oeschger cycles: Interactions between ocean and sea ice intrinsic to the Nordic seas. *Paleoceanography*, 28(3), pp.491–502.

Duplessy, J.C., Lalou, C. & Vinot, A.C., 1970. Differential Isotopic Fractionation in Benthic Foraminifera and Paleotemperatures Reassessed. *Science*, 168(3928), pp.250–251.

Emiliani, C., 1966. Paleotemperature Analysis of Caribbean Cores P6304-8 and P6304-9 and a Generalized Temperature Curve for the past 425,000 Years. *The Journal of Geology*, 74(2), pp.109–124.

Emiliani, C., 1955. Pleistocene Temperatures. *The Journal of Geology*, 63(6), pp.538–578.

EPICA Community Members et al., 2006. One-to-one coupling of glacial climate variability in Greenland and Antarctica. *Nature*, 444(7116), pp.195–198.

Epstein, S. et al., 1951. Carbonate-Water Isotopic Temperature Scale. *Geological Society of America Bulletin*, 62(4), pp.417–426.

Epstein, S. et al., 1953. Revised Carbonate-Water Isotopic Temperature Scale. *Geological Society of America Bulletin*, 64(11), pp.1315–1326.

Expedition 303 Scientists, 2006a. Expedition 303 summary. In J. E. T. Channell et al., eds. *Proceedings of the Integrated Ocean Drilling Program 303/306*. College Station TX (Integrated Ocean Drilling Program Management International, Inc.), pp. 1–30.

Expedition 303 Scientists, 2006b. Site U1304. In J. E. T. Channell et al., eds. *Proceedings of the Integrated Ocean Drilling Program, 303/306*. College Station TX (Integrated Ocean Drilling Program Management International, Inc.), pp. 1–82.

Farmer, E., 2012. Climate and Hydrography of the Subpolar North Atlantic During the Last Interglacial. *Quaternary International*, 279-280(2012), p.137.

Fisher, R. V, 1964. Maximum size, median diameter, and sorting of tephra. *Journal of Geophysical Research*, 69(2), pp.341–355.

Folk, R.L. & Ward, W.C., 1957. Brazos River Bar: A study in the significance of grain size parameters. *Journal of Sedimentary Research*, 27(1), pp.3–26.

Fratantoni, D.M., 2001. North Atlantic surface circulation during the 1990's observed with satellite-tracked drifters. *Journal of Geophysical Research: Oceans*, 106(C10), pp.22067–22093.

Fronval, T. et al., 1998. Variability in surface and deep water conditions in the nordic seas during the last interglacial period. *Quaternary Science Reviews*, 17(9-10), pp.963–985.

Fronval, T. & Jansen, E., 1997. Eemian and Early Weichselian (140–60 ka) Paleoceanography and paleoclimate in the Nordic Seas with comparisons to Holocene conditions. *Paleoceanography*, 12(3), p.443.

Fronval, T. & Jansen, E., 1996a. Late Neogene paleoclimates and paleoceanography in the Iceland-Norwegian Sea: evidence from the Iceland and Vøring Plateaus. *Proceedings of the Ocean Drilling Program*, 151(3), pp.455–468.

Fronval, T. & Jansen, E., 1996b. Rapid changes in ocean circulation and heat flux in the Nordic seas during the last interglacial period. *Nature*, 383(October), pp.806–810.

Galaasen, E.V. et al., 2014. Rapid Reductions in North Atlantic Deep Water During the Peak of the Last Interglacial Period. *Science* , 343 (6175), pp.1129–1132.

Gans, W. d., Beets, D.J. & Centineo, M.C., 2000. Late Saalian and Eemian deposits in the Amsterdam glacial basin. *Netherlands Journal of Geosciences*, 2-3(79), pp.147–160.

Geirsdóttir, Á., Miller, G.H. & Andrews, J.T., 2007. Glaciation, erosion, and landscape evolution of Iceland. *Journal of Geodynamics*, 43(1), pp.170–186.

GRIP Members, 1993. Climate instability during the last interglacial period recorded in the GRIP ice core. *Nature*, 364(6434), pp.203–207.

Grönvold, K. et al., 1995. Ash layers from Iceland in the Greenland GRIP ice core correlated with oceanic and land sediments. *Earth and Planetary Science Letters*, 135, pp.149–155.

Gross, T.F. & Williams III, A.J., 1991. Characterization of deep-sea storms. *Marine Geology*, 99(3–4), pp.281–301.

Grousset, F.E. et al., 2000. Were the North Atlantic Heinrich events triggered by the behavior of the European ice sheets? *Geology* , 28 (2), pp.123–126.

Gwiazda, R.H., Hemming, S.R. & Broecker, W.S., 1996. Tracking the sources of icebergs with lead isotopes: The provenance of ice-rafted debris in Heinrich layer 2. *Paleoceanography*, 11(1), pp.77–93.

Habicht, J.K.A., 1979. *Paleoclimate, Paleomagnetism and Continental Drift* M. K. Horn, ed., American Association of Petroleum Geologists.

Hafliðason, H., Eiriksson, J. & Kreveld, S. Van, 2000. The tephrochronology of Iceland and the North Atlantic region during the Middle and Late Quaternary: a review. *Journal of Quaternary Science*, 15(1), pp.3–22.

Hall, I.R. et al., 1998. Coherent deep flow variation in the Iceland and American basins during the last interglacial. *Earth and Planetary Science Letters*, 164(1-2), pp.15–21.

Harting, P., 1874. De bodem van het Eemdal. *Verslagen en Verhandelingen Koninklijke Academie van Wetenschappen*, 2e Reeks(8), pp.282–290.

Hayward, C., 2012. High spatial resolution electron probe microanalysis of tephras and melt inclusions without beam-induced chemical modification. *The Holocene*, 22(1), pp.119–125.

Hemming, S.R. et al., 1998. Provenance of Heinrich layers in core V28-82, northeastern Atlantic: 40Ar/39Ar ages of ice-rafted hornblende, Pb isotopes in feldspar grains, and Nd-Sr-Pb isotopes in the fine sediment fraction. *Earth and Planetary Science Letters*, 164(1-2), pp.317–333.

Hibbert, F.D. et al., 2010. British Ice Sheet dynamics inferred from North Atlantic ice-

rafted debris records spanning the last 175 000 years. *Journal of Quaternary Sceince*, 25(4, Sp. Iss. SI), pp.461–482.

Hodell, D. a. et al., 2008. Onset of "Hudson Strait" Heinrich events in the eastern North Atlantic at the end of the middle Pleistocene transition (□640 ka)? *Paleoceanography*, 23(4), pp.1–16.

Hodell, D. & Curtis, J., 2008. Oxygen and carbon isotopes of detrital carbonate in North Atlantic Heinrich Events. *Marine Geology*, 256(1-4), pp.30–35.

Hodell, D.A. et al., 2009. Surface and deep-water hydrography on Gardar Drift (Iceland Basin) during the last interglacial period. *Earth and Planetary Science Letters*, 288(1-2), pp.10–19.

Hubbard, A. et al., 2006. A modelling insight into the Icelandic Last Glacial Maximum ice sheet. *Quaternary Science Reviews*, 25(17-18), pp.2283–2296.

Hunt, J. & Hill, P.G., 1996. An inter-laboratory comparison of the electron probe microanalysis of glass geochemistry. *Quaternary International*, 34-36(95), pp.229–241.

Imbrie, J. et al., 1984. The orbital theory of Pleistocene climate: Support from a revised chronology of the marine delta 18 O record. In *Milankovitch and climate: Understanding the response to astronomical forcing*. p. 269.

Imsland, P., 1984. *Petrology, Mineralogy and Evolution of the Jan Mayen Magma System*. Visindafel., Reykjavik: Nordic Volcanological Institute, University of Iceland.

Jagan, A., 2010. *Tephra stratigraphy and geochemistry from three Icelandic lake cores: a new method for determining source volcano of tepra layers*. School of Geosciences, University of Edinburgh.

Jakobsson, S.P., 1979. Petrology of recent basalts of the Eastern Volcanic System, Iceland. *Acta Naturalia Islandica*, 26, pp.1–103.

Jakobsson, S.P., Jonasson, K. & Sigurdsson, I.A., 2008. The three igneous rock series of Iceland. *Jökull*, 58, pp.117–138.

Jessen, K. & Milthers, V., 1928. No TitleStratigraphical and paleontological studies of interglacial freshwater deposits in Jutland and Northwest Germany. *Danmarks Geologiske Undersøgelse*, 48, pp.1–1379.

Jochum, K.P. et al., 2005. Chemical Characterisation of the USGS Reference Glasses GSA-1G, GSC-1G, GSD-1G, GSE-1G, BCR-2G, BHVO-2G and BIR-1G Using EPMA, ID-TIMS, ID-ICP-MS and LA-ICP-MS. *Geostandards and Geoanalytical Research*, 29(3), pp.285–302.

Johnsen, S.J. et al., 2001. Oxygen isotope and palaeotemperature records from six Greenland ice-core stations: Camp Century, Dye-3, GRIP, GISP2, Renland and NorthGRIP. *Journal of Quaternary Science*, 16(4), pp.299–307.

Jónasson, K., 2007. Silicic volcanism in Iceland: Composition and distribution within

the active volcanic zones. *Journal of Geodynamics*, 43(1), pp.101–117.

Jouzel, J. et al., 2007. Orbital and millennial Antarctic climate variability over the past 800,000 years. *Science (New York, N.Y.)*, 317(5839), pp.793–6.

Keigwin, L.D. et al., 1994. The role of the deep ocean in North Atlantic climate change between 70 and 130 kyr ago. *Nature*, 371(6495), pp.323–326.

Kittleman, L.R., 1973. Mineralogy, Correlation, and Grain-Size Distributions of Mazama Tephra and Other Postglacial Pyroclastic Layers, Pacific Northwest. *Geological Society of America Bulletin*, 84(9), pp.2957–2980.

Knutz, P.C., Austin, W.E.N. & Jones, E.J.W., 2001. Millennial-scale depositional cycles related to British Ice Sheet variability and North Atlantic palcocirculation since 45 kyr B.P., Barra Fan, U.K. margin. *Paleoceanography*, 16(1), pp.53–64.

Kopp, R.E. et al., 2009. Probabilistic assessment of sea level during the last interglacial stage. *Nature*, 462(7275), pp.863–867.

van Kreveld, S. et al., 2000. Potential links between surging ice sheets, circulation changes, and the Dansgaard-Oescheger cycles in the Irminger Sea, 60-18kyr. *Paleoceanography*, 15(4), pp.425–442.

Kuehn, S.C., Froese, D.G. & Shane, P. a. R., 2011. The INTAV intercomparison of electron-beam microanalysis of glass by tephrochronology laboratories: Results and recommendations. *Quaternary International*, 246(1-2), pp.19–47.

Kuhs, M. et al., 2014. Iceberg-rafted tephra as a potential tool for the reconstruction of ice-sheet processes and ocean surface circulation in the glacial North Atlantic. *Geological Society, London, Special Publications*, 398(1), pp.141–155.

Kukla, G.J. et al., 2002. Last Interglacial Climates. *Quaternary Research*, 58(1), pp.2–13.

Kvamme, T. et al., 1989. Geochemistry of Pleistocene ash zones in cores from the North Atlantic. *Norsk Geologisk Tidsskrift*, 69, pp.251–272.

Lacasse, C. et al., 1996. North Atlantic deep-sea sedimentation of Late Quaternary tephra from the Iceland hotspot. *Marine Geology*, 129(3–4), pp.207–235.

Lackschewitz, K.S. & Wallrabe-Adams, H.J., 1997. Composition and origin of volcanic ash zones in late quaternary sediments from the Reykjanes ridge: Evidence for ash fallout and ice-rafting. *Marine Geology*, 136, pp.209–224.

Landais, A. et al., 2004. Evidence for stratigraphic distortion in the Greenland Ice Core Project (GRIP) ice core during Event 5e1 (120 kyr BP) from gas isotopes. *Journal of Geophysical Research: Atmospheres*, 109(D6), pp.1–8.

Lane, C.S. et al., 2012. Was the 12.1 ka Icelandic Vedde Ash one of a kind? *Quaternary Science Reviews*, 33, pp.87–99.

Larsen, G. & Eiríksson, J., 2008. Late Quaternary terrestrial tephrochronology of Iceland - Frequency of explosive eruptions type and volume of tephra deposits. *Journal of Quaternary Science*, 23(October 2007), pp.109–120.

Lea, D.W., Mashiotta, T.A. & Spero, H.J., 1999. Controls on magnesium and strontium uptake in planktonic foraminifera determined by live culturing. *Geochimica et Cosmochimica Acta*, 63(16), pp.2369–2379.

Leadbetter, S.J. & Hort, M.C., 2011. Volcanic ash hazard climatology for an eruption of Hekla Volcano, Iceland. *Journal of Volcanology and Geothermal Research*, 199(3-4), pp.230–241.

Ledbetter, M.T., 1986. A Late Pleistocene time-series of bottom-current speed in the Vema Channel. *Palaeogeography, Palaeoclimatology, Palaeoecology*, 53(1), pp.97–105.

Van Leeuwen, R.J.W. et al., 2000. Stratigraphy and integrated facies analysis of the Saalian and Eemian sediments in the Amsterdam-Terminal borehole, the Netherlands. *Geologie en Mijnbouw/Netherlands Journal of Geosciences*, 79(2-3), pp.161–196.

Lisiecki, L.E. & Raymo, M.E., 2005. A Pliocene-Pleistocene stack of 57 globally distributed benthic δ 18O records. *Paleoceanography*, 20(1), pp.1–17.

Lisiecki, L.E. & Raymo, M.E., 2009. Diachronous benthic δ 18 O responses during late Pleistocene terminations. *Paleoceanography*, 24(3), pp.1–14.

Lowe, D.J., 2011. Tephrochronology and its application: A review. *Quaternary Geochronology*, 6(2), pp.107–153.

Maaløe, S., Sørensen, I.B. & Hertogen, J., 1986. The trachybasaltic suite of Jan Mayen. *Journal of Petrology*, (27), pp.439–466.

Mangerud, J. et al., 1984. A Younger Dryas Ash Bed in western Norway, and its possible correlations with tephra in cores from the Norwegian Sea and the North Atlantic. *Quaternary Research*, 21(1), pp.85–104.

Martinson, D.G. et al., 1987. Age dating and the orbital theory of the ice ages: Development of a high-resolution 0 to 300,000-year chronostratigraphy. *Quaternary Research*, 27(1), pp.1–29.

Maslin, M., Seidov, D. & Lowe, J., 2001. Synthesis of the nature and causes of rapid climate transitions during the Quaternary. In *The Oceans and RApid Cliamte Cange: PASt, Presnt and Furure*. American Geophysical Union, pp. 9–52.

Mazaud, A. et al., 2009. Upper and lower Jaramillo polarity transitions recorded in IODP Expedition 303 North Atlantic sediments: Implications for transitional field geometry. *Physics of the Earth and Planetary Interiors*, 172(3-4), pp.131–140.

McCave, I.N. & Hall, I.R., 2006. Size sorting in marine muds: Processes, pitfalls, and prospects for paleoflow-speed proxies. *Geochemistry, Geophysics, Geosystems*, 7(10), pp.1–37.

McIntyre, A. & Ruddiman, W.F., 1972. Northeast Atlantic post-Eemian paleooceanography: a predictive analog of the future. *Quaternary Research*, 2(3), pp.350–354.

McManus, J.F. et al., 1994. High-resolution climate records from the North Atlantic during the last interglacial. *Nature*, 371(6495), pp.326–329.

Mokeddem, Z., McManus, J.F. & Oppo, D.W., 2014. Oceanographic dynamics and the end of the last interglacial in the subpolar North Atlantic. *Proceedings of the National Academy of Sciences of the United States of America*, 111(31), pp.11263–11268.

Mortensen, A.K. et al., 2005. Volcanic ash layers from the Last Glacial Termination in the NGRIP ice core. *Journal of Quaternary Science*, 20(3), pp.209–219.

Müller, H., 1974. Pollenanalytische Untersuchungen und Jahresschichtenzählungen an der eem-zeitlichen Kieselgur von Bispingen/Luhe. *Geologisches Jahrbuch*, A 21, pp.149–168.

Müller, U.C. & Kukla, G.J., 2004. North Atlantic Current and European environments during the declining stage of the last interglacial. *Geology* , 32 (12), pp.1009–1012.

NGRIP Members, 2004. High-resolution record of Northern Hemisphere climate extending into the last interglacial period. *Nature*, 431(7005), pp.147–151.

Nicholl, J. a. L. et al., 2012. A Laurentide outburst flooding event during the last interglacial period. *Nature Geoscience*, 5(12), pp.901–904.

Van Nieuwenhove, N. et al., 2011. Evidence for delayed poleward expansion of North Atlantic surface waters during the last interglacial (MIS 5e). *Quaternary Science Reviews*, 30(7-8), pp.934–946.

Oladottir, B.A. et al., 2011. Provenance of basaltic tephra from Vatnajökull subglacial volcanoes, Iceland, as determined by major- and trace-element analyses. *The Holocene*, 21(7), pp.1037–1048.

Oppo, D.W. et al., 2001. Persistent suborbital climate variability in marine isotope stage 5 and Termination II. *Palaeoceanography*, 16(3), pp.280–292.

Oppo, D.W., Horowitz, M. & Lehman, S.J., 1997. Marine core evidence for reduced deep water production during Termination II followed by a relatively stable substage 5e (Eemian). *Paleoceanography*, 12(1), pp.51–63.

Oppo, D.W., McManus, J.F. & Cullen, J.L., 2006. Evolution and demise of the Last Interglacial warmth in the subpolar North Atlantic. *Quaternary Science Reviews*, 25(23-24), pp.3268–3277.

Parrenin, F. et al., 2007. The EDC3 chronology for the EPICA Dome C ice core. *Climate of the Past Discussions*, 3, pp.575–606.

Pearce, N.J.G., Bendall, C. a. & Westgate, J. a., 2008. Comment on "Some numerical considerations in the geochemical analysis of distal microtephra" by A.M. Pollard, S.P.E. Blockley and C.S. Lane. *Applied Geochemistry*, 23(5), pp.1353–1364.

Peck, V.L. et al., 2007. The relationship of Heinrich events and their European precursors over the past 60ka BP: a multi-proxy ice-rafted debris provenance study

in the North East Atlantic. *Quaternary Science Reviews*, 26(7-8), pp.862–875.

Pelejero, C. & Grimalt, J.O., 1997. The correlation between the 37k index and sea surface temperatures in the warm boundary: The South China Sea. *Geochimica et Cosmochimica Acta*, 61(22), pp.4789–4797.

Perkins, M.E. et al., 1995. Fallout tuffs of Trapper Creek, Idaho - A record of Miocene explosive volcanism in the Snake River Plain volcanic province. *Geological Society of America Bulletin*, 107(12), pp.1484–1506.

Perkins, M.E. et al., 1998. Sequence, age, and source of silicic fallout tuffs in middle to late Miocene basins of the northern Basin and Range province. *Bulletin of the Geological Society of America*, 110(3), pp.344–360.

Peters, C. et al., 2010. Magnetic characterisation and correlation of a Younger Dryas tephra in North Atlantic marine sediments. *Journal of Quaternary Sciene*, 25(3), pp.339–347.

Petit, R.J. et al., 1999. Climate and atmospheric history of the past 420,000 years from the Vostok ice core, Antarctica. *Nature*, 399, pp.429–436.

Pisias, N.G. et al., 1984. High resolution stratigraphic correlation of benthic oxygen isotopic records spanning the last 300,000 years. *Marine Geology*, 56(1-4), pp.119–136.

Pollard, D. & Thompson, S.L., 1997. Climate and ice-sheet mass balance at the last glacial maximum from the GENESIS version 2 global climate model. *Quaternary Science Reviews*, 16(8), pp.841–863.

Ran, L. et al., 2011. Diatom-based reconstruction of palaeoceanographic changes on the North Icelandic shelf during the last millennium. *Palaeogeography, Palaeoclimatology, Palaeoecology*, 302(1-2), pp.109–119.

Rasmussen, S.O. et al., 2013. A first chronology for the North Greenland Eemian Ice Drilling (NEEM) ice core. *Clim. Past*, 9(6), pp.2713–2730.

Rasmussen, S.O. et al., 2006. A new Greenland ice core chronology for the last glacial termination. *Journal of Geophysical Research*, 111(D6), pp.1–16.

Rasmussen, T.L. et al., 1999. Climate records and changes in deep outflow from the Norwegian Sea ~150-55 ka. *Terra Nova*, 11(2-3), pp.61–66.

Raymo, M.E. et al., 2004. Stability of North Atlantic water masses in face of pronounced climate variability during the Pleistocene. *Paleoceanography*, 19(2), pp.1–13.

Reimer, P.J. et al., 2009. IntCal09 and Marine09 radiocarbon age calibration curves, 0-50,000 yeats cal BP. *Radiocarbon*, 51(4), pp.1111–1150.

Revel, M. et al., 1996. Sr and Nd isotopes as tracers of North Atlantic lithic particles: Paleoclimatic implications. *Paleoceanography*, 11(1), pp.95–113.

Robinson, S., Maslin, M. & McCave, I., 1995. Magnetic-susceptibility variations in the upper Pleistocene deep-sea sediments of the NE Atlantic - Implication for ice

rafting and paleocirculation at the last glacial maximum. *Palaeoceanography*, 10(2), pp.221–250.

Rousseau, D.-D., Kukla, G. & McManus, J., 2006. What is what in the ice and the ocean? *Quaternary Science Reviews*, 25(17-18), pp.2025–2030.

Ruddiman, W.F., 1977. Late Quaternary deposition of ice-rafted sand in the subpolar North Atlantic ((lat 40° to 65°N)l. *Bulletin of the Geological Society of America*, 88(12), pp.1813–1827.

Ruddiman, W.F. & Glover, L.K., 1972. Vertical Mixing of Ice-Rafted Volcanic Ash in North Atlantic Sediments. *Geological Society of America Bulletin*, 83(9), pp.2817–2836.

Ruddiman, W.F. & Mcintyre, A., 1981. The North Atlantic Ocean during the last deglaciation. *Palaeogeography, Palaeoclimatology, Palaeoecology*, 35(0), pp.145–214.

Ryan, W.B.F. et al., 2009. Global Multi-Resolution Topography synthesis. *Geochemistry, Geophysics, Geosystems*, 10(3), pp.1–9.

Sánchez Goñi, M.F. et al., 2000. Direct land/sea correlation of the Eemian, and its comparison with the Holocene: A high-resolution palynological record off the Iberian margin. *Geologie en Mijnbouw/Netherlands Journal of Geosciences*, 79(2-3), pp.345–354.

Sánchez Goñi, M.F. et al., 1999. High resolution palynological record off the Iberian margin: direct land-sea correlation for the Last Interglacial complex. *Earth and Planetary Science Letters*, 171(1), pp.123–137.

Sandgren, P. et al., 1999. Stratigraphic evidence for a high marine shore□line during the late Weichselian deglaciation on the Kullen Peninsula, southern Sweden. *Journal of Quaternary Science*, 14(3), pp.223–237.

Schmidt, M.W. & Hertzberg, J.E., 2011. Abrupt Climate Change During the Last Ice Age. *Nature Education Knowledge*, 3(10), p.11.

Schmidt, M.W., Spero, H.J. & Lea, D.W., 2004. Links between salinity variation in the Caribbean and North Atlantic thermohaline circulation. *Nature*, 428(March), pp.160–163.

Schoning, K., Klingberg, F. & Wastegård, S., 2001. Marine conditions in central Sweden during the early Preboreal as inferred from a stable oxygen isotope gradient. *Journal of Quaternary Science*, 16(8), pp.785–794.

Scourse, J.D. et al., 2009. Growth, dynamics and deglaciation of the last British–Irish ice sheet: the deep-sea ice-rafted detritus record. *Quaternary Science Reviews*, 28(27-28), pp.3066–3084.

Sejrup, H.P. et al., 1989. Quaternary tephrachronology on the Iceland Plateau, north of Iceland. *Journal of Quaternary Science*, 4(2), pp.109–114.

Severinghaus, J.P., 2009. Climate change: Southern see-saw seen. *Nature*, 457(7233),

pp.1093–1094.

Severinghaus, J.P. & Brook, E.J., 1999. Abrupt Climate Change at the End of the Last Glacial Period Inferred from Trapped Air in Polar Ice. *Science*, 286(5441), pp.930–934.

Shackleton, N.J. et al., 2003. Marine Isotope Substage 5e and the Eemian Interglacial. *Global and Planetary Change*, 36(3), pp.151–155.

Shackleton, N.J. et al., 2002. The Classic Marine Isotope Substage 5e. *Quaternary Research*, 58(1), pp.14–16.

Shackleton, N.J., 1969. The Last Interglacial in the Marine and Terrestrial Records. *Proceedings of the Royal Society of London B: Biological Sciences*, 174(1034), pp.135–154.

Shackleton, N.J., Hall, M.A. & Vincent, E., 2000. Phase relationships between millennial-scale events 64,000--24,000 years ago. *Paleoceanography*, 15(6), pp.565–569.

Shackleton, N.J. & Opdyke, N.D., 1973. Oxygen isotope and palaeomagnetic stratigraphy of Equatorial Pacific core V28-238: Oxygen isotope temperatures and ice volumes on a 105 year and 106 year scale. *Quaternary Research*, 3(1), pp.39–55.

Skinner, L.C. & Shackleton, N.J., 2005. An Atlantic lead over Pacific deep-water change across Termination I: implications for the application of the marine isotope stage stratigraphy. *Quaternary Science Reviews*, 24(5-6), pp.571–580.

Skinner, L.C. & Shackleton, N.J., 2006. Deconstructing Terminations I and II: revisiting the glacioeustatic paradigm based on deep-water temperature estimates. *Quaternary Science Reviews*, 25(23-24), pp.3312–3321.

Small, D., Austin, W. & Rinterknecht, V., 2013. Freshwater influx, hydrographic reorganization and the dispersal of ice-rafted detritus in the sub-polar North Atlantic Ocean during the last deglaciation. *Journal of Quaternary Science*, 28(5), pp.527–535.

Sparks, R.S.J., Wilson, L. & Sigurdsson, H., 1981. The Pyroclastic Deposits of the 1875 Eruption of Askja, Iceland. *Philosophical Transactions of the Royal Society A: Mathematical, Physical and Engineering Sciences*, 299(1447), pp.241–273.

Spero, H.J. et al., 1997. Effect of seawater carbonate concentration on foraminiferal carbon and oxygen isotopes. *Nature*, 390(6659), pp.497–500.

Steele, D. & Engwell, S., 2009. *Preparation of Tephra Samples for Electron Microprobe Analysis*, TAU, Universtiy of Edinburgh.

Stirling, C.H. et al., 1998. Timing and duration of the Last Interglacial: evidence for a restricted interval of widespread coral reef growth. *Earth and Planetary Science Letters*, 160(3–4), pp.745–762.

Svensson, A. et al., 2011. Annual layering in the NGRIP ice core during the Eemian.

Climate of the Past, 7(4), pp.1427–1437.

Svensson, A. et al., 2006. The Greenland Ice Core Chronology 2005, 15–42ka. Part 2: comparison to other records. *Quaternary Science Reviews*, 25(23-24), pp.3258–3267.

Thompson, W.G. & Goldstein, S.L., 2006. A radiometric calibration of the SPECMAP timescale. *Quaternary Science Reviews*, 25(23–24), pp.3207–3215.

Thordarson, T. & Larsen, G., 2007. Volcanism in Iceland in historical time: Volcano types, eruption styles and eruptive history. *Journal of Geodynamics*, 43(1), pp.118–152.

Turner, C., 2002. Problems of the Duration of the Eemian Interglacial in Europe North of the Alps. *Quaternary Research*, 58(1), pp.45–48.

Turney, C.S.M. et al., 2006. North European last glacial–interglacial transition (LGIT; 15–9 ka) tephrochronology: extended limits and new events. *Journal of Quaternary Science*, 21(4), pp.335–345.

Turney, C.S.M. et al., 2004. Tephrochronology of last termination sequences in Europe: a protocol for improved analytical precision and robust correlation procedures(a joint SCOTAV–INTIMATE proposal). *Journal of Quaternary Science*, 19(2), pp.111–120.

Turney, C.S.M., Harkness, D.D. & Lowe, J.J., 1997. The use of microtephra horizons to correlate Late-glacial lake sediment successions in Scotland. *Journal of Quaternary Science*, 12(1997), pp.525–531.

Turney, C.S.M. & Jones, R.T., 2010. Does the Agulhas Current amplify global temperatures during super-interglacials? *Journal of Quaternary Science*, 25(6), pp.839–843.

Turon, J.-L., 1984. Direct land/sea correlations in the last interglacial complex. *Nature*, 309(5970), pp.673–676.

Tzedakis, C., 2003. Timing and duration of Last Interglacial conditions in Europe: A chronicle of a changing chronology. *Quaternary Science Reviews*, 22(8-9), pp.763–768.

Vinther, B.M. et al., 2006. A synchronized dating of three Greenland ice cores throughout the Holocene. *Journal of Geophysical Research*, 111, pp.1–9.

Wastegård, S. et al., 2005. A tephra-based correlation between the Faroe Islands and the Norwegian Sea raises questions about chronological relationships during the last interglacial. *Terra Nova*, 17(1), pp.7–12.

Wastegård, S. et al., 2000. Extending the known distribution of the Younger Dryas Vedde Ash into northwestern Russia. *Journal of Quaternary Science*, 15(6), pp.581–586.

Wastegård, S. & Rasmussen, T.L., 2001. New tephra horizons from Oxygen Isotope Stage 5 in the North Atlantic: correlation potential for terrestrial, marine and ice-

core archives. *Quaternary Science Reviews*, 20(15), pp.1587–1593.

Watkins, S.J., Maher, B. a. & Bigg, G.R., 2007. Ocean circulation at the Last Glacial Maximum: A combined modeling and magnetic proxy-based study. *Paleoceanography*, 22(2), pp.1–20.

Wilson, S.A., 1997. The collection, preparation, and testing of USGS reference material BCR-2, Columbia River, Basalt: *U.S. Geological Survey Open-File Report*, pp.98–00x.

Zagwijn, W.H., 1961. No TitleVegetation, climate and radiocarbon datings in the Late Pleistocene of the Netherlands. Part I: Eemian and Early Weichselian. *Mededelingen van de Geologische Stichting, Nieuwe Serie*, 14, pp.15–40.